



Lawrence Berkeley Laboratory

UNIVERSITY OF CALIFORNIA

Materials & Chemical Sciences Division

The Role of Inhibitors During Electrodeposition of Thin Metallic Films

M.J. Armstrong

Ph.D. Thesis

May 1990



! LOAN COPY !
! Circulates !
! for 2 weeks !

! Bldg. 50 Library. !
! Copy 2 !

LBL-28972



DISCLAIMER

This document was prepared as an account of work sponsored by the United States Government. While this document is believed to contain correct information, neither the United States Government nor any agency thereof, nor the Regents of the University of California, nor any of their employees, makes any warranty, express or implied, or assumes any legal responsibility for the accuracy, completeness, or usefulness of any information, apparatus, product, or process disclosed, or represents that its use would not infringe privately owned rights. Reference herein to any specific commercial product, process, or service by its trade name, trademark, manufacturer, or otherwise, does not necessarily constitute or imply its endorsement, recommendation, or favoring by the United States Government or any agency thereof, or the Regents of the University of California. The views and opinions of authors expressed herein do not necessarily state or reflect those of the United States Government or any agency thereof or the Regents of the University of California.

LBL-28972

**THE ROLE OF INHIBITORS DURING
ELECTRODEPOSITION OF THIN METALLIC FILMS**

Michael J. Armstrong

(Ph.D. Thesis)

**Department of Chemical Engineering
University of California at Berkeley**

and

**Materials and Chemical Sciences Division
Lawrence Berkeley Laboratory
University of California
Berkeley, CA 94720**

This work was supported by the Director, Office of Energy Research,
Office of Basic Energy Sciences, Materials Sciences Division of the
U.S. Department of Energy under contract No. DE-AC03-76SF00098.

The Role of Inhibitors During Electrodeposition of Thin Metallic Films

Michael Jeffrey Armstrong

(Ph.D. Thesis)

with Rolf. H. Muller

Lawrence Berkeley Laboratory

Materials and Chemical Sciences Division

and

Department of Chemical Engineering

University of California, Berkeley

Berkeley, California 94720

Abstract

The role of brightening agents during the deposition of thin metal films was analyzed. The model brightening system studied was copper deposition in the presence of benzotriazole (BTA). Emphasis was placed on the early stages of deposition. The development of microtopography was characterized with *in situ* scanning tunneling microscopy. Cuprous-BTA film formation was measured with impedance spectroscopy. Copper electrochemistry was measured with double-pulse potentiometry. The incorporation of BTA, including the effects of mass transport conditions, was studied with x-ray photoelectron spectroscopy and secondary ion mass spectroscopy. A visual survey of deposits from 0.5 M CuSO₄, 0.5 M H₂SO₄ indicated that brightening occurs when the concentration of BTA is greater than 100 μM and the current density is greater than 50 mA/cm². A passive layer was

found to form during cathodic polarization of copper in 0.5 M CuSO_4 , 0.5 M H_2SO_4 with 100 and 200 μM BTA. Following breakdown of the passive layer, with increased polarization, the copper remains covered with a BTA film with a coverage following Langmuir adsorption kinetics. Benzotriazole was not incorporated into the copper deposits. The nucleation site density of Cu on Pt was only a function of overpotential irrespective of the BTA concentration. The presence of BTA increases the overpotential (resulting in an increase in nucleation rate) for a given current density which results in a decreased particle size. Benzotriazole altered the morphology of the deposited Cu. Deposits from BTA free electrolyte consisted of flat planes terminated with ledges with growth occurring at the ledges. Deposits from BTA containing electrolyte consisted of hemispheres with growth occurring uniformly on the surface. The brightening of copper deposited in the presence of BTA for a given current density is a result of an increase in the nucleation rate due to increased overpotential and the uniform growth of the nuclei surface.

A scanning tunneling microscope was adapted to perform *in situ* measurements of the topography of copper films. Software was developed to collect and display (line plot, height coded grey scale, derivative coded grey scale, and edge enhanced height coded grey scale) data from the tunneling microscope with a IBM AT compatible computer.

A handwritten signature in black ink, appearing to read "A. J. ...", is located in the bottom right corner of the page.

Acknowledgement

I am very grateful for the love and patience of my wife, Kim, who has been beside me throughout most of my stay at Berkeley. I thank my daughter, Cameron whose favorite sayings are "get a job Dad" and "come home for dinner". She gives me an excuse to play on rope swings and hunt for salamanders. I welcome Jillian, born March 1, 1990, to our family even though she keeps me up at night. My parents, Warren and Harriet, have always had faith in me even when I didn't. It is due to their parenting that I have been able to pursue this degree. If I am as good a parent to my children as they have been to me then I will consider myself successful in life. I also would like to thank my sisters Phyllis and Jeanette and my brother Steve for their support. Thanks to my in-laws Steve and Frances Barrett for sharing their daughter and being supportive.

I have enjoyed most of my stay at Berkeley. This is in large part due to the friendship I have with the Muller and Tobias students. The present Muller students Laura, Bob, Dan, and Feliz have been especially helpful by mitigating the frustration of compiling the thesis during the past year. I would like to thank Dr. Muller for his direction and support during my trip down this winding road.

This work was supported by the Director, Office of Energy Research, Office of Basic Energy Sciences, Materials Sciences Division of the US Department of Energy under contract No. DE-AC03-76SF00098.

Contents

Chapter 1: Introduction	
1.1 Purpose	1
1.2 Definition of Brightening and Leveling	2
1.3 Metal Deposition	4
1.3.1 Transport and Kinetics	4
1.3.2 Inhibition.....	5
1.3.3 Nucleation.....	6
1.3.4 Leveling and Brightening	9
1.4 Copper Deposition	13
1.4.1 Plating Baths.....	13
1.4.2 Brightening Agents	14
1.5 Benzotriazole	16
Chapter 2: Procedures	
2.1 Electrochemical Analysis	28
2.1.1 Galvanostatic Double-Pulse.....	28
2.1.2 Cyclic Voltammetry.....	29
2.1.3 Impedance.....	32
2.2 Elemental Analysis of Deposits	36
2.2.1 X-ray Photoelectron Spectroscopy.....	36
2.2.2 Secondary Ion Mass Spectroscopy	37
2.3 Scanning Tunneling Microscopy	38
2.3.1 Topography of Copper Deposits.....	46
2.3.2 Nuclei Density.....	48
Chapter 3: Results	
3.1 Survey of Addition Agents	52
3.1.1 Methyl Red.....	54
3.1.2 Rhodamine-B Chloride.....	54
3.1.3 Fluorescein.....	58
3.1.4 Benzotriazole	58
3.1.5 Polyvinyl Alcohol.....	60

3.1.6	Coumarin 343	60
3.1.7	Summary.....	60
3.2	Conditions which result in Bright Copper Deposition -- SEM Survey.....	63
3.3	Copper-Benzotriazole Film Formation.....	70
3.3.1	Film Formation in Cu Plating Solution.....	70
3.3.2	Incorporation into Electrodeposited Cu.....	83
3.4	Inhibition of Copper Reduction	95
3.4.1	Deposition rate as a function of potential and BTA Concentration.....	95
3.4.2	UPD of Cu on Pt as a function of BTA Concentration .	100
3.5	Micro Topography.....	105
3.5.1	Growth of Copper Deposits	105
3.5.2	Nucleation Density.....	108
Chapter 4: Conclusions		
4.1	Nucleation and Growth Phenomena.....	116
4.2	Summary of Conclusions.....	117
4.3	Future Directions	118
4.3.1	Copper-Benzotriazole System.....	118
4.3.2	STM Technique	120
Appendix A: Impedance Spectroscopy Software		
1	Introduction	122
2	Multimode waveform -- MKCV (make curve).....	122
3	Data Acquisition -- ACQUIRE.C.....	123
4	Impedance Calculation -- IMP-FFT	126
5	Source Code Listing.....	127
5.1	MKCV (fortran).....	127
5.2	IMP-FFT (fortran).....	130
Appendix B: Scanning Tunneling Microscopy Software		
1	Introduction	136
2	Data Acquisition	136
2.1	STMPLE3.....	137
2.2	STMPLE4.....	143
3	Data Display -- RE2	144

4	Data Manipulation	144
4.1	SUBTRACT.....	144
4.2	ENHANCE.....	145
4.3	DX.....	145
4.4	MOOTH.....	147
5	Source Code	151
5.1	STMPLE3.....	151
5.2	STMPLE4.....	161
5.3	RE2.....	171
5.4	SUBTRACT.....	174
5.5	ENHANCE.....	177
5.6	DX.....	180
5.7	SMOOTH.....	183
5.8	Subroutines.....	186
5.8.1	<i>Display</i>	186
5.8.2	<i>Grey64</i>	192
5.8.3	<i>Disp2</i>	193

Chapter 1. Introduction

1.1. Purpose

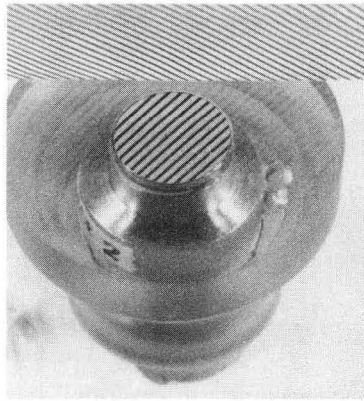
Virtually all commercial plating baths contain one or more addition agents for the purpose of modifying the physical properties of the deposit. An inhibitor is defined here as any addition agent (excluding complexing agents) which inhibits the electrodeposition of the metal. Small amounts, 10^{-6} M, of inhibitor can have large effects on deposit properties such as morphology, corrosion resistance, hardness, and ductility. The purpose of this work was to study the effect of inhibitors on the morphology of thin metal films and relate these effects to processes occurring during mirror bright metal deposition.

In spite of the extensive use of inhibitors in commercial plating baths for the purpose of brightening there is still much to be learned about how these agents function. Historically the choice of agents and the conditions of their use has not been based on a theory of their function but has been arrived at by trial and error augmented by practical knowledge of previously used materials. The difficulty in forming a generalized mechanism by which agents affect the deposit brightness is in part due to the large number of different materials which are effective. Another hindrance is the large volume of data needed to characterize the deposition process

for each additive used due to the complexity of the electroplating process. With a better understanding of the brightening process it will be possible to choose an agent with a minimum of developmental costs. Two characteristics of metal deposition in the presence of brightening agents include randomization of grain growth and reduction of grain size [1.1]. This work focuses upon these two phenomena during the deposition of copper from plating baths containing benzotriazole (BTA). Benzotriazole is a proven brightening agent [1.2]. The formation of BTA films on copper deposits and incorporation of BTA into copper deposits was also investigated.

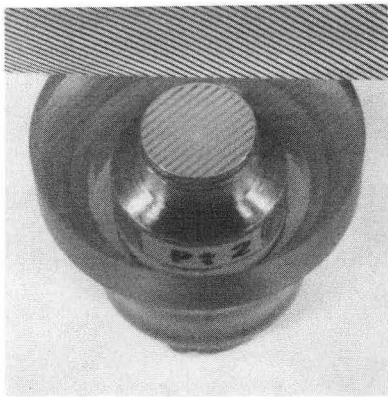
1.2. Definition of Brightening and Leveling

The smoothing of a surface through cathodic deposition is broken into two classifications, leveling and brightening, which are defined by the size of roughness. Leveling is associated with smoothing features of a size greater than the wavelength of visible light, generally $0.5 \mu\text{m}$ and above. Brightening is associated with the smoothing of features sizes on the order of or less than the wavelength of visible light ($< 0.5 \mu\text{m}$). The brightness of an object is related to the ability of the object to specularly reflect light. With increasing brightness more light is specularly reflected and less light is scattered. The contrast of a reflected image from a surface increases as less light is scattered by roughness. The reflected image of a parallel line pattern from several copper deposits with different degrees of roughness is shown in figure 1.1. In this figure the increase of contrast in the reflected image is apparent as the brightness increases.



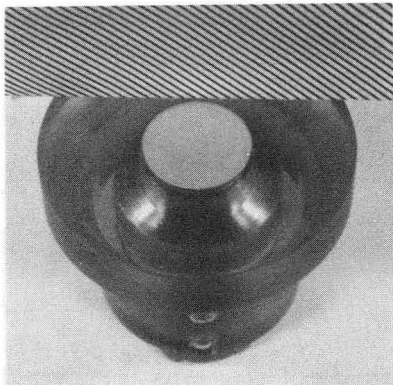
Bright

roughness $< 200 \text{ \AA}$



Milky

$200 \text{ \AA} < \text{roughness} < 3000 \text{ \AA}$



Matte

$3000 \text{ \AA} < \text{roughness}$

Figure 1.1. Reflected image of a parallel line pattern from surfaces with roughness wavelengths of (a) $0.02 \mu\text{m}$, (b) $0.3 \mu\text{m}$, and (c) $1 \mu\text{m}$. The reported roughness for figure (a) was measured by scanning tunneling microscopy on a similarly prepared surface. For figures (b) and (c) the roughness corresponds to the spatial frequency of features imaged with scanning electron microscopy. The parallel line pattern is on the rectangular object in the top of each photo. The deposit is the inner disk below the parallel line pattern. The contrast decreases with increasing roughness. (XBB 894-3299)

1.3. Metal Deposition

Metal deposition involves three processes: transport of reacting species to the surface, nucleation of crystals, and continued growth of crystals. A very brief review of theory concerning mass transport, nucleation, and crystal growth during metal deposition is presented here. Kindler has presented a literature review of theory and experimental work concerning the electrodeposition of metals. [1.3].

1.3.1. Transport and Kinetics

Within the electrolyte the transport of reacting species to the surface occurs by convection, diffusion, and migration. For the one dimensional case the flux, N_j , of each ionic species, j , can be written as

$$N_j = -D_j \frac{dC_j}{dx} + z_j u_j C_j \frac{d\phi}{dx} + C_j v \quad (1.1)$$

where D is the diffusion coefficient, C is the concentration, x is the coordinate normal to the surface, z is the charge carried, u is the mobility, ϕ is the potential, and v is the velocity normal to the surface. The current density at an electrode is expressed by

$$i = \sum n_j F N_j \quad (1.2)$$

where F is Faraday's constant and n is the number of electrons transferred from the reactant to the electrode.

The current density is related to the electrode potential and interfacial reactant concentration by the kinetics of the charge transfer reaction. A frequently used description of the kinetics in the absence of mass transfer limitation is the

Butler-Volmer expression [1.4]

$$i = i_0 \left[\exp \left(\frac{(1-\alpha)nF}{RT} \eta \right) - \exp \left(\frac{-\alpha nF}{RT} \eta \right) \right] \quad (1.3)$$

where i is the current density, i_0 is the exchange current density, α is the transfer coefficient for the cathodic reaction, η is the kinetic polarization, n is the number of electrons transferred, F is Faraday's constant, R is the gas constant, and T is the absolute temperature. The Butler-Volmer equation can be approximated at low surface overpotentials by a linear expression

$$i = i_0 \frac{nF}{RT} \eta \quad (1.4)$$

and at high surface overpotentials by the Tafel equations.

$$\text{cathodic} \quad i = i_0 \exp \left(\frac{-\alpha nF}{RT} \eta \right) \quad (1.5)$$

and

$$\text{anodic} \quad i = i_0 \exp \left(\frac{(1-\alpha)nF}{RT} \eta \right) \quad (1.6)$$

1.3.2. Inhibition

Theoretical treatments of inhibition are based on the adsorption of inhibitor to the electrochemical interface [1.5, 1.6]. The adsorbed inhibitor may form an electrostatic field at the interface altering the rate of discharge of metal ions and the inhibitor may physically block the metal ions from reaching the interface and reduce the effective surface area for reaction. In general the current density in the presence of inhibitor can be represented by the expression

$$i_\theta = i_{\theta=0} f(\theta) \quad (1.7)$$

where i_θ is the current density on a surface with a inhibitor coverage of θ and $f(\theta)$

is a function of theta. In the case of physical blocking of the surface by inhibitor $f(\theta) = (1-\theta)$.

1.3.3. Nucleation and Continued Growth

A study of brightening requires an understanding of the mechanism of nucleation and growth of crystals from which metal deposits form. It is the size and shape of the crystals which determines the minimum possible roughness of a deposit surface.

Theoretical treatments on a global scale of the nucleation of new crystals generally assume that nucleation occurs at active sites on an electrode surface and that all nucleations require the same energy [1.7]. Using these assumptions the number of nuclei appearing on active sites can be given in a first-order approximation [1.7]

$$N(t) = N_0 [1 - \exp(-\int_0^t \alpha(t) dt)] \quad (1.8)$$

where $N(t)$ is the observed number of nuclei as a function of time, N_0 is the total number of active sites, and $\alpha(t)$ is a potential-dependent activation rate for sites. Recently the assumption of a unique energy for nucleation has been relaxed and a broad range of energies was included in modeling the nucleation process [1.8]. Allowing for a broad range of site energies results in the following relationship for the total number of nuclei.

$$N(t) = \int_0^t (N_0 \alpha(t) \exp(-\int_0^t \alpha(t) dt)) dt \quad (1.9)$$

This nucleation model agrees with experimental data [1.9].

Several mechanisms are possible in which the adsorption of inhibitor molecules to a surface may increase the nucleation rate.

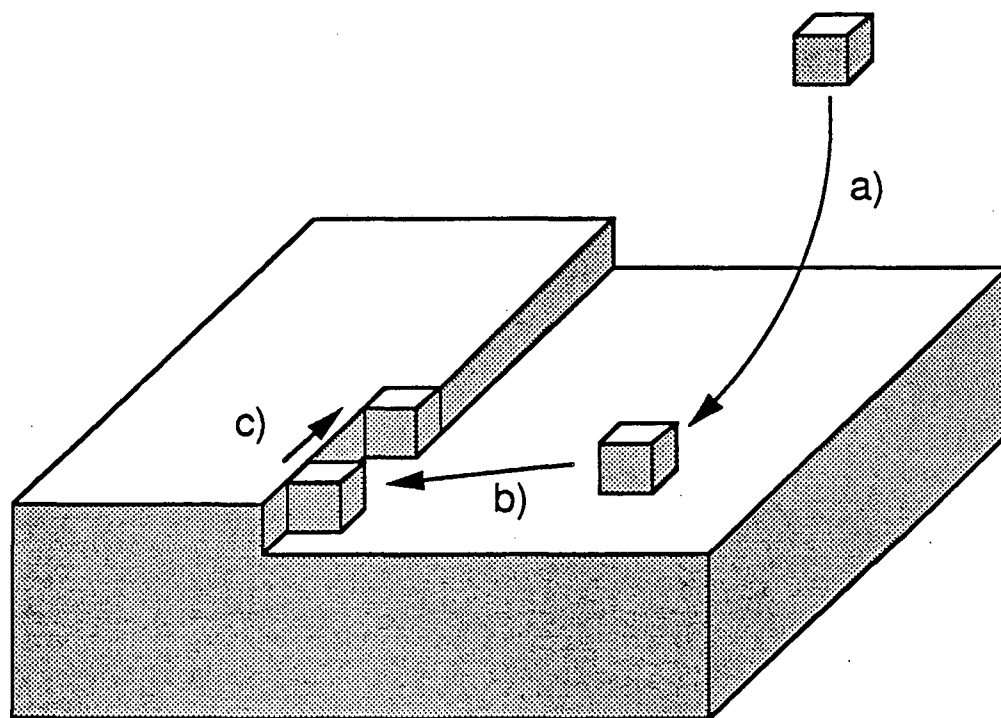
- 1) Increasing the overpotential for the deposition process
- 2) Stabilizing nuclei on less favored nucleation sites
- 3) Preventing continued growth of existing nuclei by adsorption to active growth sites

The practice of formulating bright plating baths remains an art in which the most prominent tools are intuition and trial and error. Research into the mechanism of brightening has proceeded slowly for many decades. In interpreting experimental observations, researchers have proposed mechanisms of brightening based on the solid-electrolyte interface [1.10] and/or the mass-transfer boundary layer [1.1]. It has been determined that mass transfer of inhibitor and structural properties of the deposit are both important in the brightening process [1.10].

The process of continued growth of a metal deposit is assumed to occur in the following manner (fig. 1.2) [1.11, 1.12].

- 1) Diffusion of the reacting ion from bulk solution to the surface
- 2) Surface diffusion of the ion to a kink or step site with incorporation into the lattice
- 3) Completion of the charge transfer

Deposition on dislocation-free planar surfaces occurs at kink sites along ledges on the surface. The addition of atoms to a kink site results in a propagation of the kink site along the ledge to the edge of the crystal at which point another kink site must be nucleated on the ledge.



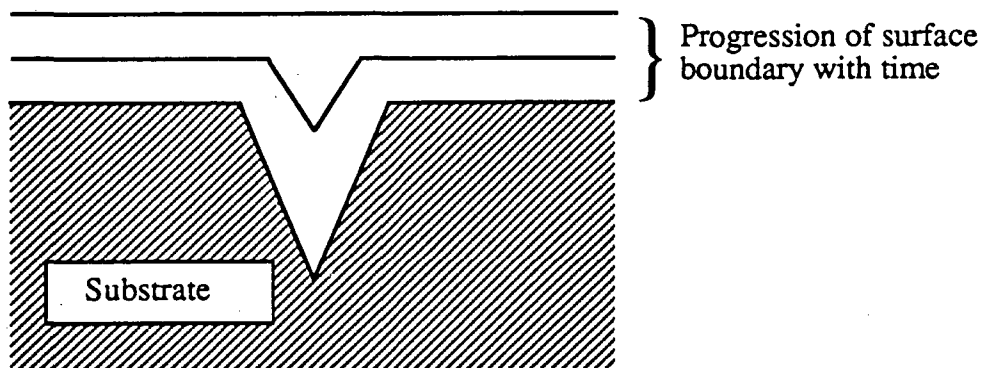
XBL 902-590

Figure 1.2. Pathway by which an atom may be incorporated into a crystal lattice, a) diffusion of the reacting ion from bulk solution to the surface, b) and c) surface diffusion of the adatom to a step or kink site with incorporation into the lattice, and completion of the charge transfer. (XBL 902-590)

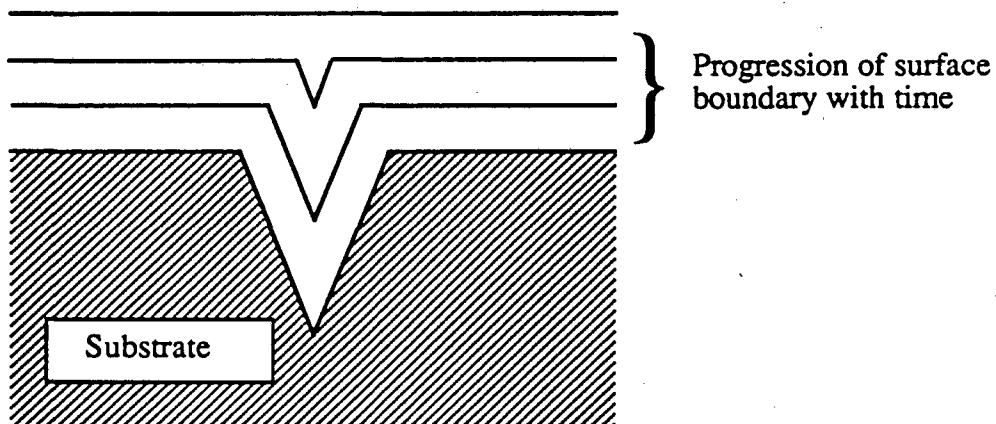
1.3.4. Leveling and Brightening

Leveling and brightening can be broken down as to whether the smoothing of the surface is passive (geometric) or active (true). In the case of passive brightening the ratio of current density in the valleys to that on the peaks of roughness is equal to 1 (fig. 1.3-a). Passive brightening can occur without any additives to the plating bath. Active brightening occurs when the ratio of current density in the valleys to that on the peaks of roughness is greater than 1 (fig. 1.3-b). Active brightening requires some agent, such as an inhibitor, to promote deposition into the valley. Active brightening requires less deposited material than passive brightening for the same degree of brightening.

The growth of crystallites results in a rough surface. The roughness depends on the size of the crystallites. The size is determined by the duration of growth which depends on nucleation rate. Anisotropy of the kinetics between the different crystal faces gives the electrodeposited crystals a characteristic shape. In order to remove the effect of grain size on the smoothness of a surface, additives are added to the plating bath which eliminate the anisotropy in the kinetics. The effect of this type of additive is often referred to as "randomization". With uniform kinetics of the crystal faces the shape of a growing crystal is controlled by mass transport alone. To remove the effect of grain shape one can reduce the grain size such that the size is much less than the desired surface smoothness. Additives to plating baths can reduce the grain size. This effect is referred to as "grain refinement". Both randomization and grain refinement increase the smoothness obtainable but do not depend on whether active or passive brightening occurs.



(a)



(b)

XBL 902-589

Figure 1.3. Definition of true and geometric leveling. (a) true leveling, current density in the valley is higher than the plain, (b) geometric leveling, uniform current density. (XBL 902-589)

Active brightening can be assisted by a difference in inhibitor flux between peaks and recesses of the surface when the inhibitor is consumed at the surface. A spatial variation of the interfacial concentration of inhibitor exist between the valleys and peaks of a rough surface when the mass transfer boundary layer thickness is comparable to the depth of the roughness. The inhibitor can be consumed by reaction and incorporation at the deposit surface. The variation of inhibitor concentration between peak and recess will be greatest at the diffusion limited delivery of inhibitor. In order for this mechanism to produce leveling or brightening the inhibition must increase with inhibitor concentration. This mechanism works best under the conditions that

- 1) characteristic dimension of roughness and diffusion layer is the same,
- 2) concentration of inhibitor at the surface is in the region where the derivative of overpotential with respect to inhibitor concentration is large,
- 3) the delivery of the inhibitor to the surface is at the diffusion limit,
- 4) current density is much less than limiting current.

Studies of the inhibitor incorporation and reaction rates have provided experimental evidence of leveling governed by the transport of the additive. Leveling was found to occur when the delivery of inhibitor to the deposit was diffusion limited [1.13, 1.14]. In addition several features of diffusion control have been revealed by studies on incorporation of inhibitor. By radiotracer and preferential etching methods, the preferred incorporation of inhibitors to peaks has been detected [1.13, 1.15]. Also the most effective concentration of inhibitor to produce leveling has been shown to be in the range where the derivative of

overpotential with respect to inhibitor concentration is large [1.16].

Significant contributions towards understanding diffusion controlled leveling and brightening have been made by the following.

Foulke and Kardos proposed a theory based on local variation of polarization caused by the local diffusion boundary layer thickness [1.17]. Their concepts were supported by measurements of the influence of agitation on polarization and measurements of leveling agent consumption. Watson and Edwards also proposed this theory for leveling at about the same time [1.13]. In addition they proposed to predict the degree of leveling from the dependence of electrode potential on additive concentration and on current density. Their work also showed greater incorporation of inhibitor on peaks than in valleys. Rodger, Ware, and Fellows studied the incorporation of thiourea in nickel deposits [1.14]. They determined the incorporation rate of inhibitor to be independent of current density and proportional to inhibitor concentration. They also showed an increase in incorporation with agitation.

Extension of the diffusion controlled leveling mechanism to brightening has been opposed by Vagramyan and Baraloshkina [1.10]. Vagramyan and Baraloshkina suggest that the inhibitor is uniformly accessible to a surface with roughness characteristic of bright deposits ($<0.3 \mu\text{m}$). They point to the relatively small difference in diffusion boundary thickness of peaks and valleys on a bright surface. Kardos disagreed with this argument and suggested that the lateral diffusion of inhibitor to peaks is important enough to produce an interfacial concentration gradient over the roughness [1.18]. More recently Gerenrot and

Leichkis proposed, for brightening to occur, the requirement of a film of the same order of thickness as existing roughness to act as a diffusion barrier to the inhibitor [1.19].

1.4. Copper Deposition

1.4.1. Plating Baths

Electrodeposited copper is used widely. Applications of copper electrodeposition include corrosion protection, undercoating for other plated metals, electroforming, and electrorefining. There are two types of plating baths used for copper deposition based on whether or not copper is complexed.

Complexed copper plating baths are made generally with cyanide or pyrophosphate anions. The copper complexed plating baths are generally used in cases where the substrate material is sensitive to acid baths. The cyanide based plating baths are alkaline with copper complexed with cyanide, $\text{Cu}(\text{CN})_3^{-2}$. The pyrophosphate based baths are slightly basic with copper complexed as $\text{Cu}(\text{P}_2\text{O}_7)_2^{-6}$ and $(\text{CuP}_2\text{O}_7)^{-2}$. The complexed bath has better throwing power than the acid baths but the current density obtainable is lower. The remainder of this discussion will be focused on the acid baths which is the area of this research. A good review of copper cyanide and copper pyrophosphate plating can be found in Modern Electroplating [1.20].

Acid copper plating is generally performed in an acidic sulfate or fluoroborate

electrolytes. The advantage of using an acid bath over an alkaline complexed bath are higher conductivity and lower overpotential at the cathode and anode. Also at low pH the high current densities can be obtained without the formation of spongy deposits containing occluded salts and oxides. The baths are also easily controlled and cheaper, but as mentioned before they have less throwing power. A typical sulfate plating bath would consist of 0.75 M CuSO_4 and 0.75 M H_2SO_4 with addition agents for modifying deposit properties such as brightness.

In aqueous solutions of copper ions both monovalent, cuprous, and divalent, cupric, ions coexist. The reduction of cupric ions proceeds via a two step mechanism [1.21, 1.22].



Reaction 1.10 has been shown to be the rate limiting step [1.21, 1.22]. This two step reduction is followed by surface diffusion of the adatom to a growth site. The standard potential, E_0 for reactions 1.10 and 1.11 are 0.169 and 0.522 respectively. Assuming reaction 1.11 is fast, the concentration of Cu^+ ion, C_{Cu^+} , at a copper electrode of potential E can be determined with the Nernst equation.

$$E = E_0 - \frac{RT}{F} \ln \left(\frac{1}{C_{\text{Cu}^+}} \right) \quad (1.12)$$

1.4.2. Brightening Agents

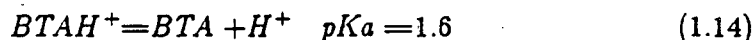
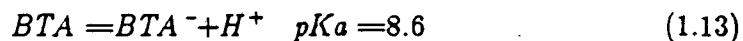
Deposits from additive free electrolytes are columnar whereas deposits from brightener containing electrolyte are fine grained [1.23]. Brightening agents belong

to several classes of compounds including amines, sulfonic acids, azo dyes, and many others. One of the first to be used for bright copper plating is thiourea. Thiourea is thought to decompose at the surface releasing sulfide ions, this has been supported by the observation of the incorporation of sulfide in nickel deposits [1.14] and the adsorption of sulfide on palladium [1.24] in thiourea containing electrolytes. At concentrations less than 0.1 mM, thiourea lowers the cathodic overpotential in acidic electrolytes [1.25]. It is postulated by Barnes that the sulfide prevents chemisorption of hydrogen to the copper surface [1.25]. Barnes suggest that the hydride ion is displaced by HS^- which being highly polarizable stimulates reduction of copper ions and causes a coarser deposit grain size [1.26]. Thiourea becomes an inhibitor at higher concentrations. These higher concentrations, 1 to 10 mM, result in leveling and brightening of copper deposits. Ke has investigated the crystallographic dependencies of thiourea adsorption and copper plating [1.27]. Without inhibitor present the deposit topography was dependent on the underlying surface. With thiourea the deposit was polycrystalline and independent of underlying surface. A radiotracer study showed thiourea to be strongly adsorbed and nonselective of crystal orientation. Hoffer and Hintermann studied the structure of thiourea inhibited copper deposition with X-ray diffraction [1.28]. In this study they found the grain size to be minimum at 18 nm with 20 ppm of thiourea in a acid copper sulfate plating bath. Thiourea, which decreases ductility of the deposit, has since been replaced by better brighteners [1.21]. Many of the brighteners are sulfur containing compounds such as sulfonated aryl and alkyl substitution products of acetylthiourea and sulfonated aromatic compounds [1.28]. Brighteners are frequently grouped into two classes [1.29]. Class I brighteners are

those additives which effect a milky plate for electrodeposited metals, and have no critical upper limit of concentration. Plating in the presence of these brighteners does not result in leveling. Class II brighteners promote leveling and increase the brightness obtainable when used with class I brighteners. Class I brighteners are not incorporated and class II are incorporated into deposits. Examples of class I and II brighteners are shown in table 1.1.

1.5. Benzotriazole

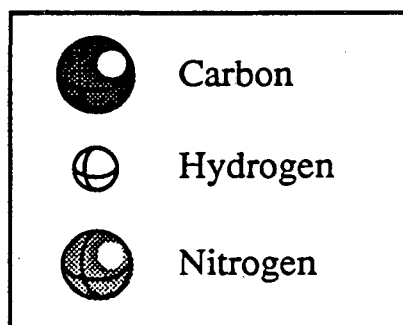
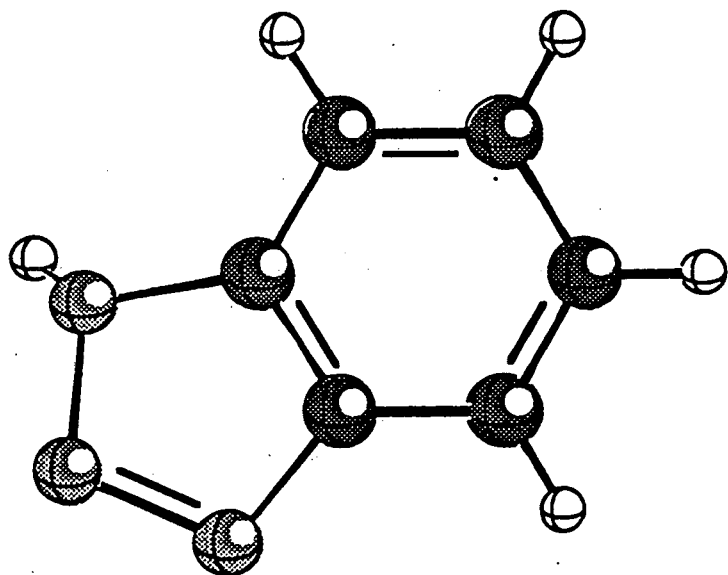
Benzotriazole, whose structure is shown in figure 1.4, is a strong inhibitor of electrochemical reactions of copper. It is used as a corrosion inhibitor and a brightening agent. At concentrations above 1 mM, BTA forms thin films composed of Cu-BTA on the surface of copper [1.30]. The corrosion inhibition at high BTA concentrations is due to the Cu-BTA barrier film and BTA adsorbed to the copper surface [1.31, 1.32]. The degree of inhibition by BTA decreases with acidity [1.32, 1.33], this may be the result of protonation of the BTA anion [1.32]. The ionization constants for benzotriazole have been determined for the following reactions [1.34].



In acidic solutions with the pH below 1.6 most of the BTA is in cationic form. Benzotriazole does not electrochemically react at the potentials used in this study (-400 to +250 mv relative to copper) [1.31]. It is thought that BTA forms a complex with cuprous and cupric ions in a copper sulfate solution [1.35]. The

Brighteners	
Class I	Class II
1,5 Naphthalene disulfonic acid	Butyndiol
<i>p</i> -Toluene sulfonamide	Butenediol
Saccharin	Coumarin
Benzene sulfonic acid	Ethylene cyanohydrin
Cyclohexyl sulfonic acid	Formaldehyde
2-Butyne-1,4-disulfonic acid	Fuchsin
	Pyridine
	Thiourea

Table 1.1. Examples of class I and II brighteners.



XBL 902-588

Figure 1.4. Benzotriazole molecule. (XBL 902-588)

solubility of the cuprous-BTA complex has been reported to be 35 mM in an aqueous solution of pH=5.5 [1.36] however cuprous-BTA inclusions have been reported in copper deposits formed in 200 μ M BTA [1.2]. The neutral benzotriazole molecule was thought to chemisorb to the copper surface [1.37] however recent experimental evidence suggest that the anion of BTA is adsorbed on the surface, even in the presence of cuprous-BTA overlayers [1.32].

Sheshadri proposed the mechanism for BTA inhibited copper deposition in which copper is deposited by the reduction of a cuprous-BTA film adsorbed on the copper surface [1.38]. Sheshadri proposed that BTA molecules released during reduction would immediately recombine with copper and adsorb to the surface. Sheshadri measured different Tafel slopes for BTA containing and BTA free solutions. He attributed this difference to reaction mechanisms in which cuprous ion was reduce from BTA free electrolyte and cuprous-BTA complex was reduced from BTA containing electrolyte. Sheshadri also measured exchange currents of copper in BTA containing electrolyte which were an order of magnitude less than in BTA free solution. The growth habit of copper deposits remained the same between BTA free and BTA containing electrolytes. The main difference Sheshadri found was a reduction of feature size in the BTA containing solution which was indicative of an increased nucleation rate. Others have also found BTA to refine the grain size of deposits [1.39].

Walker et al. [1.39- 1.42] have studied the effects of 1 mM Benzotriazole on Cu deposition at several temperatures and varying degrees of agitation. The focus of these studies was on the hardness and stress of the deposits. Adherence and

cracking of the deposit were dependent on the stress of the deposit. Deposits with high tensile stress tended to peel whereas deposits with compressive stress did not. In presence of Benzotriazole the deposit stress was tensile or compressive depending on temperature and current density. Compressive stress was favored by high temperature and low current density [1.41]. Walker indicated an aging effect for benzotriazole in which the stress of deposits depended on immersion time [1.31]. The aging effect was apparent immediately and continued over several days. Walker reported that the current efficiency was reduced by the addition of benzotriazole to the plating baths [1.40]. Cross sections of deposits showed a layered structure which was assumed to be the result of cuprous benzotriazolate inclusions [1.40, 1.42]. It was also found that the degree of layering increased with agitation [1.42]. Also Walker reported that surface smoothness increased and deposit grain size decreased with agitation [1.42]. The brightest deposit was obtained with 2 mM benzotriazole.

Prall and Shreir performed a survey of conditions in which copper was deposited in the presence of benzotriazole [1.2]. They recorded BTA content and the appearance of copper deposits at several concentrations of BTA, Cu^{2+} , and H^{+} and as a function of current density, temperature, and agitation.

In general they recorded increases in BTA content with:

- 1 increase in the concentration of BTA
- 2 increase in temperature
- 3 decrease in the concentration of copper sulfate
- 4 increase in pH to a maximum at pH 1.5 when further increase in pH reduces inclusion content
- 5 increase in agitation

The grain structure of the copper deposits changed from coarsely crystalline deposit to a semi-bright deposit at a BTA concentration of 0.024 g/l (200 μ M BTA) when deposited at 20 mA /cm² from an electrolyte of 0.5 M H₂SO₄ and 0.5 M CuSO₄. This structure change was accompanied by a sudden increase in BTA inclusion content and the formation of bands within the deposit high in Cu(I)-BTA. They suggest that this observation can be explained by a mechanism involving the formation of a cathodic film of Cu(I)-BTA which periodically precipitates. Very bright deposits were obtained with 0.192 g/l BTA (1.6 mM BTA) and 0.240 g/l BTA (2.0 mM BTA).

References

- [1.1] O. Kardos and D.G. Foulke, "Applications of Mass Transfer Theory: Electrodeposition on Small-Scale Profiles", in *Advances in Electrochemistry and Electrochemical Engineering*, Vol 2, C.W. Tobias Ed., Interscience, New York, 1962
- [1.2] J. K. Prall and L. L. Shreir, "A Study of Benzotriazole as an Addition Agent for Acid Copper Sulphate Solutions", *Trans. Inst. Metal Finishing*, 41, 29 (1964)
- [1.3] A. Kindler, *The Morphology of Electrodeposited Copper*, PhD Thesis, Univ. Calif., Berkeley, Lawrence Berkeley Laboratory LBL 12838 (1981)
- [1.4] J. Newman, *Electrochemical Systems*, Prentice Hall Inc., Englewood Cliffs, N.J. (1973)
- [1.5] E. Dutkiewicz and A. Puacz, "Electrode Process in the Presence of a Surface Active Substance with Accelerating-Inhibiting Properties", *J. Electroanal. Chem.*, 100 (1979) 947
- [1.6] S. F. Timashev, "Effect of the Adsorption of Surface-Active Materials on Electrochemical Reaction Kinetics", *Electrokhimiya*, 15 (1979) 333
- [1.7] J. A. Harrison and H. R. Thirsk, *The Fundamentals of Metal Deposition in Electroanalytical Chemistry* (edited by A. J. Bard) Vol. 5, pp. 67-147 Academic Press, New York (1971)

- [1.8] S. Fletcher and T. Lwin, "A General Probabilistic Model of Electrochemical Nucleation", *Electrochem Acta*, 28 (1983) 237
- [1.9] R. L. Deutscher and S. Fletcher, "Microelectrode Assemblies for Nucleation Studies" in **Electrochemistry Current and Potential Applications**, proceedings of the 7th Australian Electrochemistry Conference, Sydney, 15-19 February 1988
- [1.10] A. T. Vagramyan and N. K. Baraloshkina, "Investigation of Reflectivity and Structure of Electrodeposited Nickel during Electrolysis", *Plating*, 54 (1967) 930
- [1.11] H. Gerischer, "Mechanism of Electrolytic Deposition and Solution of Metals", *Z. Elektrochem*, 62, 256 (1958)
- [1.12] B. E. Conway and J. O. M. Bockris, "Calculation of Potential Energy Profile Diagrams For Processes in Electrolytic Metal Deposition", *Electrochimica Acta*, 3, 340 (1961)
- [1.13] S. A. Watson and J. Edwards, "Leveling in Electrodeposition", *Trans. Inst. Metal Finishing*, 34, 167 (1957)
- [1.14] G. T. Rogers, M. J. Ware, and R. V. Fellows, "The Incorporation of Sulfur in Electrodeposited Nickel, Using Thiourea as a Brightener and Leveler", *J. Electrochem. Soc.*, 107, 677
- [1.15] S. E. Beacom and B. J. Riley, "Leveling in Bright Ni Electroplating Baths", *J. Electrochem. Soc.*, 106 (1959) 309
- [1.16] C. C. Roth and H. Leidheiser, *J. Electrochem. Soc.*, 100 (1953)

- [1.17] D.G. Foulke and O. Kardos, "Current Distribution on Macroprofiles I", *Proc. Am. Electroplater's Soc.*, 43 (1956) 172
- [1.18] O. Kardos, discussion of reference [1.10], *Plating*, 55 (1968) 90
- [1.19] Yu. E. Gerenrot and D. L. Leichkis, "Adsorption-Diffusion Model of Brightening During Metal Electrocrystallization", *Elektrokhimiya*, 13 (1977) 941
- [1.20] R. R. Bair and A. K. Graham, *Copper Plating From Cyanide Baths in Modern Electroplating* (F. A. Lowenheim Ed.), 3rd ed., pp 165-182, John Wiley & Sons, New York, 1974
- [1.21] U. Bertocci and D.R. Turner, *Copper in Encyclopedia of Electrochemistry of the Elements* (A. J. Bard editor), Vol. 2, p 384, Marcel Dekker Inc., New York (1974)
- [1.22] E. Mattisson and J. O'M. Bockris, "Galvanostatic Studies of the Kinetics of Deposition and Solution in the Cu+Cu Sulfate System", *Trans. Faraday Soc.*, 55 (1959) 1586
- [1.23] W. H. Safranek, *Acid Copper Electroplating and Electroforming in Modern Electroplating* (F. A. Lowenheim Ed.), 3rd ed., pp 183-203, John Wiley & Sons, New York, 1974
- [1.24] R.V. Bucur and P. Marginean, "Interaction Between Thiourea and Palladium Electrodes", *Electrochimica Acta*, 29 (1984) 1297
- [1.25] S.C. Barnes, "The Effect of Thiocompounds on the Structure of Copper Electrodeposits", *J. Electrochem. Soc.*, 111, (1964) 296
- [1.26] L.L. Shreir and J. W. Smith, "Effects of Addition Agents on the

Cathode Polarization Potential During the Electrodeposition of Copper",
Trans. Faraday Soc., 50 (1954) 393

[1.27] B. Ke, J.J. Hoekstra, B.C. Sison, Jr., and D. Trivich, "Role of Thiourea in the Electrodeposition of Copper", *J. Electrochem. Soc.*, 106 (1959) 382

[1.28] E.M. Hofer and H.E. Hintermann, "Defects in the Structure of Electrodeposited Copper", *J. Electrochem. Soc.*, 112 (1965) 167

[1.29] H. Brown and B. B. Knapp, "Nickel" in *Modern Electroplating* (F. A. Lowenheim Ed.), 3rd ed., John Wiley & Sons, New York, 1974

[1.30] S. L. F. A. DaCosta, J. C. Rubim, and S. M. L. Agostinho, "Spectroelectrochemical Study of the Corrosion of a Copper Electrode in Deaerated 1.0 M HCl Solutions Containing Fe(III) Effect of the Corrosion Inhibitor Benzotriazole", *J. Electroanal. Chem.* 220 (1987) 259

[1.31] N.D. Hobbins and R.F. Roberts, "An Ellipsometric Study of Thin Films Formed on Copper by Aqueous Benzotriazole and Benzimidazole", *Surf. Tech.*, 9 (1979) 235

[1.32] M.M. Musiani, G. Mengoli, M. Fleischmann, and R.B. Lowry, "An Electrochemical and SERS Investigation of the Influence of pH on the Effectiveness of Some Corrosion inhibitors of Copper", *J. Electroanal. Chem.*, 217 (1987) 187

[1.32] Yu.M. Loshkarev, V.A. Omel'chenko, V.F. Vargalyuk, V.V. Trofimenko, L.P. Snetkova, and A.A. Rysakov, "Effect of Trace Amounts

of Organic Complexing Agents on the Electroreduction of Metals I.

Cathodic Deposition of Copper in the Presence of Benzotriazole",

Elektrokhimiya, 10 (1974) 723

[1.33] L.I. Mal'kova, Yu.M. Loshkarev, M.A. Loshkarev, V.A.

Omel'chenko, A.A. Rysakov, and V.S. Ivanko, "Electrolytic Copper Plating

of Steel From Sulfuric Acid Solutions with Organic Additives",

Elektrokhimiya, 13 (1977) 1483

[1.34] A. Albert, R. Goldacre, and J. Phillips, "The Strength of

Heterocyclic Bases", *J. Amer. Chem. Soc.*, 70 (1948) 2240

[1.35] J.K. Prall and L.L. Shreir, "Effect of Codeposited Material on the

Corrosion Behavior of Electrodeposits", *Corros. Sci.*, 1 (1961) 181

[1.36] P. G. Fox, G. Lewis, and P. J. Boden, "Chemical Aspects of the

Corrosion Inhibition of Copper by Benzotriazole", *Corros. Sci.*, 19 (1979)

457

[1.37] S.M. Mayanna and T.H.V. Setty, "Effect of Benzotriazole on the

Dissolution of Copper Single Crystal Planes in Dilute Sulfuric Acid",

Corros. Sci., 15 (1975) 627

[1.38] B.S. Sheshadri, "Effect of Thioglycolic Acid and Benzotriazole on

the Cathodic Polarization of Copper on Copper Single Crystal Planes",

Electroanal. Chem., 61 (1975) 353

[1.39] R. Walker, "Stress in Copper Electrodeposit Made With

Benzotriazole as Addition Agent", *Electrochimica Acta*, 13 (1968) 1861

[1.40] R. Walker and A. Ward, "Stress in Copper Electrodeposits From

the Sulfate Bath", *Electrochimica Acta*, 15 (1970) 673

[1.41] R. Walker, "Effect of Benzotriazole on the Stress in Copper Electrodeposits", *Plating*, 57 (1970) 610

[1.42] R. Walker and R. C. Benn, "Effect of Benzotriazole on the Hardness of Copper Electrodeposits", *Electrochimica Acta*, 16 (1971) 1081

Chapter 2. Procedures

2.1. Electrochemical Analysis

2.1.1. Galvanostatic Double-Pulse

A galvanostatic double-pulse method was used to measure the current-voltage behavior of copper plating electrolytes in the presence of BTA. The overpotential for Cu deposition was measured for 0, 100 and 200 μM BTA in 0.5 M CuSO_4 and 0.5 M H_2SO_4 . The first pulse, 100 mA/cm^2 by 2 s, serves to form a thin copper deposit, 740 Å thick assuming a compact film, on a Pt substrate. The potential is measured during the second pulse at a current less than 100 mA/cm^2 . The magnitude of the second pulse was varied whereas the magnitude and duration of the first pulse remained constant. The first pulse was kept constant to minimize the difference in active surface area between potential measurements. The potential of the electrode was measured within a few seconds following the step to the final current density. A polycrystalline Pt disk, 8 mm dia., embedded in epoxy and polished with a final polish of 0.05 μm alumina was used for the deposit substrate. A Pt counter electrode and a Cu (99.999% Cu) wire reference electrode were used

in the electrochemical cell. The Pt substrate was dipped in a 20% HNO_3 and 10 % H_2O_2 solution prior to each measurement. The rotating disk setup described in the voltammetry apparatus section was used during all measurements. The rotation speed was set at 700 rpm resulting in a 18 μm mass transfer boundary layer thickness, δ , as determined by the Levich equation

$$\delta = 1.6\omega^{-1/2}v^{1/6}D^{1/3} \quad (2.1)$$

where ω is the rotation rate, v is the viscosity, and D is the diffusivity.

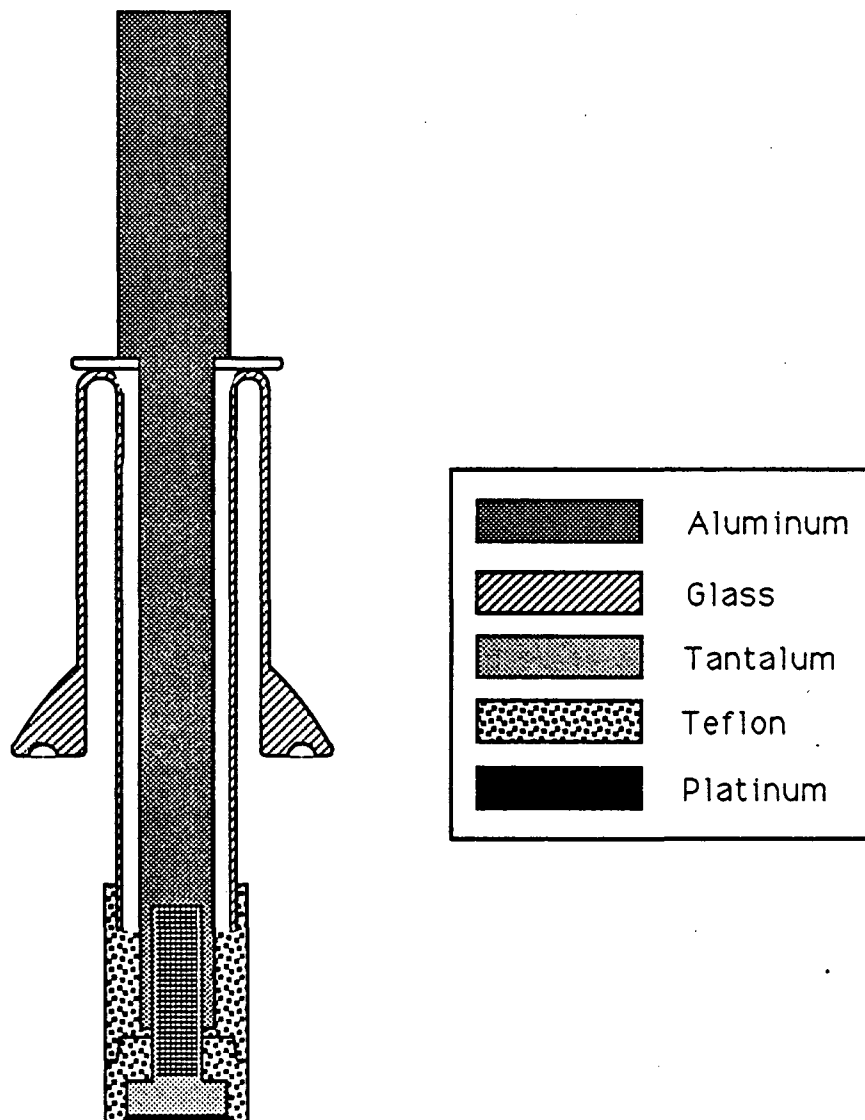
2.1.2. Cyclic Voltammetry

In cyclic voltammetry the electrode potential is cycled between two potentials with a linear sweep [2.1]. The current response to cyclic voltammetry is useful for identification of steps of an electrochemical reaction and identification of species in solution. Cyclic voltammetry was used in this study to determine the effects of BTA on the deposition of the first monolayer of Cu on Pt. The first layer of Cu deposited on Pt is referred to as the underpotential deposit because the layer forms at potentials anodic of bulk Cu. Cyclic voltammetry was performed with a PAR 273 programmable potentiostat with current-voltage data recorded on a HP 7044A X-Y recorder. The underpotential deposits of copper were formed in nitrogen purged electrolyte within a glass and Teflon cell (fig. 2.1 and 2.2).

The nitrogen bubbler provided the only agitation of the electrolyte. The cell had tapered joints to insert the reference and counter electrodes, a gas sparger, and a gas vent. The sample was held in a Teflon holder inserted through a port to the



Figure 2.1. Electrochemical cell used for cyclic voltammetry. Ports for reference electrode, counter electrode, N_2 sparger, and vent are located on top of the cell. Quartz windows, used for ellipsometry of the working electrode, are compression sealed with Teflon gaskets to ports located on the side. The working electrode is mounted in a Teflon holder and inserted through the large port. The working electrode holder is sealed with a Viton gasket. (CBB 893-2069)



XBL 902-574

Figure 2.2. Cross section of working electrode holder for electrochemical cell in figure 2.1. The electrode is held in a Teflon mount which is sealed by compression to the Teflon portion of the holder. The Teflon portion of the holder is attached to the glass tube with shrink Teflon tubing which has a WTF Teflon melt-liner.
(XBL 902-574)

cell. The sample holder was sealed against electrolyte leaks by compression against Teflon and Viton gaskets. The underpotential deposition (UPD) of Cu onto Pt was measured as a current during cyclic linear sweep voltammetry. For UPD of Cu on Pt the substrate potential was cycled between 800 and -30 mV relative to Cu at a sweep rate of 20 mV/s. The Pt substrate was prepared with a final polish with 0.05 μm alumina. The Pt electrode was cleaned in nitric acid prior to each change in BTA concentration. Two copper wires (99.999% Cu) were used for both the reference and counter electrodes. The reference and counter electrodes were inserted directly in the cell. The supporting electrolyte in each case was 0.5 N NaClO_4 acidified to pH 2 with HClO_4 . For UPD of Cu on Pt 10 mM Cu^{2+} was added by addition of $\text{Cu}(\text{OH})_2$ to the supporting electrolyte.

2.1.3. Impedance

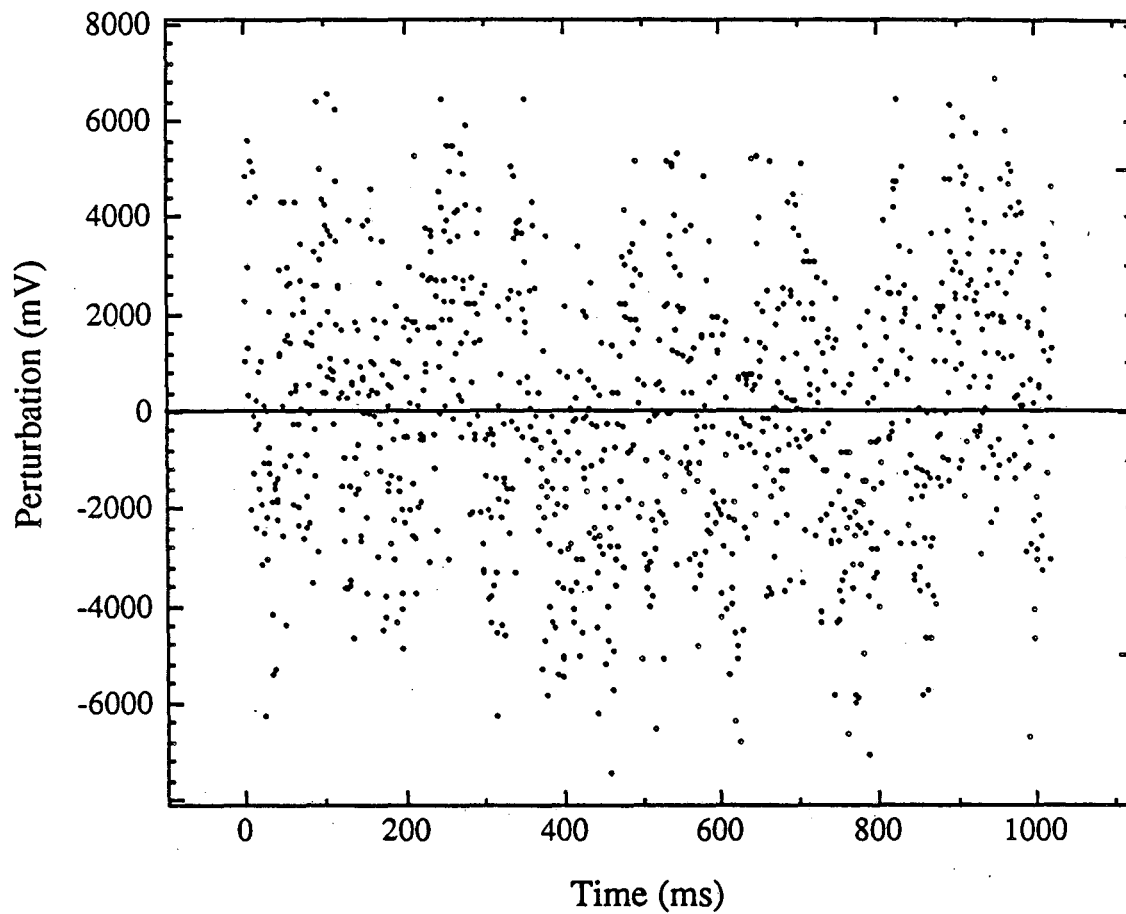
For impedance measurements sinusoidal current or potential perturbations are applied to the electrochemical interface. Reaction kinetics and interface structure can be determined from the frequency dependence of the complex impedance, $Z_{cell}(\omega)$. Impedance measurements were used in this research to monitor the formation and breakdown of resistive films during copper deposition.

Impedance was determined using a fast Fourier transform of the current response to an applied potential program containing 20 frequencies between 1 and 512 Hz, appendix A. Each frequency component begins with a different phase with respect to the other frequency components at the beginning of the potential

program. The potential program was digitally represented by 1024 chronological steps (fig. 2.3). A PAR 273 potentiostat was programmed with the potential program. The impedance measurement was the result of averaging 96 sweeps (1 sec/sweep) of the program. Both the potential and current were measured such that the error due to frequency response of the potentiostat controller would be eliminated. The program was superimposed on the bias voltage such that impedance data could be obtained at several applied voltages. The amplitude of the program was adjusted such that the potential was kept within 10 mV of the set bias voltage. The resolution of the digitally applied program was 3 μ V. The recorded current and potential response was then used as input to a FFT program, IMP_FFT (appendix A), which gave an output in terms of real, Z_r , and imaginary, Z_i , components of impedance as a function of frequency.

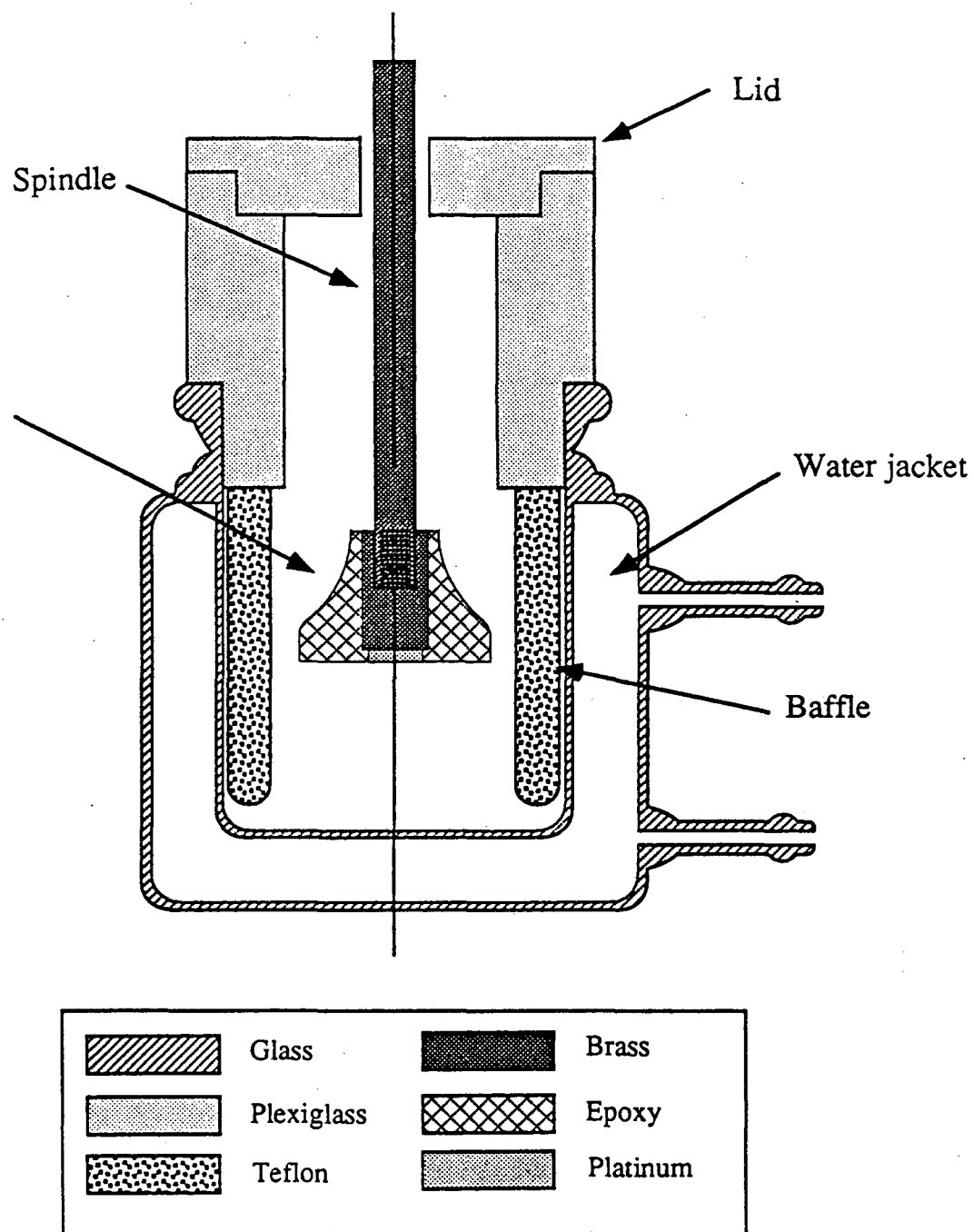
A rotating disk electrode in a glass cell with a plexiglass cover was used for impedance measurements (fig. 2.4). The cover had openings to allow insertion of the rotating disk, gas sparger, and counter and reference electrodes.

The complex impedance and its frequency dependence was measured during copper deposition in electrolyte of 0.5 M CuSO_4 , 0.5 M H_2SO_4 , and 100 or 200 μ M BTA. The substrate was formed by plating Cu onto a 8 mm dia. Pt disk polished with 0.05 μ m alumina. The Pt substrate was rotated at 500 rpm giving an effective boundary layer of 21 μ m. Nitrogen gas was bubbled through the electrolyte during all measurements. Copper wire (99.999% Cu) was used as the reference electrode and Pt sheet was used as the counter electrode. Use of the Pt avoids the breakdown of BTA which occurs on Cu anodes [2.2].



XBL 902-593

Figure 2.3. Potential program applied during impedance measurements. The end points for each step are plotted. (XBL 902-593)



XBL 902-573

Figure 2.4. Electrochemical cell used for impedance measurements.
(XBL 902-573)

2.2. Elemental Analysis of Deposits

BTA contains 3 N atoms per molecule. The N content of a deposit has been used to identify the presence of BTA in Cu. The nitrogen content of copper films deposited from electrolytes containing BTA was determined with X-ray photoelectron spectroscopy, XPS, and secondary ion mass spectroscopy, SIMS. The results of these measurements were used to gain understanding of the incorporation and placement of BTA within copper deposits.

2.2.1. X-ray Photoelectron Spectroscopy

The identification of elements and their chemical states by measurement of the energy of ejected electrons is referred to as "X-ray photoelectron spectroscopy" (XPS). An X-ray light source of well defined energy is used to stimulate the ejection of core-level electrons. These electrons have unique energies characteristic of the elemental composition of the surface. Detectable shifts in the core-level energies caused by changes in the valence are used to determine the chemical state of the elements. In this research XPS was used to measure the nitrogen content of electrodeposits.

X-ray photoelectron spectroscopy was performed with a PHI 8600. This XPS apparatus uses a Mg or Al X-ray source and a spherical electron analyzer. For depth profiling a 5 keV Ar ion source was rastered across the sample surface.

A polycrystalline Au substrate was used for the deposit substrate. The

substrate was prepared by vapor deposition of Au on highly doped Si wafers. A layer of Au with 18 At-% Si was first applied to promote adhesion of Au to the Si surface. This procedure produced optically smooth surfaces with rms roughness on the order of 200 Å as measured with scanning tunneling microscopy. The Au covered Si wafer was attached with silver paint to a rotating disk electrode with edges of the wafer masked with a resist polymer.

2.2.2. Secondary Ion Mass Spectrometry

Secondary ion mass spectroscopy was used to determine depth profiles of the N content of copper deposits formed under modulated mass transport conditions. The measurement of the flux of secondary ionized particles ejected from a surface during ion bombardment is named secondary ion mass spectroscopy (SIMS). SIMS has a very high sensitivity, greater than 1 part in 10^6 , for detection of secondary ions. A PHI 5600 secondary ion mass spectrometer was used in this investigation.

Cu deposits were formed from electrolyte containing 0.5 M CuSO_4 and 0.5 M H_2SO_4 electrolyte containing 0 and 100 μM BTA. The deposits were deposited in the rotating disk apparatus described in the impedance equipment section. The mass transfer boundary layer was modulated by periodically stepping the rotation rate between 200 and 1800 rpm. A polycrystalline Au substrate was used for the deposit substrate. The substrate was prepared by sputter deposition of 400 Å of Au on polished stainless steel. The stainless steel substrate was polished with 0.25 μm diamond paste. The steel substrate was machined to fit the sample holder of SIMS

analysis equipment, figure 2.5.

2.3. Scanning Tunneling Microscopy

Previously optical methods had been used for topographical characterization of surfaces undergoing electrochemical modification. These methods include ellipsometry, light scattering, and optical microscopy. The optical methods are not invasive, that is they do not alter the surface or surrounding electrolyte. Ellipsometry provides a method for measuring the optical properties of a surface. Film thickness, coverage, and refractive index for one or multiple films can be derived from the measured optical properties. Light scattering provides a measure of roughness and its characteristic length. Optical microscopy provides a visual record of the surface. Optical microscopy is good for measuring the size of features larger than several micrometers. With the development of scanning tunneling microscopy (STM) in ionic environments, a new method is available to directly measure deposit growth [2.3]. STM was applied in this investigation to obtain a qualitative description of the surface and a quantitative measure of the density of nuclei of Cu deposited on Pt as they are affected by the presence of BTA.

Tunneling of electrons between two materials of different potential occurs at very small separations on the order of 1 nm. Scanning tunneling microscopy uses this phenomenon in the following way [2.4]. The tip is rastered laterally across the surface while the tip height is measured. If the tip position is controlled in order to maintain a constant current the gap between the tip and surface remains virtually

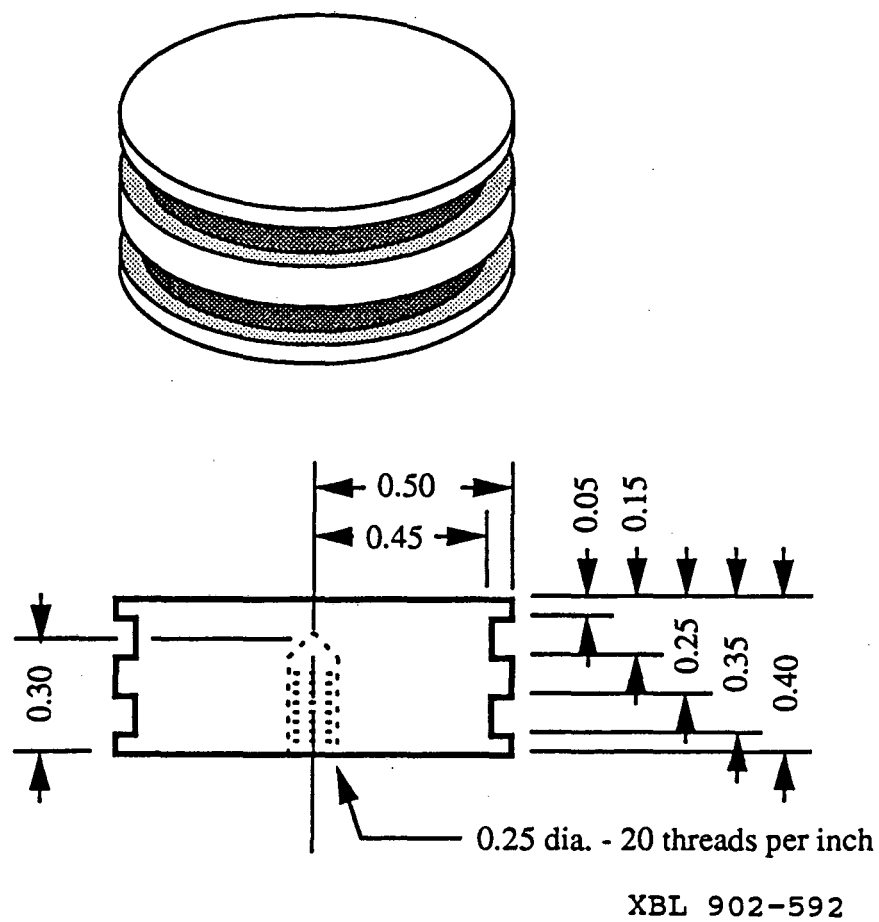
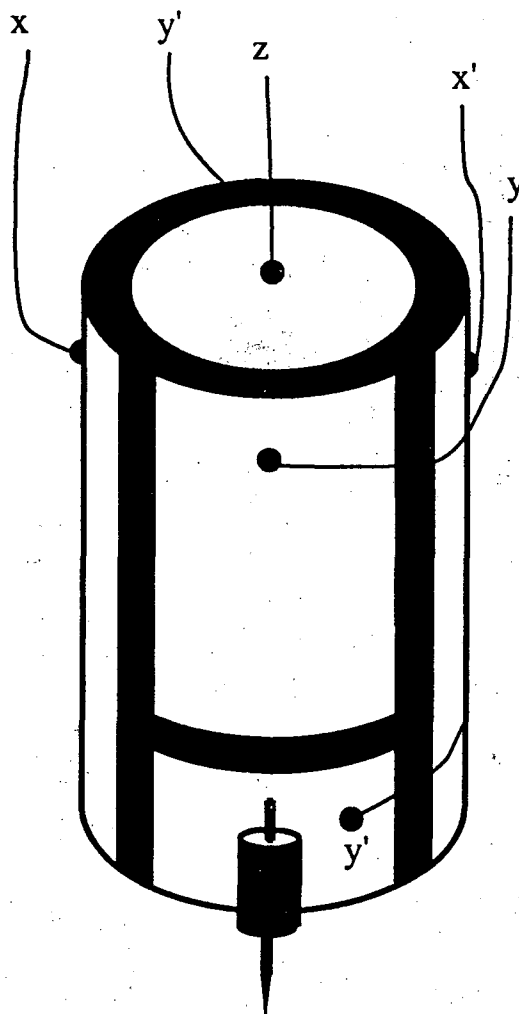


Figure 2.5. Isometric and side view of steel substrate used for secondary ion mass spectroscopy of copper films. Units in inches. (XBL 902-592)

constant. The tunneling current is very sensitive to the tip position since tunneling current varies exponentially with the gap. Sub-angstrom resolution of height and lateral positions is made possible by the use of piezoelectric positioners. A commercially available STM, Nanoscope I [2.5], was used in this investigation (fig. 2.6). The STM uses a single-tube piezoelectric positioner for x, y, and z translation. The single-tube piezoelectric STM was developed by Binnig and Smith in 1986 [2.6]. The advantage of this design over the tripod configuration [2.7] includes simplicity (fewer parts), a higher mechanical resonance frequency, and stability. The mechanical resonance frequency restricts the scan frequency thus the cylindrical piezoelectric STM can scan faster than a tripod piezoelectric STM. Piezoelectric materials expand or contract perpendicular to an applied electric field. Six electrodes on the Digital Instruments single tube piezoelectric are used to obtain the x, y, and z translations (fig. 2.7). The outside of the tube has five electrodes and the inside of the tube has one. The z translation is obtained by applying a potential to the single inside electrode of the tube. The x-y motion is obtained by controlling the voltage on orthogonally placed electrodes on the outside of the tube. The expansion or contraction of the piezoelectric tube in the axial direction by the x-y electrodes results in bending of tube and results in the x-y translation. Each pair of the x and y electrodes is held at opposite polarity to enhance the x and y movement. To compensate for coupling of the y and z motion there is a third y electrode on the tip side of the piezoelectric tube which is held at the potential of the y' electrode (Fig. 2.7). Two scanners are available for the Nanoscope I with lateral ranges of $0.6\mu\text{m}$ and $9\mu\text{m}$. The $9\mu\text{m}$ scanner had a $3\mu\text{m}$ vertical range, z,



Figure 2.6. Scanning tunneling microscope configured for *in-situ* probing of electrochemical deposits. Components from left to right include the display, keyboard, oscilloscope, computer, STM power supply, vibration isolation table, and scanner with electrochemical cell and tunneling probe. (CBB 880-10611)



XBL 902-594

Figure 2.7. Digital Instruments single tube piezoelectric positioner. The y' electrode completely covers the back of the tube and partially covers the front. The z electrode completely covers the inner surface of the tube. x translation is achieved by polarizing the x and x' electrodes at opposite polarity. y translation is achieved by polarizing the y and y' electrodes at opposite polarity. z translation is achieved by polarizing the z electrode. All potentials are with respect to STM power supply ground. (XBL 902-594)

and the $0.6\mu\text{m}$ scanner had a $0.6\mu\text{m}$ vertical range.

A PC based data acquisition system was used to record a 200×320 point map of the z position. Software was developed to perform x - y control, data collection, data manipulation, and data display functions (appendix B). A triangular wave form sweep of the x position was digitally simulated. The y position was updated following each cycle of the x sweep. The z position was collected with a constant x sweep direction starting $1/2$ x sweep cycle following an update of the y position. The fastest rate obtainable by the A/D-D/A data acquisition board for updating the x position and recording the z position is 4 kHz which corresponds to 0.1 s per raster line (200 pts/line) or 32 s per complete scan (320 lines/scan). Generally the rastering speed is limited by the ability of the z position controller to follow the surface.

A Pt $\langle 110 \rangle$ single crystal with a 9 by 12 mm surface was used for the working electrode and Cu was used for the reference electrode. A 0.05 ml well for electrolyte on the working electrode was made by welding polypropylene tubing onto the surface at approximately 160 C (fig. 2.8). This well of 3 mm height and 6 mm in diameter was connected to the reference and counter electrodes by $1/16$ Teflon tubing. Electrical connection to the Pt electrode was made with conducting paint.

Electrical connections to the electrochemical cell are shown in figure 2.9. An alternative cell configuration, also used for deposition studies, was constructed of a 6 mm diameter ring of 20 mil Pt wire in which the electrolyte was held on the surface by surface tension. The Pt ring was also the counter electrode. A reference

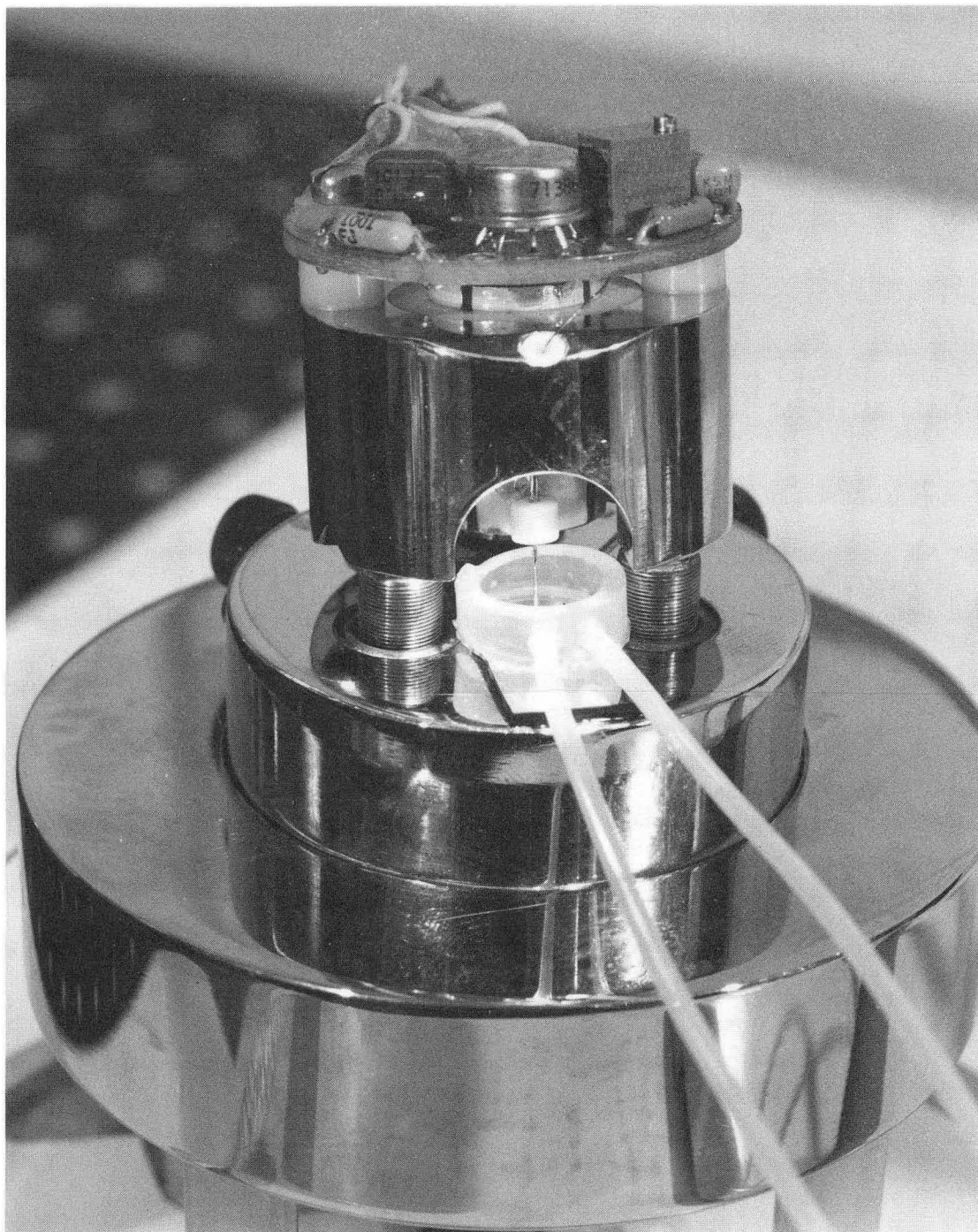


Figure 2.8. STM scanner, $0.6\mu\text{m}$ x-y-z range, and electrochemical cell used for *in-situ* STM. The electrochemical cell is 6 mm in diameter. The counter and reference electrodes are connected to the cell by separate Teflon tubes (entering the picture from the lower right corner) filled with electrolyte. (CBB 880-10609)

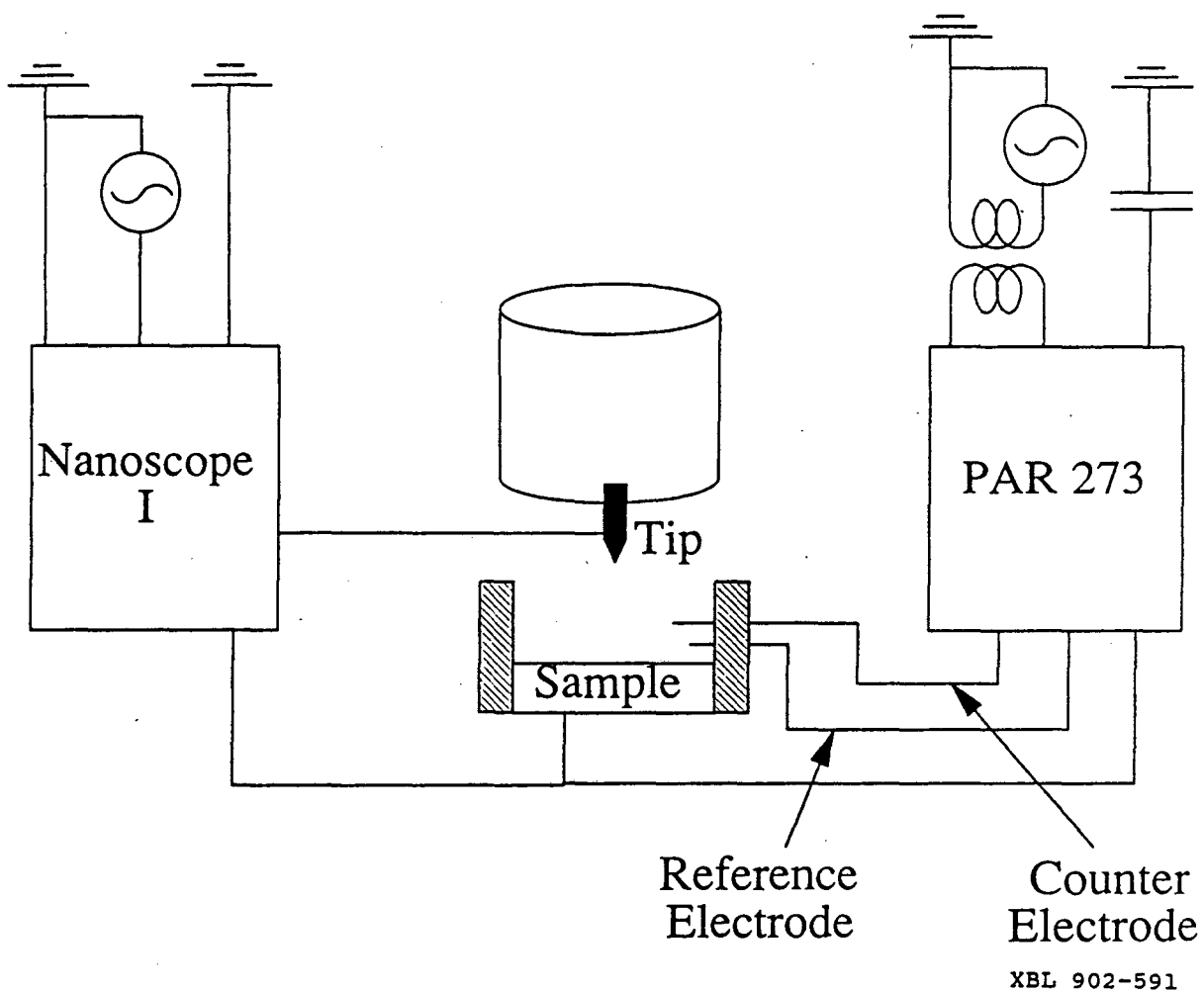


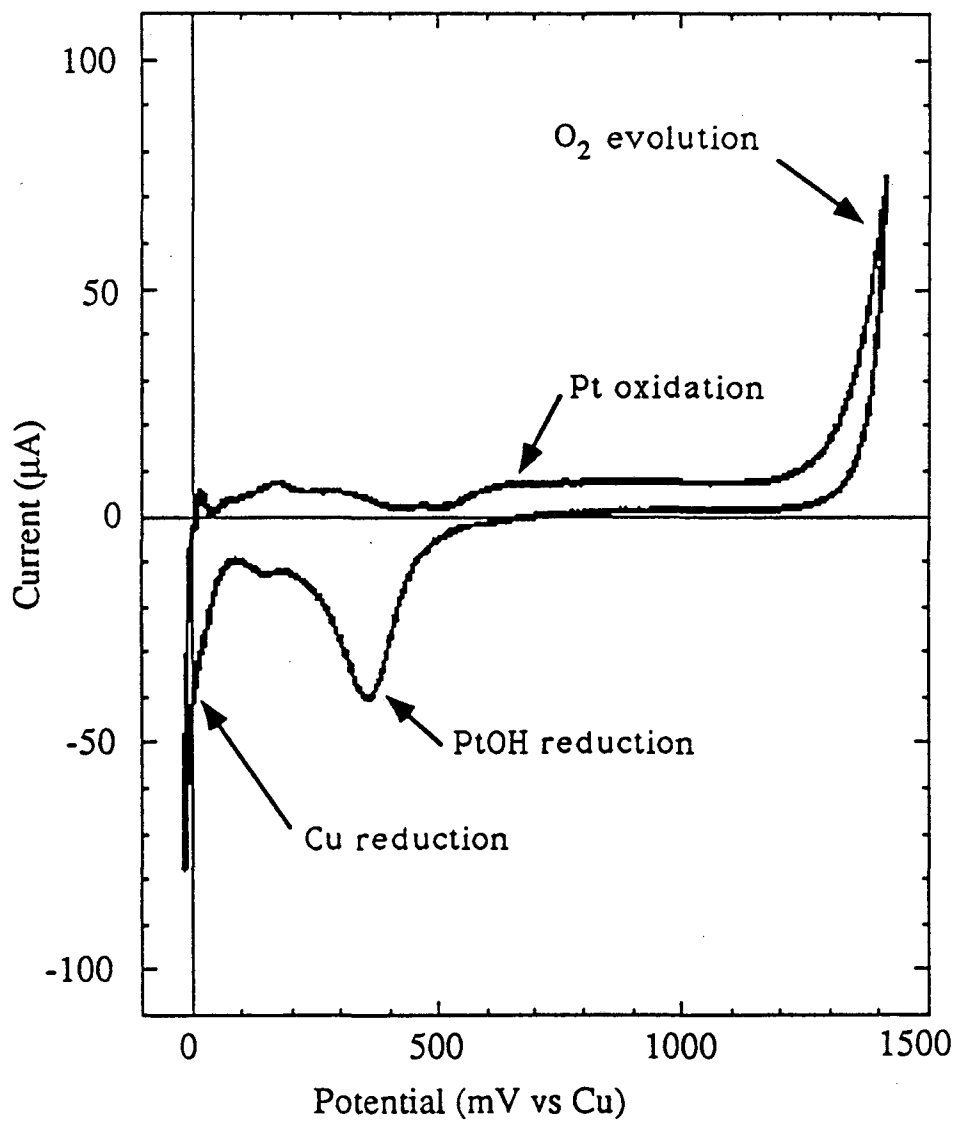
Figure 2.9. Electrical connections to the electrochemical cell used for *in-situ* STM. The PAR 273 is isolated from the building ground by a transformer in parallel with a 100 μF capacitor. (XBL 902-591)

electrode made from Cu wire was inserted directly in the Pt ring cell. The Pt substrate potential and current was controlled with a PAR 273 potentiostat. The potentiostat was isolated from ground with an isolation transformer. An AC ground of the PAR 273 was provided with a 100 μ F capacitor inserted between the Nanoscope I chassis and the PAR 273 ground. This provided a high frequency shunt to reduce noise in the system. With the DC ground isolation, no low frequency current can pass from the PAR 273 to ground.

The Pt<110> substrate was mechanically polished with 0.05 μ m alumina, etched in warm *aqua regia*, and flame annealed. STM was performed in the constant current mode. The tunneling current was set to 1 to 2 nA above the background current. Typical background currents were 0.2 to 2 nA with a dependence on the probe potential. During STM it is important to hold the tip potential such that faradaic processes are minimized. In our system the tip potential was bounded by copper deposition (0 mV vs Cu) and O₂ evolution (1200 mV vs Cu) (fig. 2.10). The tip potential was held at 30 mV vs the substrate.

2.3.1. Topography of Copper Deposits

The development of the topography was followed with STM. Sequential images of growing deposits were recorded. The composition of the electrolyte was 10 mM Cu (ClO₄)₂, 0.5 M NaClO₄, and 0.1 M HClO₄ with and without 10 μ M BTA. The reference and counter electrodes were made from 10 mil 99.999% copper wire.



XBL 902-595

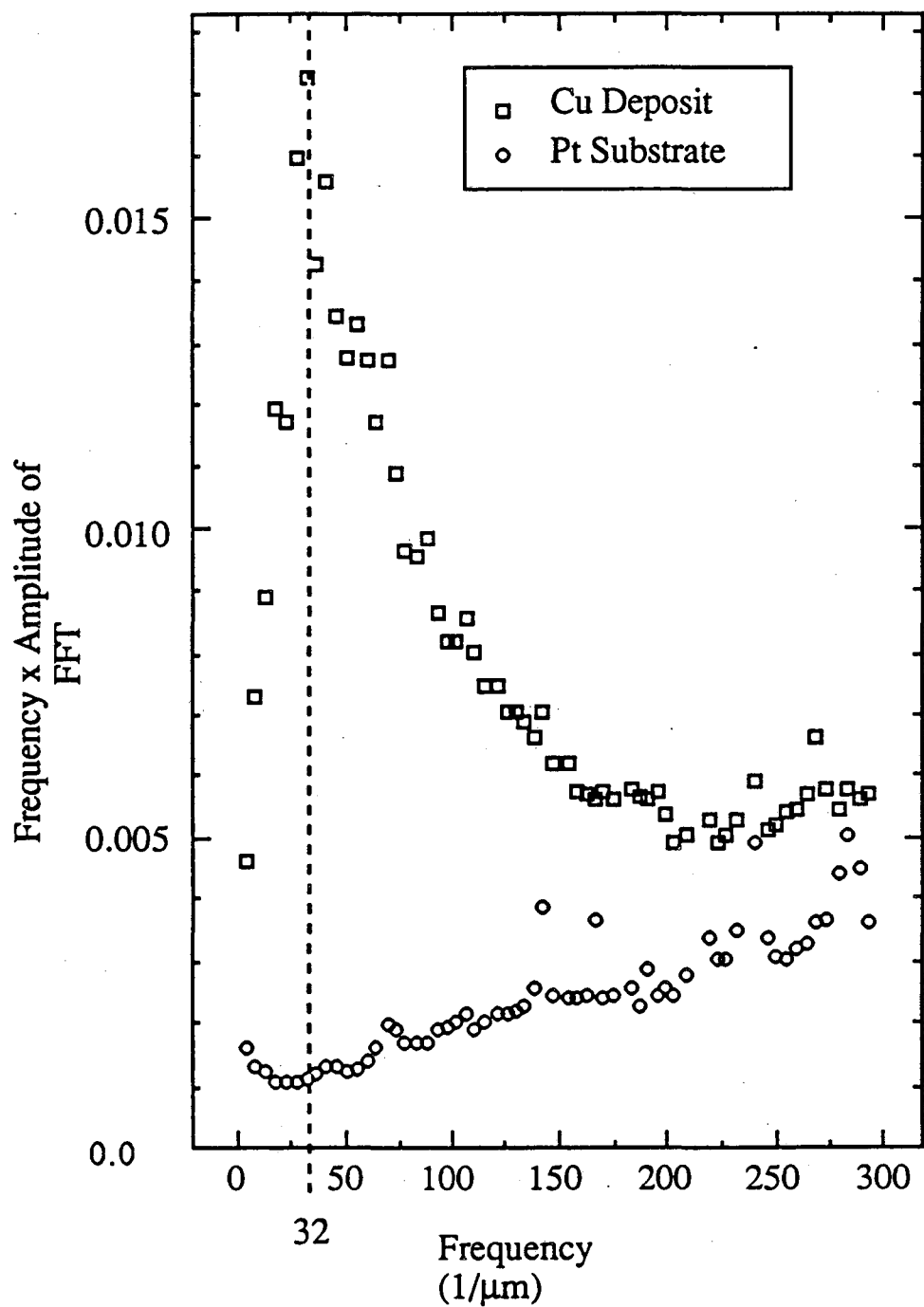
Figure 2.10. Cyclic voltammetry of Pt in 0.5 M CuSO₄ and 0.5 M H₂SO₄.
(XBL 902-595)

2.3.2. Nuclei Density

The nuclei density of Cu on Pt was measured following galvanostatic deposition of 15 mC/cm^2 (54 Å compact film) of Cu. The composition of the electrolyte was 0.5 M CuSO_4 and 0.5 M H_2SO_4 with 50, 100, or 200 μM BTA. Prior to each deposition the substrate was cleaned by passing an anodic current of 1.6 A/cm^2 for approximately 4 s followed by a change in electrolyte. Following the pulse the substrate was held galvanostatically at a current corresponding to the oxygen reduction current to prevent deposit dissolution. The oxygen reduction current was measured on the Pt substrate at 2 mV vs. Cu prior to Cu deposition. STM was performed in the constant current mode. The tunneling probe was withdrawn from solution during the cathodic pulse to prevent shielding of the substrate by the tip. A profile of the nucleated deposit and of the substrate were taken. The deposit was removed by electrochemical dissolution in order to determine the profile of the substrate.

The nuclei density was estimated from a one dimensional fast Fourier transform (FFT) of the z height with respect to the scan direction. The amplitudes from the FFT of the data were averaged over the 320 raster lines of the STM scan. It was assumed that the ratio of height to width of nuclei was constant and independent of the size of the nuclei. If the nuclei on the surface are touching and not overlapping, the characteristic frequency, f_c , of the nuclei is equal to the inverse of the nuclei width such that the product of the amplitude and frequency is constant irrespective of nuclei density. The characteristic frequency of nuclei was experimentally determined as the frequency at the peak value of the product of

amplitude and frequency from a FFT of the surface (fig. 11). The nuclei density, Γ_n , was estimated as $(f_s)^2$.



XBL 902-572

Figure 2.11. FFT of the probe height with respect to distance in the scan direction of (a) Cu deposit and (b) the underlying Pt substrate. The Cu deposit was formed with a 100 mA/cm^2 pulse for 200 ms from 0.5 M CuSO_4 , $0.5 \text{ M H}_2\text{SO}_4$, and $100 \text{ } \mu\text{M BTA}$. (XBL 902-572)

References

- [2.1] A. J. Bard and L. R. Faulkner, "Electrochemical Methods", John Wiley & Sons, USA, 1980, pp. 213-243
- [2.2] J. K. Prall and L. L. Shreir, "A Study of Benzotriazole as an Addition Agent for Acid Copper Sulphate Solutions", *Transactions of the Institute of Metal Finishing*, 41 (1964) 29
- [2.3] B. Drake, R. Sonnenfeld, J. Schneir, and P. K. Hansma, "Scanning Tunneling Microscopy of Processes at Liquid-Solid Interfaces", *Surf. Sci.*, 181 (1987) 92
- [2.4] P. K. Hansma and J. Tersoff, "Scanning Tunneling Microscopy", *J. Appl. Phys.*, 61 (1987) R1
- [2.5] Nanoscope I, Digital Instruments Inc., Santa Barbara, California, USA
- [2.6] G. Binnig and D.P.E. Smith, "Single-Tube Three-Dimensional Scanner for Scanning Tunneling Microscopy", *Rev. Sci. Instrum.*, 57 (1986) 1688
- [2.7] G. Binnig, H. Rohrer, Ch. Gerber, and E. Weibel, "Surface Studies by Scanning Tunneling Microscopy", *Phys. Rev. Lett.*, 49 (1982) 57

Chapter 3. Results

3.1. Survey of Addition Agents

Six addition agents were screened for brightening of Cu deposits during electrodeposition. A qualitative measure of appearance was made according to figure 1.1. In addition, overpotential during deposition was measured with each addition agent. Rhodamine-B chloride [3.1] and benzotriazole [3.2], have been shown to be brighteners for lead and copper respectively. Several of the compounds were chosen because they absorb light at visible wavelengths. At the time of this survey, the formation of inhibitor films on copper deposits was to be studied with spectroscopic ellipsometry. The object of this survey was to determine which additives result in the brightest deposit with the lowest overpotential. A summary of the results of this survey are in table 3.1.

The electrolyte used during deposition was composed of 0.13 M Cu (ClO₄)₂ and 0.1 M HClO₄. The deposits were formed galvanostatically at 4 mA /cm² onto polycrystalline Pt sheet in a stagnant solution. A total charge of 2.4 C /cm² (720 nm compact Cu deposit assuming 100 % current efficiency) was passed for each deposit.

Addition Agent	Concentration (μM)	Visual Appearance	Overpotential at 4 mA/cm^2 (mV)
Methyl red	26	matte	-130
Fluorescein	27	milky	-370
Rhodamine-B chloride	76	milky	-210
Benzotriazole	10	bright	-400
Poly vinyl alcohol		bright	-870
Coumarin 343	10	matte	-210

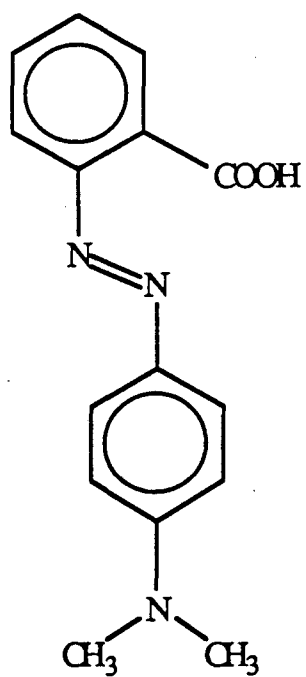
Table 3.1. Summary of addition agent effectiveness for brightening copper. 2.4 C/cm^2 copper deposit, 4 mA/cm^2 , $0.13 \text{ M Cu}(\text{ClO}_4)_2$, 0.1 M HClO_4 .

3.1.1. Methyl Red

Methyl red is an acid-base indicator dye that has a color transition in the pH range of 4.8 to 6.0. Its structure is shown in figure 3.1. Methyl red was chosen as an inhibitor candidate because it is electrochemically active and absorbs light in the visible spectrum. The compound is electrochemically reduced at potentials below 100 mV vs Cu (fig. 3.2). The study of the deposition of metal in the presence of a concentration gradient of inhibitor would be possible with methyl red. Methyl red failed to induce bright Cu deposition under the conditions of this test. An overpotential of 0.13 V was necessary to plate copper from electrolyte containing 1.4 mM methyl red. The deposit texture was matte.

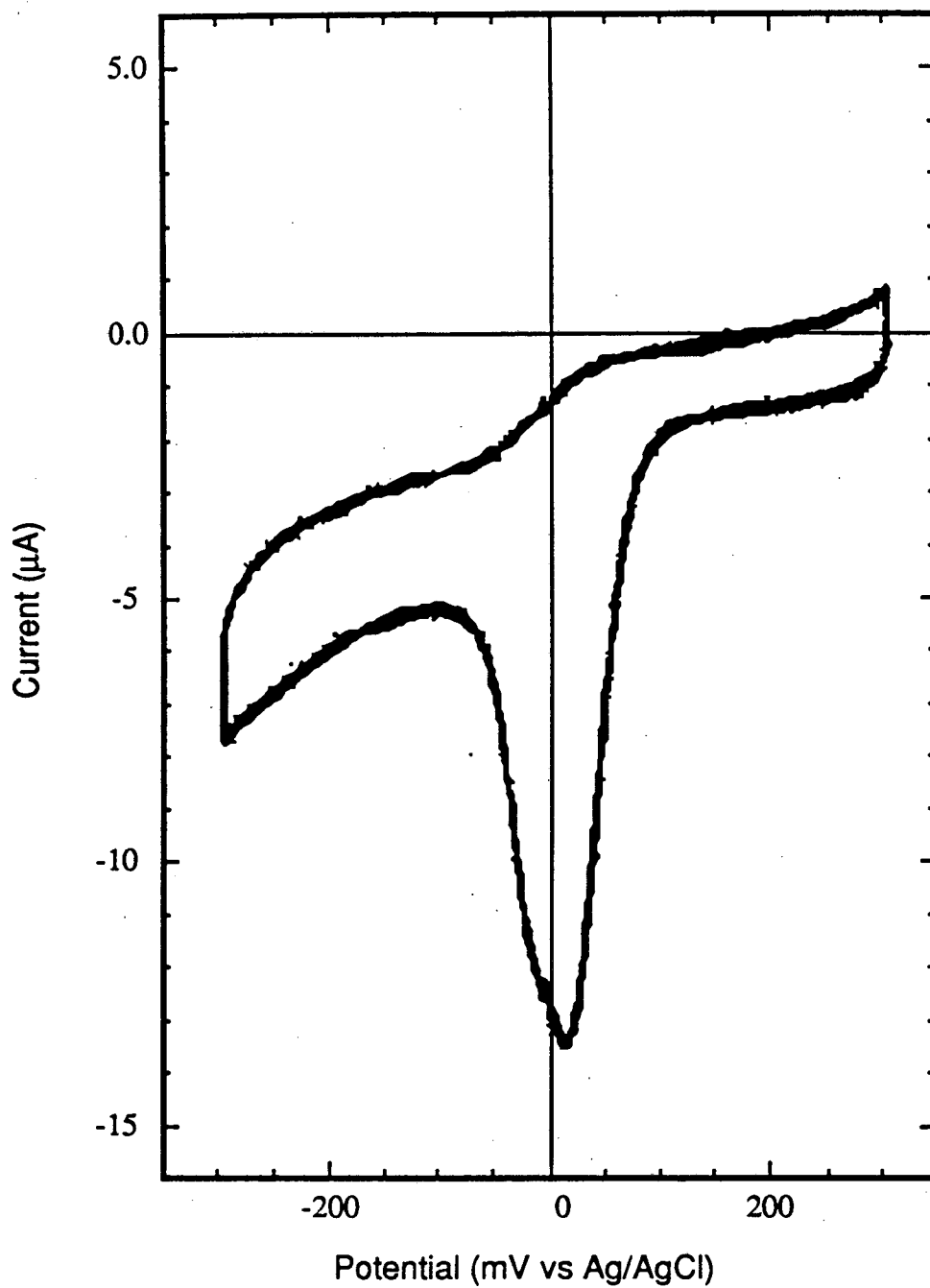
3.1.2. Rhodamine-B Chloride

Rhodamine-B chloride was chosen as a brightening candidate because it has been shown to be a brightener for lead deposition and it absorbs light in the visible spectrum. Its structure is shown in figure 3.3. Rhodamine-B chloride did not electrochemically react in the voltage span. Deposition of Cu from electrolyte containing 76 μ M rhodamine-B chloride yielded milky deposits. An overpotential of 0.21 V was required for deposition at 4 mA /cm².



XBL 902-596

Figure 3.1. Structure of Methyl Red. (XBL 902-596)



XBL 902-597

Figure 3.2. Cyclic voltammetry of 26 μM methyl red on a Au electrode with a supporting electrolyte of 1 M NaClO_4 at $\text{pH} = 3$. (XBL 902-597)

3.1.3. Fluorescein

Fluorescein is a highly fluorescent dye. This compound was chosen as a brightener candidate because it absorbs light in the visible spectrum and it has a structure similar to rhodamine-B chloride. Its structure is shown in figure 3.4. Fluorescein did not electrochemically react in the voltage span used for Cu deposition in these studies. Above a pH of 3.5 and in the presence of fluorescein a passive layer forms on Cu during cathodic polarization in copper plating electrolyte. The passive layer was identified as cuprous oxide, Cu_2O , by Raman spectroscopy. During deposition of the passive film in pH=5.5 electrolyte the color of the copper surface changed from copper at 0 mV vs Cu, to yellow at -75 mV, to red at -115 mV, and then to yellow at -145. Above -145 mV vs Cu the film began to break down. Deposition of Cu from 0.13 M $\text{Cu}(\text{ClO}_4)_2$ and 0.1 M HClO_4 yielded milky deposits. In this electrolyte an overpotential of 0.37 V was required for deposition at 4 mA /cm².

3.1.4. Benzotriazole

Benzotriazole is used as a corrosion inhibitor and as a brightening agent for use with copper. Its structure is shown in figure 1.5. Benzotriazole does not electrochemically react in the voltage span used for Cu deposition in these studies. Further information can be found in section 1.5. Deposition of Cu from electrolyte containing 10 μM benzotriazole yielded milky-bright deposits. An overpotential of 0.40 V was required for deposition at 4 mA /cm².

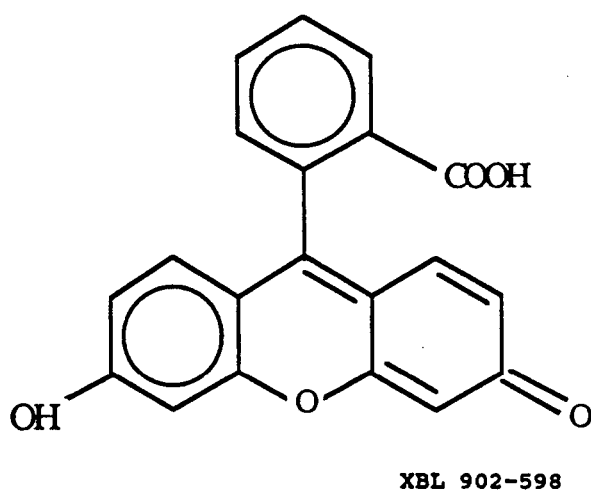


Figure 3.4. Structure of Fluorescein. (XBL 902-598)

3.1.5. Polyvinyl Alcohol

A low molecular weight polyvinyl alcohol, PVA, was screened as a possible brightener. The structure of PVA is shown in figure 3.5. Deposition of Cu from electrolyte containing PVA yielded bright deposits. An overpotential of 0.87 V was required for deposition at 4 mA /cm².

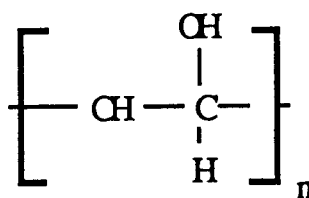
3.1.6. Coumarin 343

Coumarin 343 is a laser dye. This compound was chosen as a brightener candidate because it is structurally related to coumarin, a proven brightener [3.3], and it absorbs light in the visible spectrum. The structure of Coumarin 343 is shown in figure 3.6. Deposition of Cu from electrolyte containing 10 μM coumarin 343 yielded very rough deposits. A overpotential of 0.21 V was required for deposition at 4 mA /cm².

3.1.7. Summary

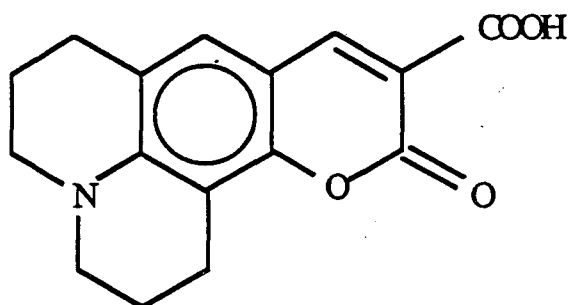
Polyvinyl alcohol, benzotriazole, and fluorescein were the best brightening agents. They also resulted in the highest overpotential during deposition.

Benzotriazole was chosen for further study for several reasons. There is a large amount of literature on the effect of benzotriazole on copper corrosion and a lesser amount on the effect of benzotriazole on Cu deposition. There are several analytical tools which can detect benzotriazole film formation on copper surfaces and



XBL 902-601

Figure 3.5. Structure of a unit cell of polyvinyl alcohol. (XBL 902-601)



XBL 902-602

Figure 3.6. Structure of coumarin 343. (XBL 902-602)

incorporation into copper deposits. Benzotriazole is a strong Raman scatterer. Unfortunately later in the progress of research it was found that the benzotriazole film which formed in the Cu plating electrolytes was too thin to detect with the available Raman spectrometry system. The identification of incorporated BTA is based on a 21 mole percent nitrogen content of BTA. The N was detected by depth profiling with techniques of X-ray photoelectron spectroscopy and secondary ion mass spectrometry.

3.2. Conditions which result in Bright Copper Deposition-- SEM Survey

A visual and microscopic survey of electrochemically deposited copper films was conducted to identify conditions which result in bright copper deposition. The effects of current density and BTA concentration on appearance were investigated. Copper was plated from a 0.5 M CuSO_4 and 0.5 M H_2SO_4 electrolyte containing 0, 15, 34, and 100 μM BTA at current densities of 50, 25, and 12.5 mA/cm^2 . For each set of conditions 8 C/cm^2 of charge was passed, corresponding to 2.4 μm of Cu. A polycrystalline Pt disk, 1.6 cm dia., polished to a mirror finish with a final polish of 0.05 μm alumina, was used for the deposit substrate. This surface was cleaned with nitric acid between deposits.

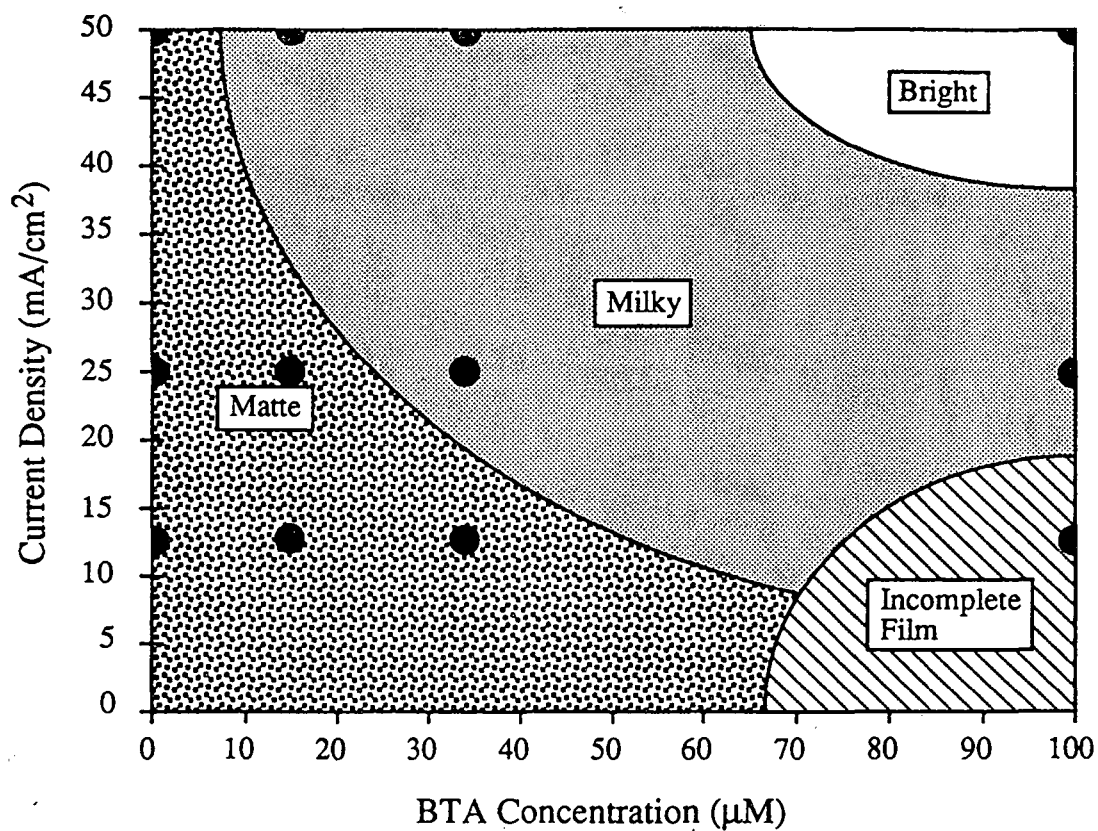
The rotating disk setup described in the voltammetry apparatus section was used for all deposits. The rotation speed was set at 700 rpm resulting in a 18 μm mass transfer boundary layer thickness as calculated by the Levich equation.

$$\delta = 1.6\omega^{-1/2}v^{1/6}D^{1/3} \quad (3.1)$$

The visual appearance of the deposits was graded according to figure 1.1. Bright deposits scattered very little light and reflected images could be seen in detail, milky deposits scattered light however a reflected image could still be seen, and matte deposits scattered light and no or very little reflected image could be resolved.

The results of this survey are summarized in figure 3.7. Deposition from BTA free electrolyte resulted in matte deposits at 12.5, 25, and 50 mA/cm² (fig. 3.8). Deposition from electrolyte with 15 μM BTA resulted in matte deposits at current densities of 12.5 and 25 mA/cm² and a milky deposit at 50 mA/cm² (fig. 3.9). It appears that there is a transition from large to fine particle deposits between 25 and 50 mA/cm². The deposits consisted of large particles surrounded by many fine particles. At 34 μM BTA matte deposition occurs at 12.5 mA/cm² and milky deposition occurs at 25 and 50 mA/cm² (fig. 3.10). With the addition of 100 μM BTA to the electrolyte bright deposits were obtained at 25 and 50 mA/cm², figure 3.11. A partial coverage of the substrate by a bright deposit was obtained at a global current density of 12.5 mA/cm². Partial coverage by the deposit was obtained whether or not the deposit was uniformly nucleated over the electrode by a 40 mA/cm² - 20 s pulse. There is apparently a critical current density or overpotential which must be achieved in order to sustain deposition from electrolyte with 100 μM BTA.

An important observation of BTA inhibited deposition is an abrupt transition to finer grain deposition and a bright appearance with an increase in current density. The transition occurs at lower current densities with increasing BTA concentration. Proposed mechanisms to explain the effect of BTA on grain



XBL 902-577

Figure 3.7. Visual appearance of copper deposits of the SEM survey as a function of the current density and benzotriazole concentration. Each data point, •, represents a 2.4 µm Cu film deposited on a rotating disk electrode (700 rpm) in 0.5 M CuSO₄, 0.5 M H₂SO₄. The borders of each shaded area are arbitrarily drawn between neighboring data points. (XBL 902-577)

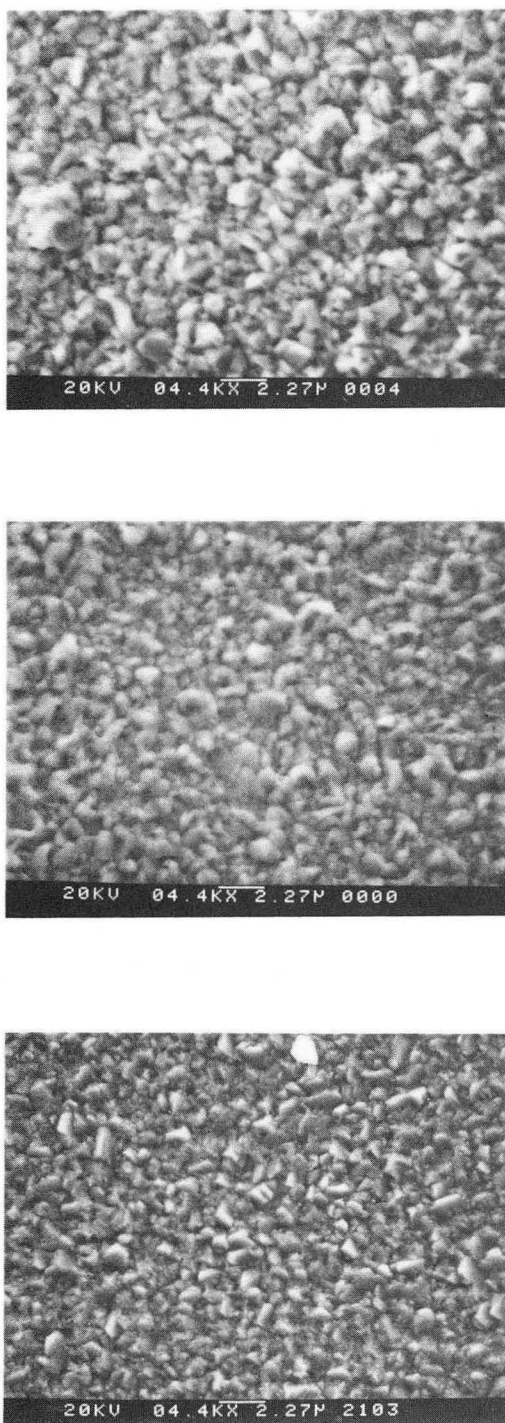


Figure 3.8. SEM of 8 C/cm^2 of Cu deposited from 0.5 M CuSO_4 and $0.5 \text{ M H}_2\text{SO}_4$ at (top) 12.5 , (center) 25 , and (bottom) 50 mA/cm^2 . Rotating disk, Pt, 700 rpm . Small change in the particle size with current density in absence of BTA. (XBB 897-5794)

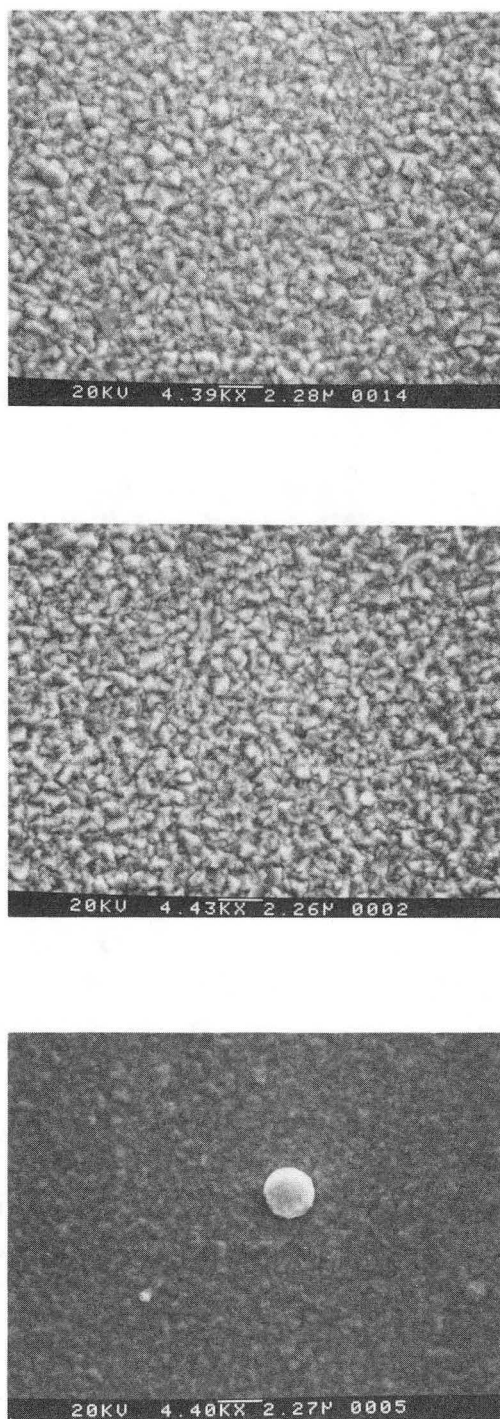


Figure 3.9. SEM of 8 C/cm^2 of Cu deposited from 0.5 M CuSO_4 , $0.5 \text{ M H}_2\text{SO}_4$, and $15 \text{ }\mu\text{M BTA}$ at (top) 12.5 , (center) 25 , and (bottom) 50 mA/cm^2 . Rotating disk, Pt, 700 rpm . Transition from coarse to fine particle deposition between 25 and 50 mA/cm^2 . (XBB 880-10923)

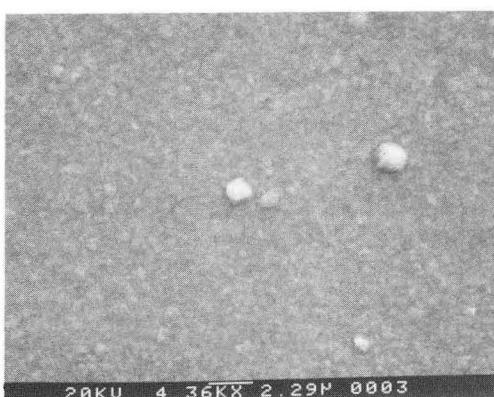
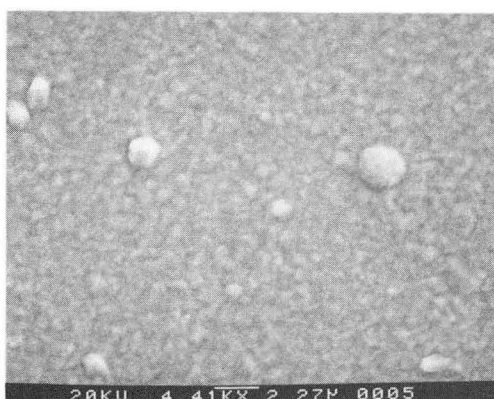
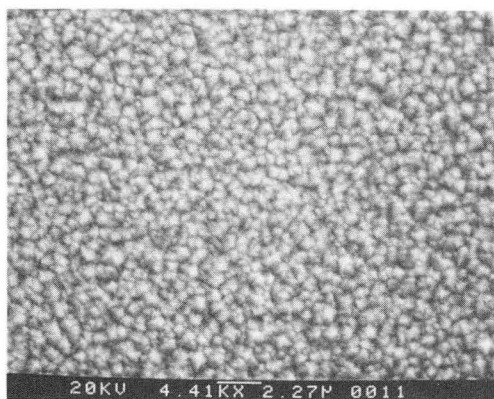


Figure 3.10. SEM of 8 C/cm^2 of Cu deposited from 0.5 M CuSO_4 , 0.5 M H_2SO_4 , and $34 \mu\text{M}$ BTA at (top) 12.5, (center) 25, and (bottom) 50 mA/cm^2 . Rotating disk, Pt, 700 rpm. Transition from coarse to fine particle deposition at approximately 25 mA/cm^2 . (XBB 880-10922)

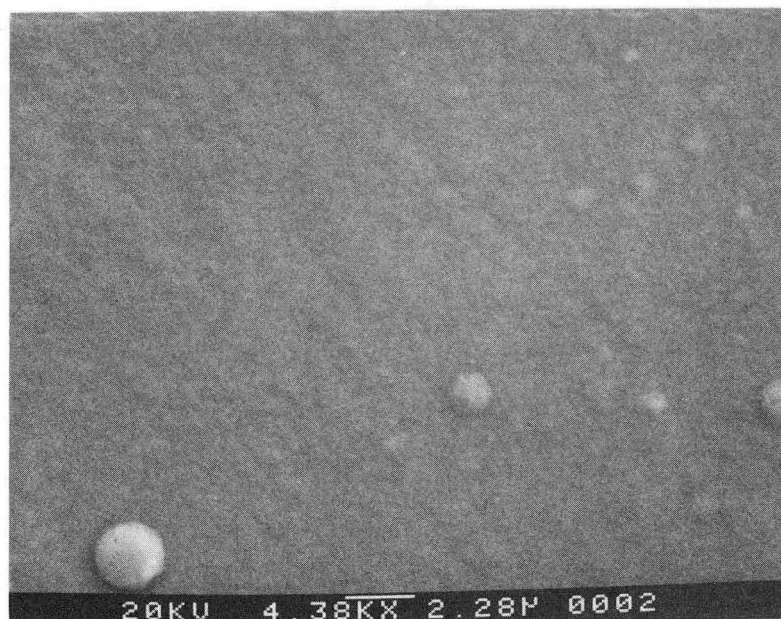
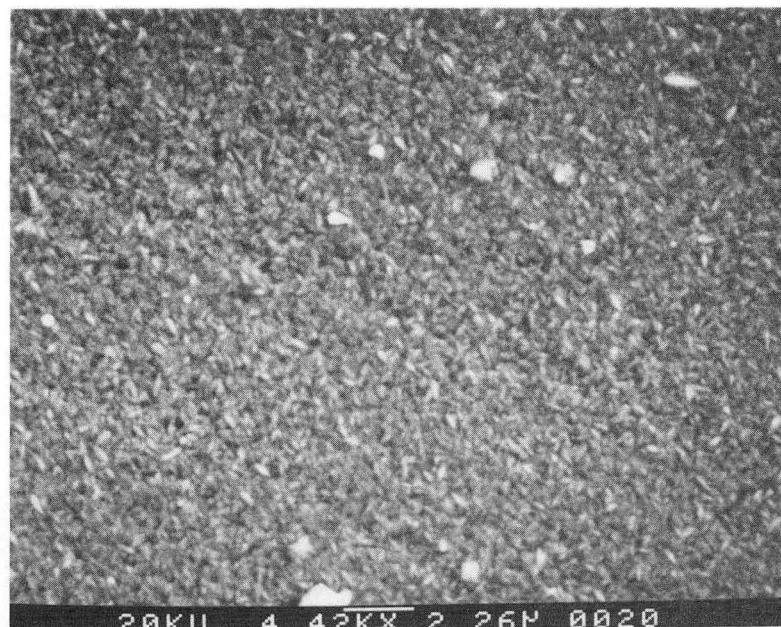


Figure 3.11. SEM of 8 C/cm^2 of Cu deposited from 0.5 M CuSO_4 , $0.5 \text{ M H}_2\text{SO}_4$, and $100 \mu\text{M BTA}$ at (top) 25 and (bottom) 50 mA/cm^2 . Rotating disk, Pt, 700 rpm . Fine particle deposition at both 25 and 50 mA/cm^2 . (XBB 897-5793)

size should include an explanation of this transition.

3.3. Copper-Benzotriazole Film Formation

The formation of cuprous-BTA films on copper substrates was discussed in section 1.5. There are at least four reasons why the formation of a film on the surface is important to discussion of the brightening mechanism: 1) the formation of a film will result in a diffusion barrier to Cu ions and increase the resistance at the surface, 2) the film may block active growth sites inducing a higher nucleation rate, 3) the film may affect the kinetics of the reduction reaction occurring at the surface, 4) the film can be incorporated into the deposit affecting the rate of inhibitor consumption. The following experiments were conducted to investigate the formation of BTA and Cu-BTA films on copper substrates from copper free and 0.5 M CuSO_4 electrolytes. The films were studied with impedance spectroscopy. In addition, the incorporation of BTA in electrodeposited copper was studied using X-ray photoelectron spectroscopy (XPS) and secondary ion mass spectrometry (SIMS).

3.3.1. Film Formation in Cu Plating Solution

The frequency dependence of the complex impedance of electrochemical reactions can give information on ohmic, kinetic, and mass transfer resistance and double layer capacitance. Impedance measurements are useful for detecting the

formation of a film on an electrode surface. In this series of experiments impedance measurements were used to establish the conditions under which Cu-BTA films exist on Cu substrates in Cu plating electrolyte. In addition qualitative information on the mass transfer of reactants was obtained from the low frequency dependence of the impedance.

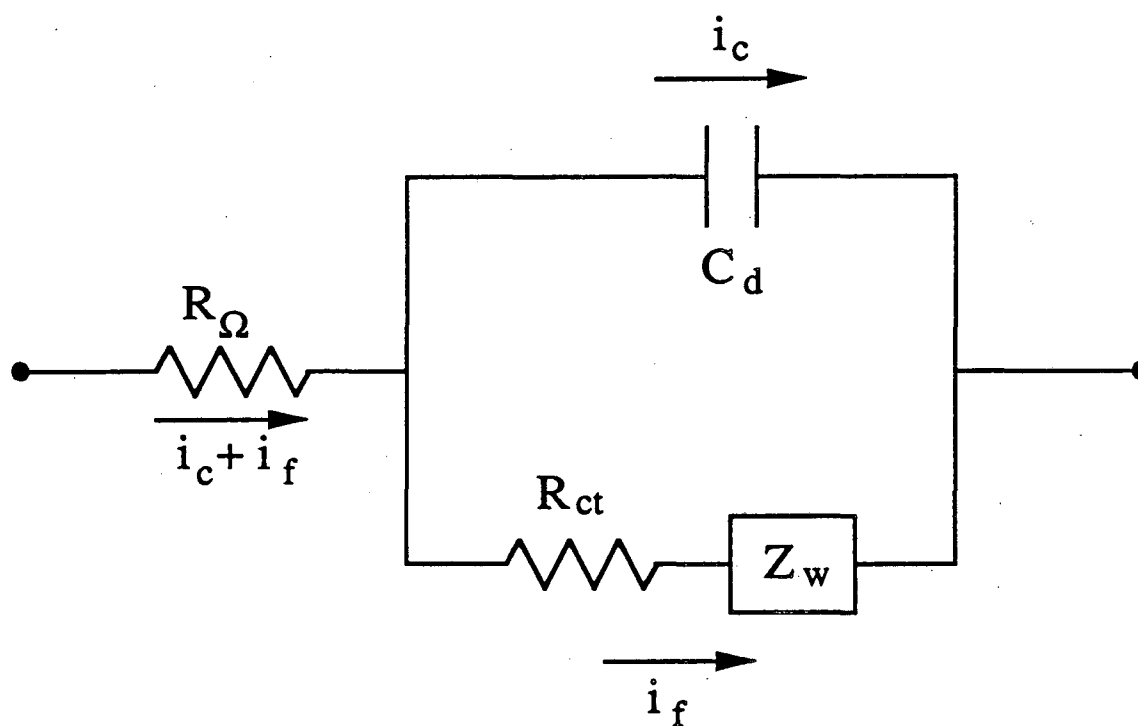
The interpretation of impedance measurements is helped by representing the electrochemical cell by an equivalent circuit. Figure 3.12 shows a representation of an electrochemical cell by a circuit containing an ohmic resistance through the cell, R_{Ω} , charge transfer resistance, R_{ct} , double layer capacitance, C_d , and Warburg impedance, Z_w . The Warburg impedance represents an impedance due to mass transfer. For the case of semi-infinite diffusion the following relationship has been derived.

$$Z_w = \frac{\sigma}{\omega^{1/2}} + \frac{1}{\sigma\omega^{1/2}} j \quad (3.2)$$

where

$$\sigma = \frac{1}{n^2 F^2 A \sqrt{2}} \left(\frac{1}{D_O^{1/2} C_O^*} + \frac{1}{D_R^{1/2} C_R^*} \right) \quad (3.3)$$

C_O^* is the concentration of the oxidized form of the reactant at the surface and C_R^* is the concentration of the reduced form of the reactant at the surface. The derivation of the Warburg impedance of a system with a finite boundary layer is considerably more complex [3.4]. Impedance data from a rotating disk can be treated as though semi-infinite diffusion is in effect if the dimensionless frequency, K , is greater than 10 [3.4].



XBL 902-603

Figure 3.12. Equivalent circuit representation of electrochemical cell. R_{Ω} is the ohmic resistance of the cell, R_{ct} is the charge transfer resistance, C_d is the double layer capacitance, Z_w is the Warburg impedance, i_c is the current due to charging of the electrochemical interface, and i_f is the current due to faradaic reactions. (XBL 902-603)

$$K = \frac{\omega}{\Omega} \left(\frac{9\nu}{a^2 D} \right)^{1/3} \quad (3.4)$$

where ω is the potential modulation frequency, Ω is the disk rotation rate, ν is the kinematic viscosity, D is the diffusivity, and $a = 0.51023$. A more complete derivation of the Warburg impedance for semi-infinite diffusion can be found in Bard and Faulkner [3.5]. The total impedance of the equivalent circuit is

$$Z_{\text{Re}} = R_{\Omega} + \frac{(R_{ct} + \sigma\omega^{-1/2})(C_d \sigma\omega^{1/2} + 1)}{\omega^2 C_d^2 (R_{ct} + \sigma\omega^{-1/2})^2 + (C_d \sigma\omega^{1/2} + 1)^2} \quad (3.5)$$

$$Z_{\text{Im}} = \frac{\omega C_d (R_{ct} + \sigma\omega^{-1/2})^2 + \sigma\omega^{-1/2} (C_d \sigma\omega^{1/2} + 1)}{\omega^2 C_d^2 (R_{ct} + \sigma\omega^{-1/2})^2 + (C_d \sigma\omega^{1/2} + 1)^2} \quad (3.6)$$

The impedance of the circuit at the low frequency limit is

$$Z_{\text{Re}} = R_{\Omega} + R_{ct} + \sigma\omega^{-1/2} \quad (3.7)$$

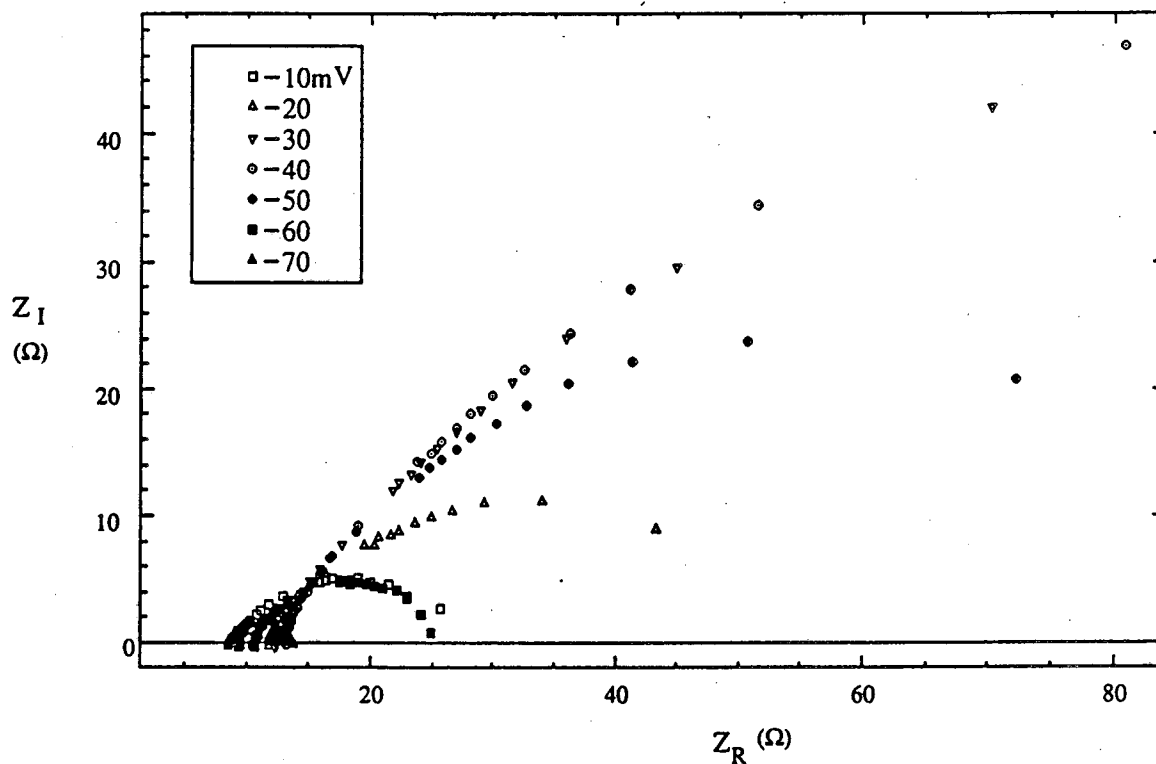
$$Z_{\text{Im}} = 2\sigma^2 C_d + \sigma\omega^{-1/2} \quad (3.8)$$

where Z_{Re} and Z_{Im} are the real and imaginary components of the equivalent circuit impedance. Such an impedance is represented by a linear line on a Nyquist plot (imaginary versus real) with a slope of one. At the high frequency limit the mass transfer resistance becomes unimportant and the following relationship results.

$$\left(Z_{\text{Re}} - R_{\Omega} - \frac{R_{ct}}{2} \right)^2 + Z_{\text{Im}}^2 = \left(\frac{R_{ct}}{2} \right)^2 \quad (3.9)$$

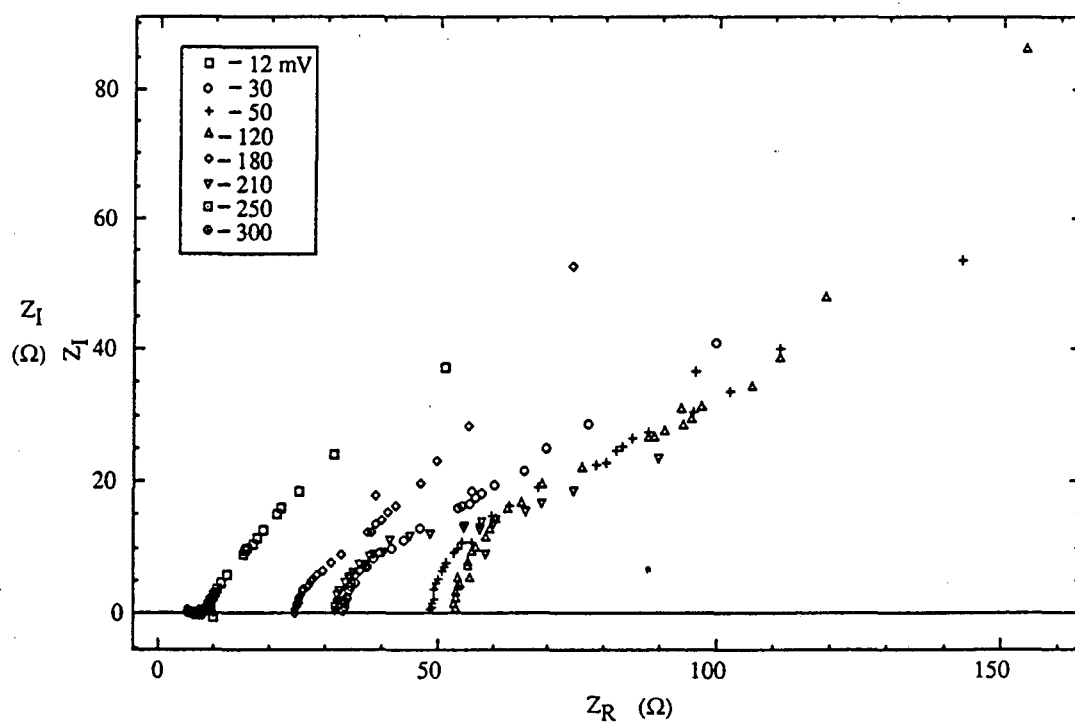
This relationship results in a semicircle with a center at $Z_{\text{Re}} = R_{\Omega} + R_{ct}/2$ and $Z_{\text{Im}} = 0$.

Figures 3.13 and 14 are Nyquist plots of impedance measurements of Cu deposition from 100 and 200 μM BTA electrolytes. These measurements were performed on a rotating disk electrode, 500 rpm, with a 10 mV amplitude potential perturbation between 1 and 512 Hz. The corresponding dimensionless frequency was in the range of $K = 4$ to 2000. Semi-infinite diffusion was assumed in the



XBL 902-612

Figure 3.13. Nyquist plot of the impedance (1 to 512 Hz) of Cu in 0.5 M CuSO_4 , 0.5 M H_2SO_4 , and 100 μM BTA plotted at several overpotentials as labeled. 8 mm diameter rotating disk electrode (500 rpm). Pt counter electrode and Cu reference electrode. (XBL 902-612)

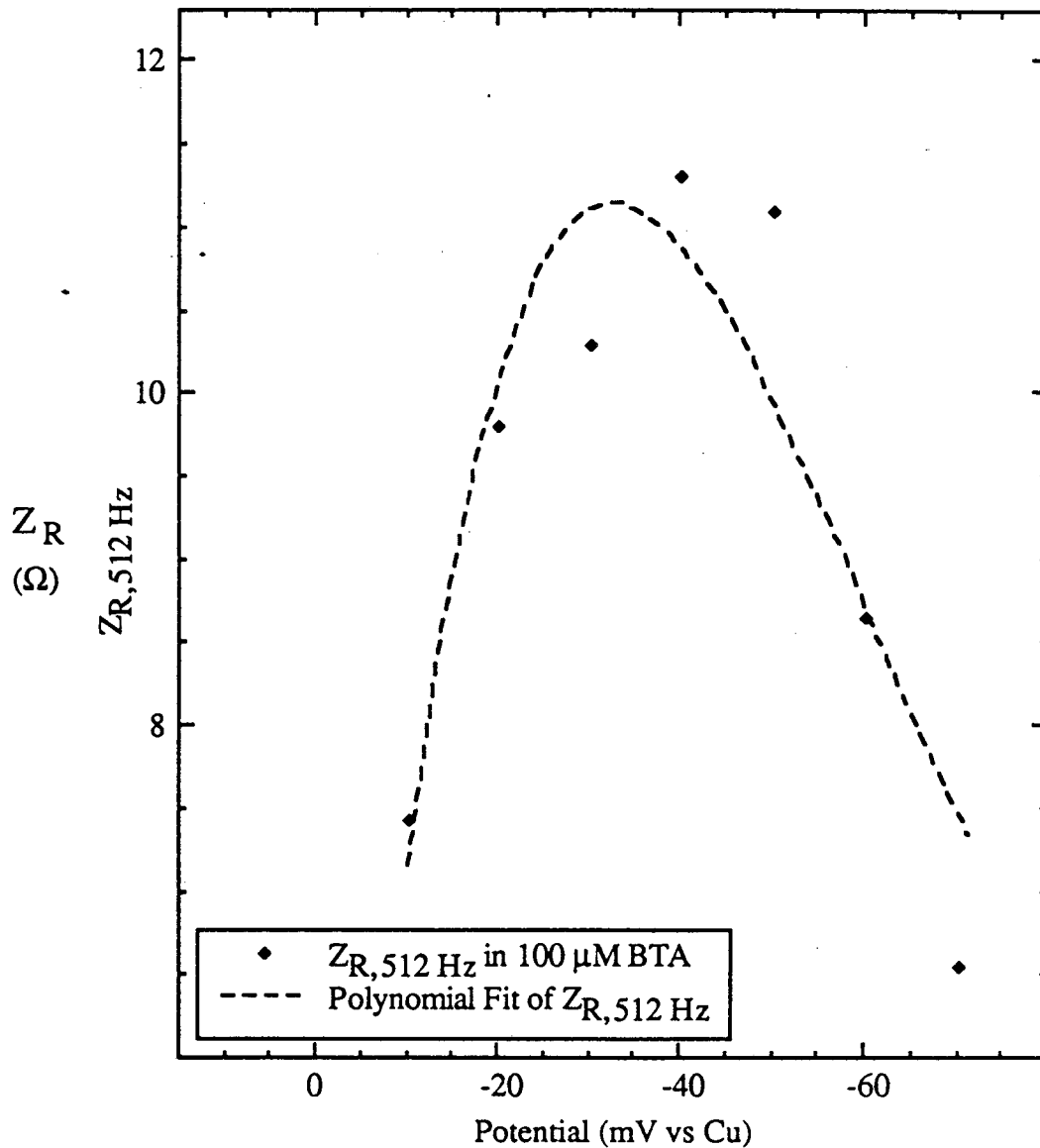


XBL 902-611

Figure 3.14. Nyquist plot of the impedance (1 to 512 Hz) of Cu in 0.5 M CuSO₄, 0.5 M H₂SO₄, and 200 μM BTA plotted at several overpotentials as labeled. 8 mm diameter rotating disk electrode (500 rpm). Pt counter electrode and Cu reference electrode. (XBL 902-611)

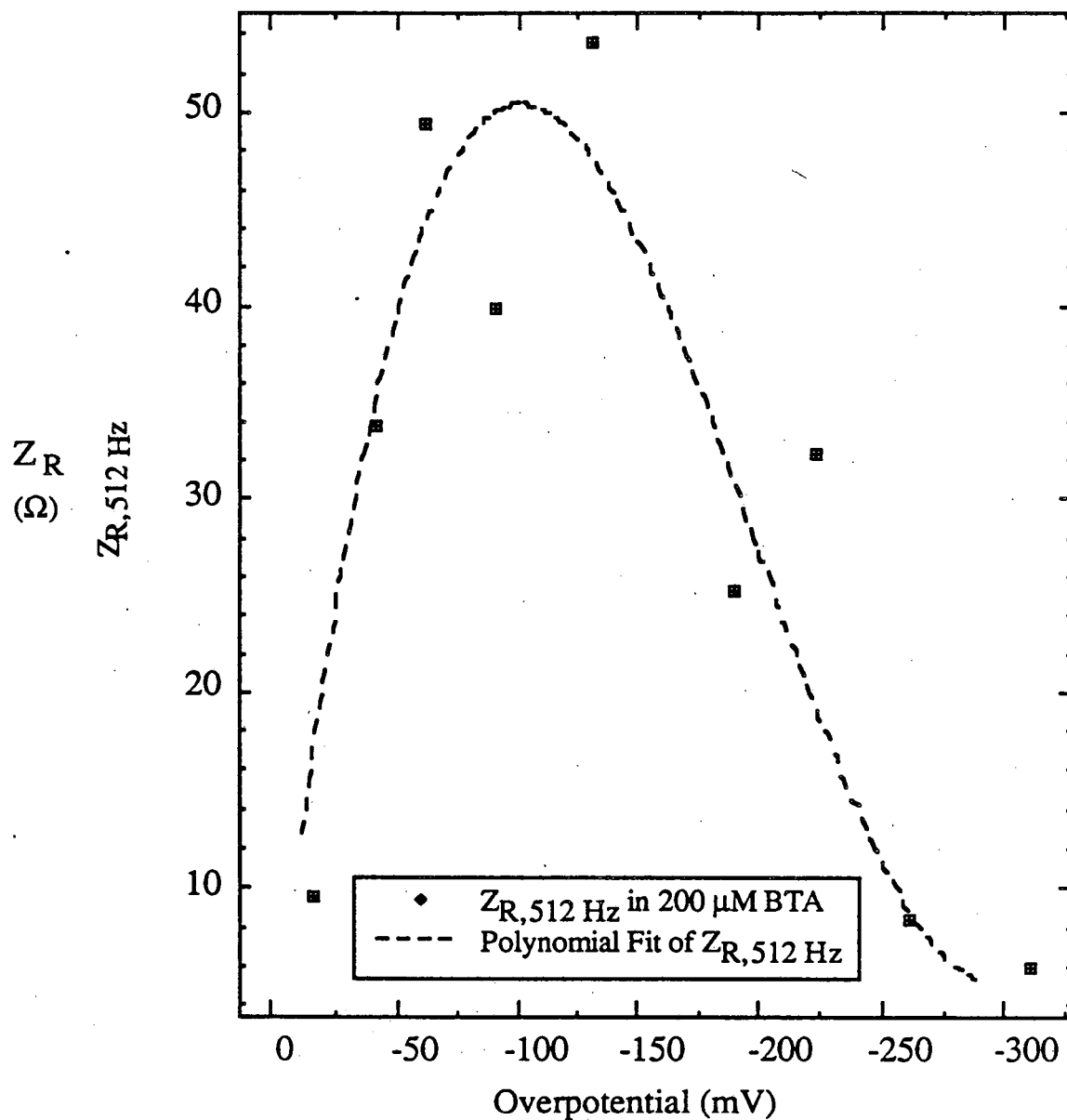
treatment of the measured impedance spectra. Characteristic of the BTA containing electrolytes was a high ohmic resistance which reached a maximum value at potentials cathodic of the open circuit potential for Cu, figures 3.15 and 3.16. The scatter present in these figures results from the experimental procedure in which the impedance measurements are performed at the electrode bias potentials in a random order. There was some hysteresis in the measured ohmic drop as a function of potential. The high ohmic resistance of the BTA inhibited copper deposition is probably due to the formation of a cuprous-BTA layer on the surface. The cuprous-BTA complex is very insoluble and has been shown to be present in trace amounts in Cu electrodeposits formed from solutions containing greater than 200 μM BTA [3.2]. Benzotriazole may inhibit the reduction of Cu^+ ions to the neutral metal resulting in a build up of Cu^+ at the surface and precipitation of a Cu-BTA film. At high current densities the break down of the Cu-BTA film may result from two mechanisms: 1) dissolution of the film due to a decrease of cuprous ion concentration by reduction of cuprous ion to copper metal and 2) physical removal of the Cu-BTA film by incorporation into the metal deposit.

A Warburg like diffusion resistance is observed at low current densities, figure 3.17. The Warburg like frequency response of impedance at low current densities is an indication that the rate of electrochemical reaction is mass transport controlled. The species which are electrochemically active in the potential range of the measurements are Cu^{2+} and Cu^+ . In addition there is the possibility of direct reduction of the cupric-BTA complex to cuprous-BTA. For the reduction of Cu^{2+} to Cu metal a Warburg impedance of $\sigma = 0.14$ was calculated from equation 3.3 for a diffusion coefficient of 0.75×10^{-5} [3.6] and a concentration of 0.5 M. If the rate



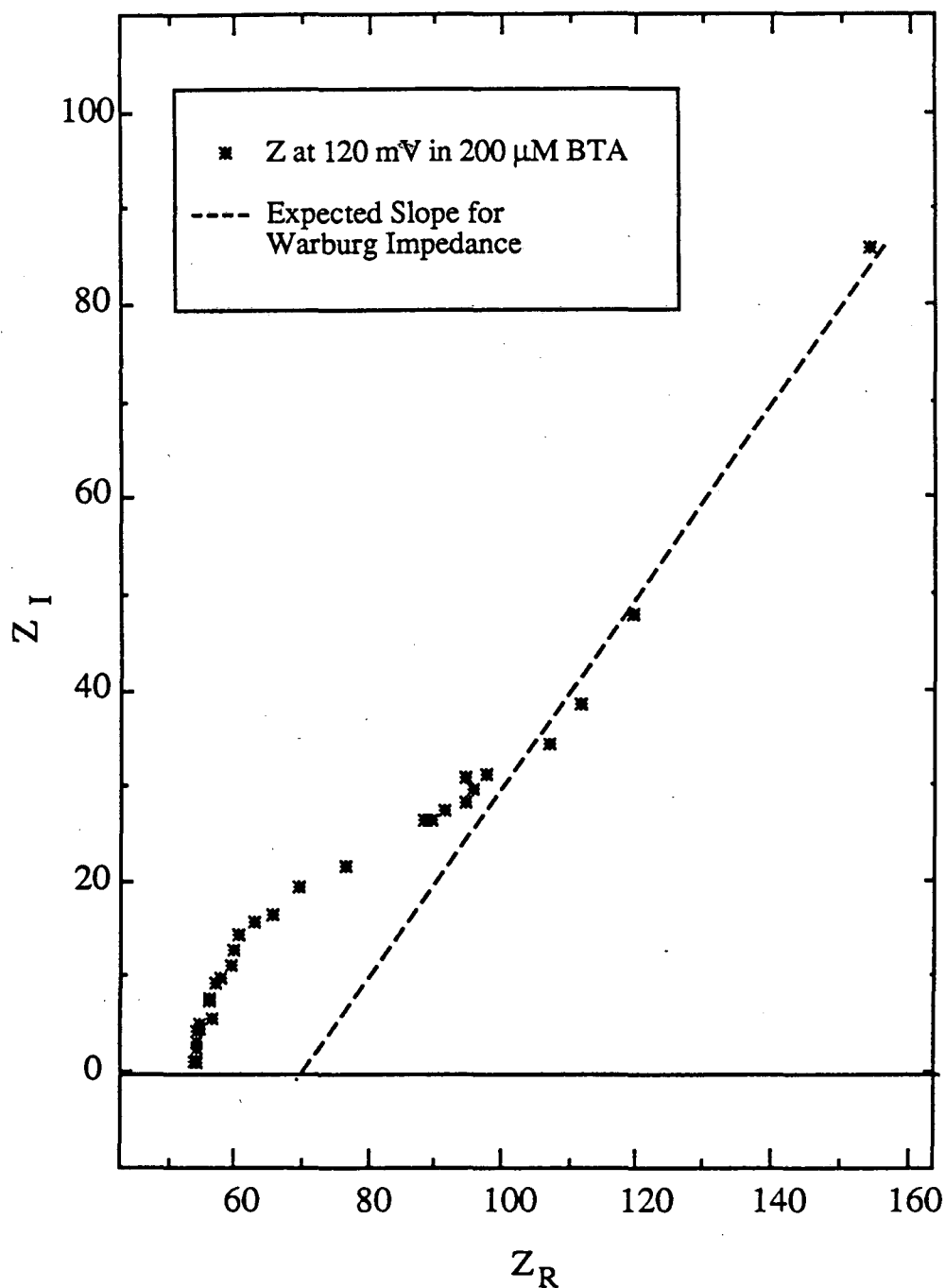
XBL 902-579

Figure 3.15. Z_R at 512 Hz as a function of potential measured from Cu in 0.5 M CuSO_4 , 0.5M H_2SO_4 , and 100 μM BTA. The presence of a maximum of the ohmic resistance indicates the buildup and breakdown of resistive film on the electrode with polarization. 8 mm diameter rotating disk electrode (500 rpm). Pt counter electrode and Cu reference electrode. (XBL 902-579)



XBL 902-580

Figure 3.16. Z_R at 512 Hz as a function of potential measured from Cu in 0.5 M CuSO_4 , 0.5M H_2SO_4 , and 200 μM BTA. The presence of a maximum of the ohmic resistance indicates the buildup and breakdown of resistive film on the electrode with polarization. (XBL 902-580)



XBL 902-578

Figure 3.17. Nyquist plot of Z (1 to 512) from a Cu electrode in 0.5 M CuSO_4 , 0.5M H_2SO_4 , and 200 μM BTA at -120 mV relative Cu at open circuit and 0.088 mA/cm^2 . The dashed line represents the expected slope of data following a Warburg behavior. (XBL 902-578)

limiting step is the diffusion of cuprous ion due to the reduction of Cu^+ to Cu metal or reduction of Cu^{2+} to Cu^+ the Warburg impedance would be $\sigma = 147$ calculated from equation 3.3 for a diffusion coefficient of 1.3×10^{-5} [3.6] and a concentration of 0.7 mM. The cuprous ion concentration was calculated assuming an equilibrium between cuprous ion, cupric ion, and copper metal

$$C_{\text{Cu}^+} = (C_{\text{Cu}^{2+}} K_{\text{eq}})^{1/2} \quad (3.10)$$

where $K_{\text{eq}} = 10^{-6}$ M [3.6]. For the reduction of Cu^{2+} -BTA(aq) to Cu^+ -BTA(s) a Warburg impedance of $\sigma = 1200$ was calculated from equation 3.3 assuming a diffusion coefficient of 1×10^{-5} and a concentration of 100 μM . Should the transport of Cu^{2+} -BTA be the rate limiting process the Warburg impedance should be inversely proportional to the concentration of BTA. The measured frequency response was fitted by equations 3.7 and 3.5. The parameters R_{Ω} , R_{ct} , C_d , and σ were determined by minimizing the sum of squares error between calculated and measured values of Z_{Re} and Z_{Im} . The derivation of the Warburg impedance from the data is complicated by the presence of the resistive film. The impedance model does not take into account the possibility of the modulation of the film thickness by the applied potential program. Nor does the model take into account inhomogeneous coverage of the surface by the film. The best fit of the model to any of the impedance spectra occurred at the potential where the ohmic drop was at a maximum in which case the derivative of the ohmic drop with respect to potential was zero. The measured Warburg impedance falls in the range of 100 to 200 $\Omega\text{-s}^{1/2}$ and is not inversely related to the BTA concentration (tables 3.2 and 3.3). It appears that the cuprous ion is the rate controlling species. The increase in the ohmic drop through solution with increased overpotential is the result of an

Overpotential (mV vs Cu)	$R_{\Omega} + R_{ct}$ (Ω)	σ ($\Omega\text{-s}^{1/2}$)
20	6.0 to 7.6	106 to 145
30	6.9 to 8.3	138 to 151
40	6.7 to 8.3	170 to 180
50	6.5	182

Table 3.2. Least squares fit of the parameters of equation 3.7 to the impedance spectra (1 to 512 Hz) of Cu in 0.5 M CuSO_4 , 0.5 M H_2SO_4 , 100 μM BTA.

Overpotential (mV vs Cu)	R_{Ω} (Ω)	R_{ct} (Ω)	σ ($\Omega\text{-s}^{1/2}$)	C_d (μF)
12	6.0 to 8.6		107 to 112	
33	34.3	14.2	136	117
54	50.7	23.3	184	94
124	54.5	28.5	186	77
184	25.7	8.66	107	216

Table 3.3. Least squares fit of the parameters of equation 3.5 to the impedance spectra (1 to 512 Hz) of Cu in 0.5 M CuSO_4 , 0.5 M H_2SO_4 , 200 μM BTA. Equation 3.7 was used for determining $R_{\Omega}+R_{ct}$ and σ from the impedance spectra recorded at a 12 mV overpotential.

increased cuprous-BTA film thickness. This would indicate that there is a buildup of cuprous ion resulting from the reduction of Cu^{2+} to Cu^+ .

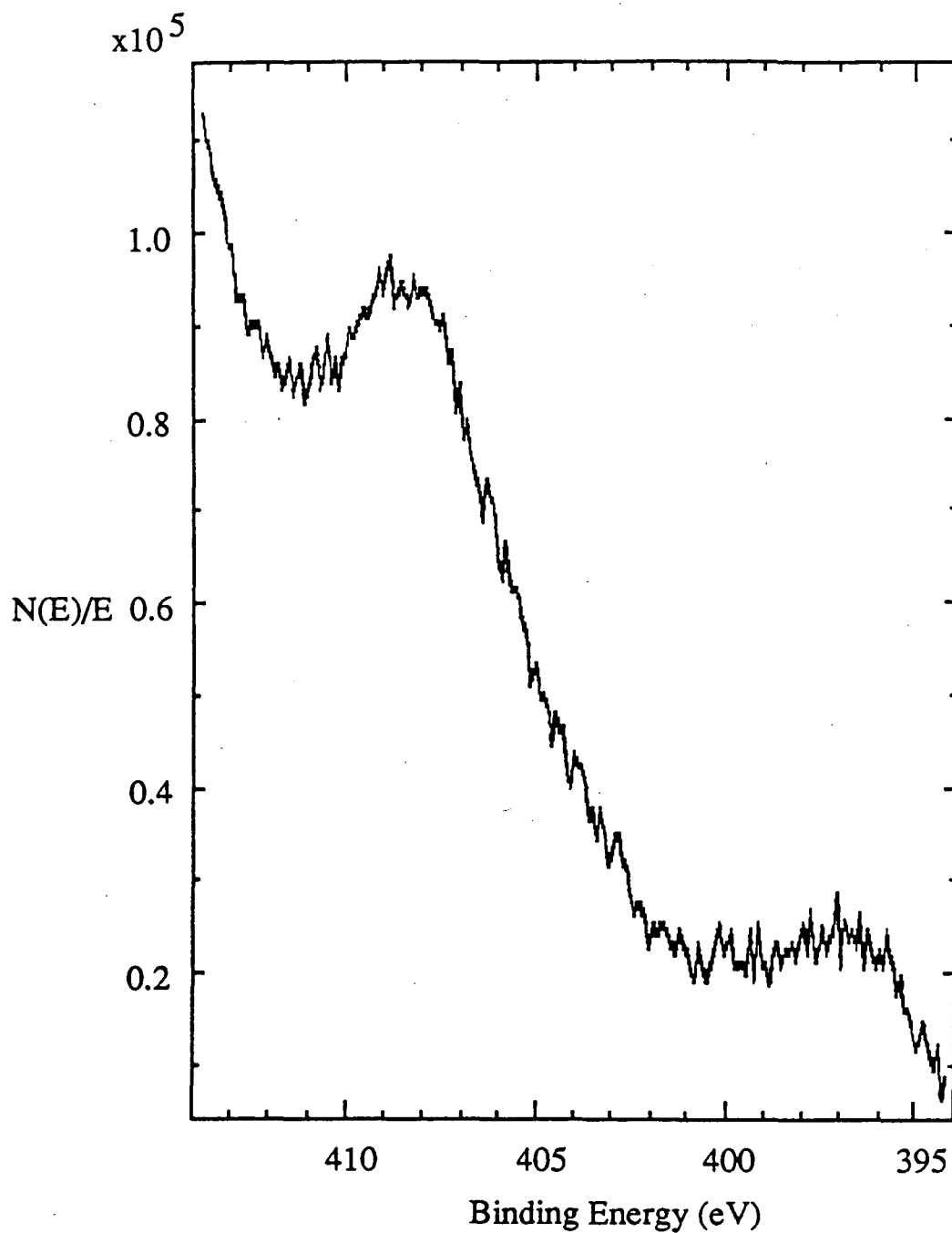
3.3.2. Incorporation into Electroplated Cu

The incorporation of BTA into copper deposits was studied with X-ray photoelectron spectroscopy (XPS) and secondary ion mass spectrometry (SIMS) to measure the nitrogen content of deposits. The rate at which BTA is incorporated in copper deposits during plating is important in consideration of brightening mechanisms based on inhibitor concentration gradient in solution. The depth profile of nitrogen concentration in the copper deposits is directly related to the rate of BTA consumption from incorporation and reaction. The following series of experiments were performed to determine whether the rate of BTA incorporation is related to the convective transport conditions.

X-ray photoelectron spectroscopy of copper electrodeposits was used to determine the deposit nitrogen content. The deposits were formed galvanostatically at 10 mA/cm^2 in 0.5 M CuSO_4 , $0.5 \text{ M H}_2\text{SO}_4$, and 0 and $34 \mu\text{M}$ BTA. The rotating disk setup described in the voltammetry apparatus section was used for all deposits. The rotation speed was set at 700 rpm resulting in a $18 \mu\text{m}$ mass transfer boundary layer thickness as calculated by equation (3.1). The films were rinsed in distilled water and dried before insertion into the ultrahigh vacuum system employed for XPS. The XPS measurements were conducted with a PHI 5300 XPS system sensitive to 0.1 atomic % coverage of copper by nitrogen.

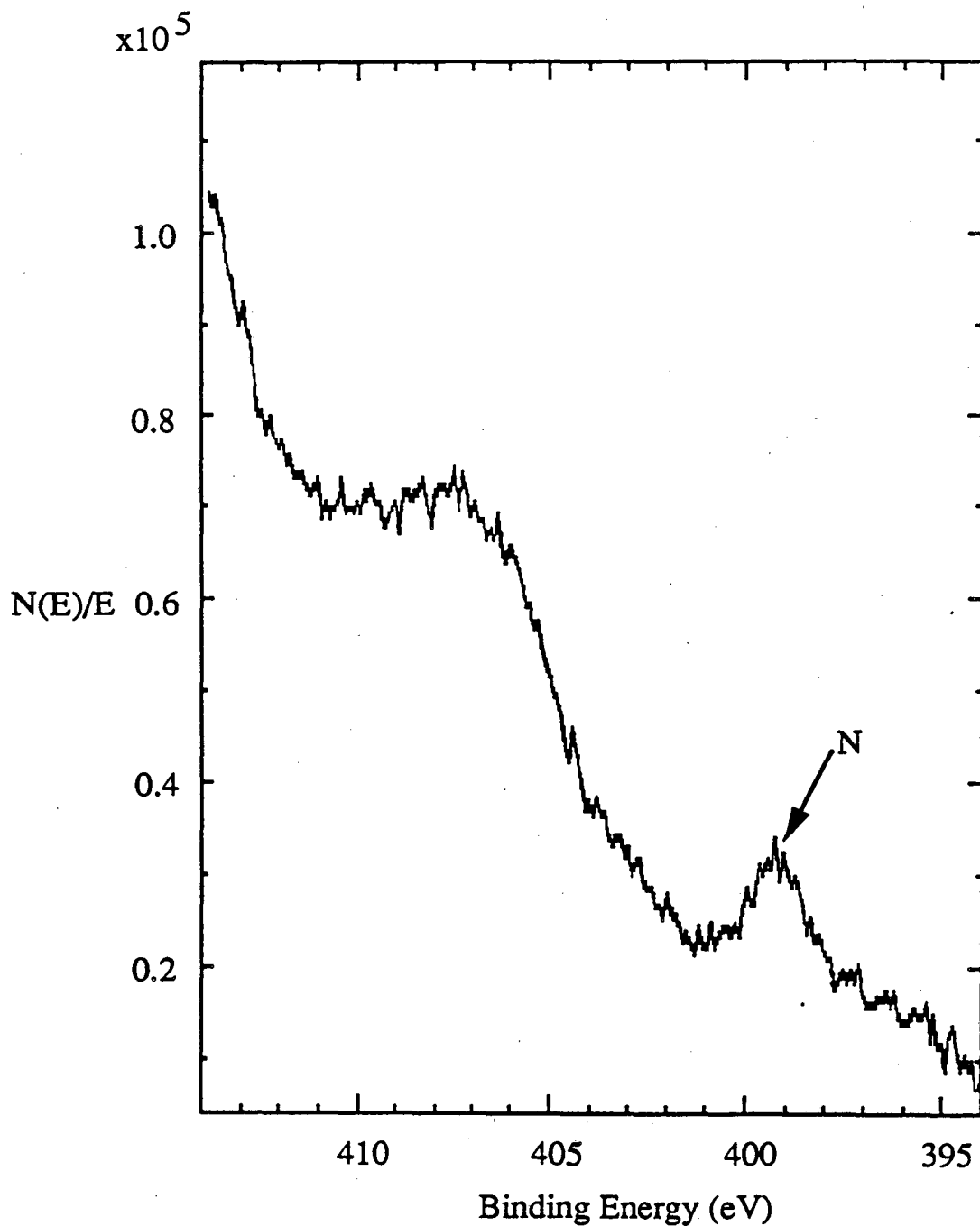
Figure 3.18 shows the result of an XPS measurement of electron emissions between 394 and 414 eV from Cu electrodeposited without BTA. There was no inflection or apparent peak at 400 eV where a emission of a photoelectron from the nitrogen 1s orbital is expected. The XPS measurements from Cu film electrodeposited without BTA showed no indications of N content on the initial surface or following etching of the surface by ion bombardment. Figure 3.19 shows the result of an XPS measurement of electron emissions between 394 and 414 eV from Cu electrodeposited in the presence of 34 μM BTA. The XPS measurements of the Cu film prior to ion bombardment showed a peak at 400 eV associated with 3% coverage of the surface by N. Following removal of a few hundred angstroms of deposit by ion bombardment there was no indication of the N photoelectron emission indicating either less than 0.1 % N was incorporated within the deposit or that the action of ion bombardment selectively removed the BTA from the deposit (fig. 3.20). The XPS measurements indicate the presence of BTA at the surface of copper deposits but no BTA is evident within the deposit. The concentration of BTA in solution is sufficient to obtain a N content of 2% in copper electrodeposited under the experiment conditions if the incorporation rate of BTA is mass transfer limited.

The SIMS method was employed to determine if there is fluctuation of the N content with depth into copper deposits when the deposits are formed during modulation of the mass transport boundary layer thickness or modulation of the current density. The transport conditions were varied by applying a step function to the rotation rate of the deposit substrate. If the incorporation rate of benzotriazole is mass transport limited then the ratio of Cu to BTA should vary



XBL 902-576

Figure 3.18. X-ray photoelectron spectroscopy of the surface of a copper film electrodeposited onto a Au rotating disk, 1000 rpm, at 5.5 mA/cm^2 in an electrolyte consisting of 0.5 M CuSO_4 and $0.5 \text{ M H}_2\text{SO}_4$. No peak at 400 eV due to N occurs. (XBL 902-576)



XBL 902-584

Figure 3.19. X-ray photoelectron spectroscopy of the surface of a copper film electrodeposited onto a Au rotating disk, 1000 rpm, at 5.5 mA/cm^2 in a electrolyte consisting of 0.5 M CuSO_4 , $0.5 \text{ M H}_2\text{SO}_4$, and $34 \mu\text{M BTA}$. The peak at 400 eV is due to the N 1s orbital. (XBL 902-584)

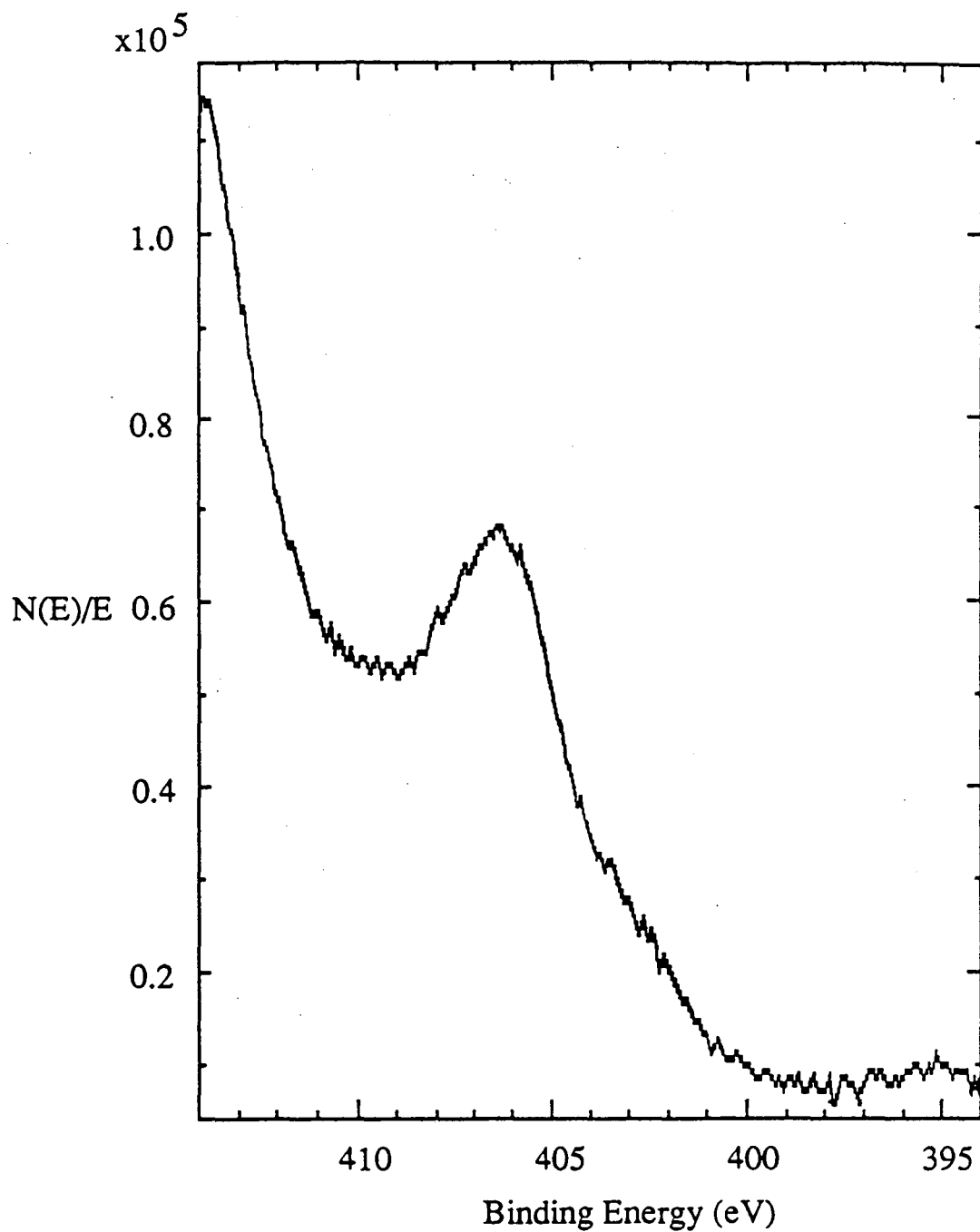


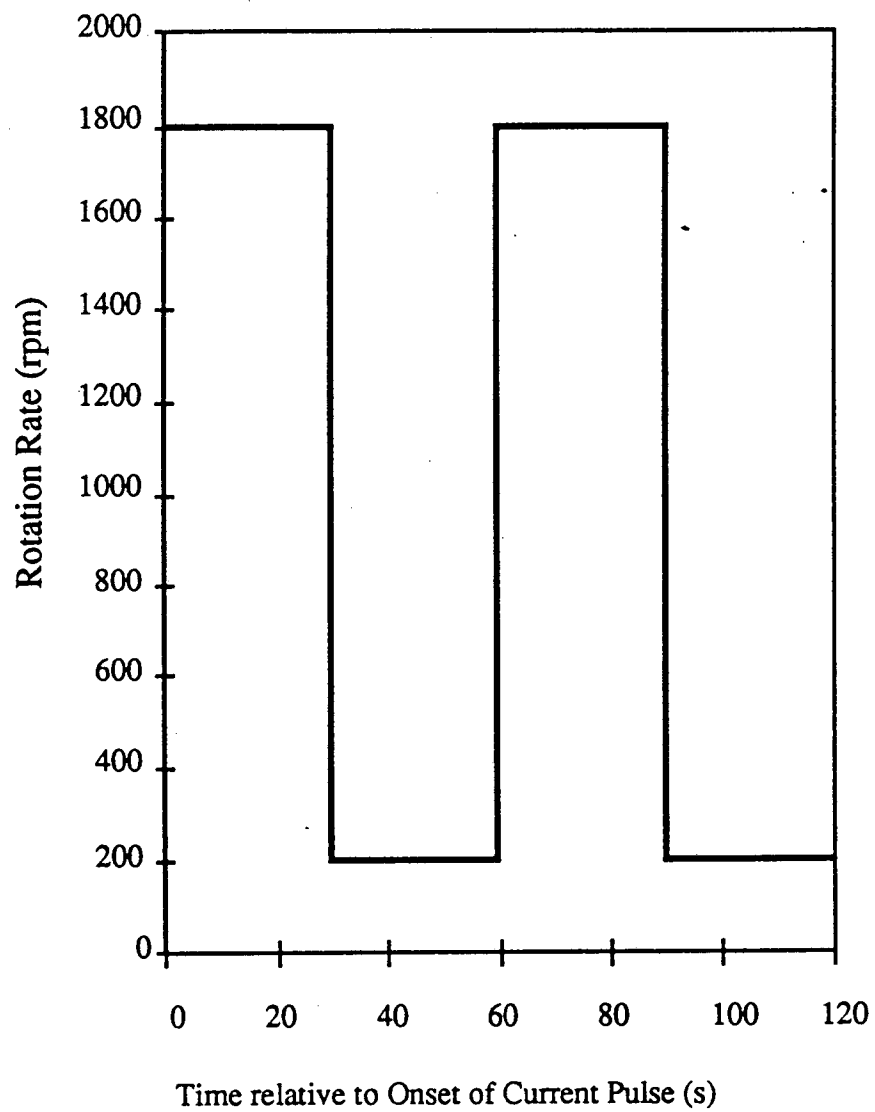
Figure 3.20. X-ray photoelectron spectroscopy following ion bombardment of the surface of a copper film electrodeposited onto a Au rotating disk, 1000 rpm, at 5.5 mA/cm^2 in a electrolyte consisting of 0.5 M CuSO_4 , $0.5 \text{ M H}_2\text{SO}_4$, and $34 \text{ }\mu\text{M}$ BTA. There is no peak at 400 eV due to the N 1s orbital. (XBL 905-1571)

with the changing transport conditions. Copper was electrodeposited galvanostatically much below limiting current to minimize the concentration gradient of Cu. The nitrogen content of the deposit should vary with a period equivalent to the step function if there is a correspondence between rotation rate and BTA incorporation.

In this series of experiments, copper was plated from a 0.5 M CuSO_4 and 0.5 M H_2SO_4 electrolyte containing 0 and 100 μM BTA at current densities of 10 and 20 mA/cm^2 . In each set of conditions 1.2 C/cm^2 of charge was passed. Assuming a compact Cu film, a thickness of 0.40 μm was expected.

The rotation speed of the electrode was varied between 200 and 1800 rpm with a step function (fig. 3.21). The mass transfer boundary layer was 34 and 12 μm and limiting current was 220 and 670 mA/cm^2 at 200 and 1800 rpm respectively as calculated by equation (3.1).

Figures 3.22 and 3.23 are plots of the 14 m/e peak corresponding to nitrogen during a depth profile of deposits made at 10 mA/cm^2 with 0 and 100 μM BTA. The increase in the 14 m/e signal at the right hand side of the figures corresponds to the breakthrough by ion etching into the gold covered steel substrate. A general increase in all m/e signal occurs during breakthrough due to a change in the ionization cross section and sputter rates when entering the new material. There was no periodicity in the nitrogen content with or without BTA present. The source of the nitrogen in the deposit from BTA free electrolyte is the CuSO_4 salt used for making the 0.5 M CuSO_4 solution. The nitrogen content of the analytical grade CuSO_4 used in the solution preparation was reported to be less than 10 ppm.



XBL 902-583

Figure 3.21. Rotation rate as a function of time during deposition of Cu at 10 mA/cm² for the modulated boundary layer deposits. (XBL 902-583)

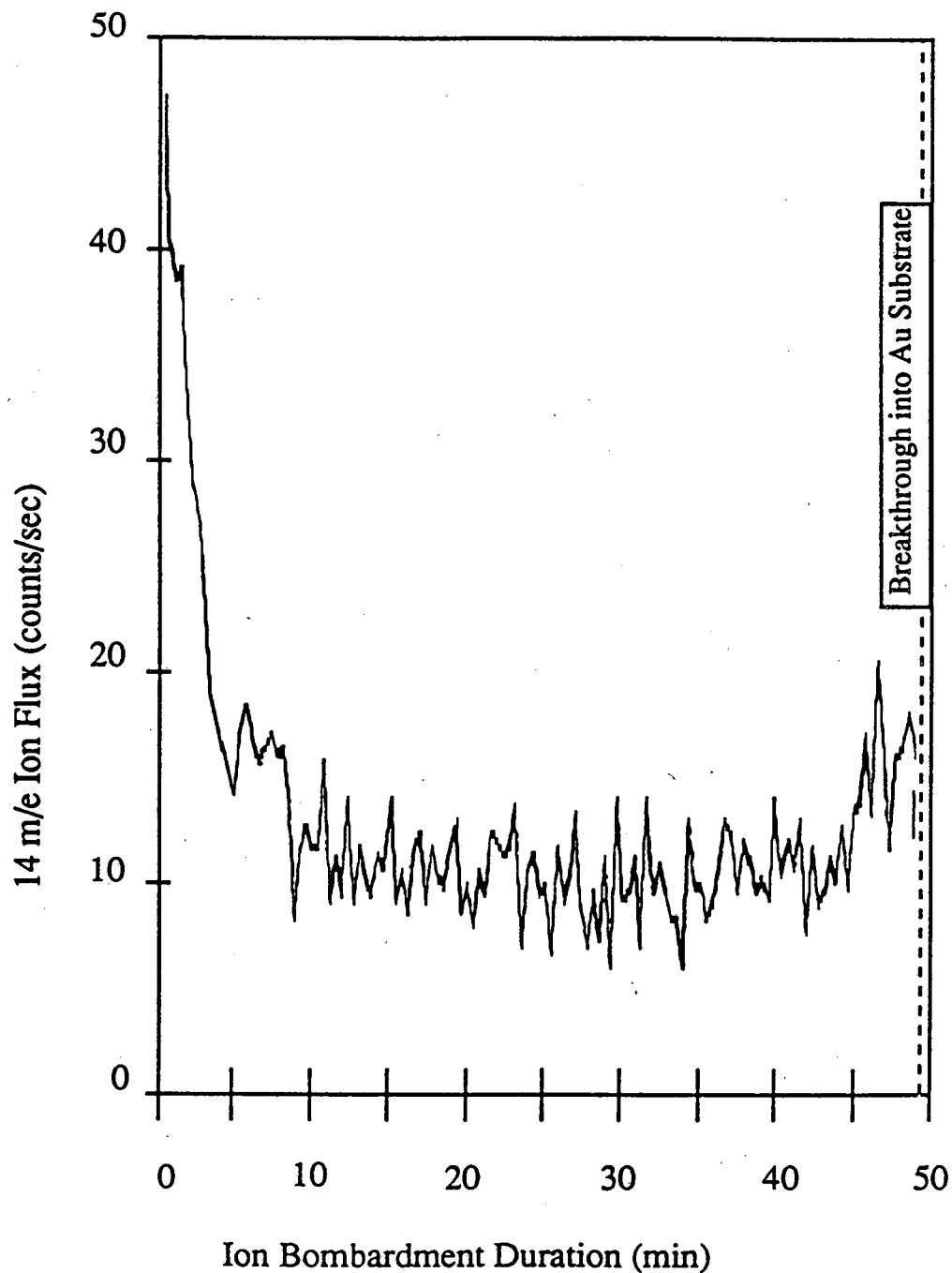
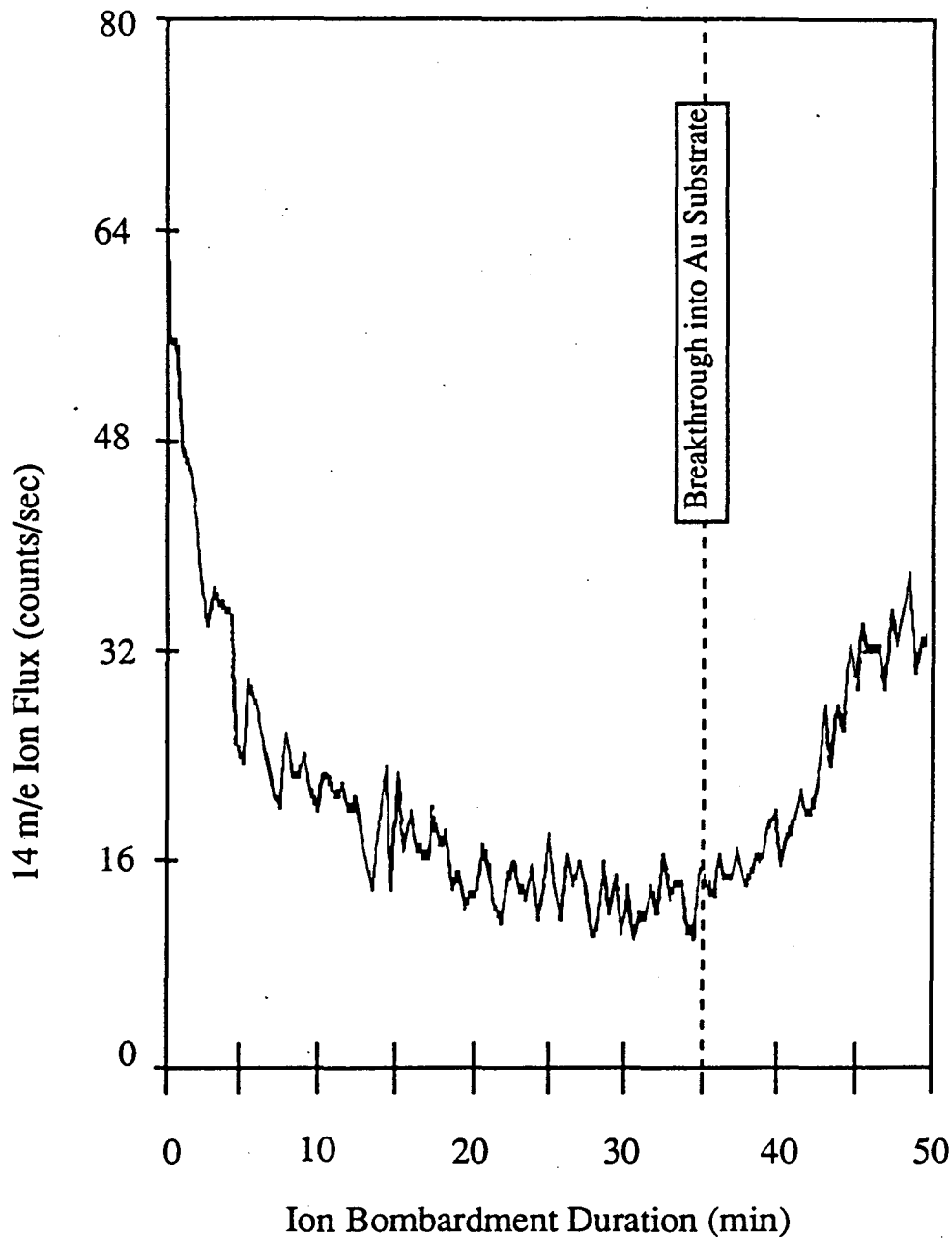


Figure 3.22. Amplitude of the 14 m/e signal during SIMS as a function of ion bombardment duration from a 10 mA/cm^2 modulated boundary layer deposit in BTA free electrolyte. Breakthrough into the Au substrate, as indicated by an increase in the amplitude of the 197 m/e (Au) signal, occurs following 48 min of ion bombardment. There are no modulations in the N content corresponding to the changes in rotation rate of the substrate. (XBL 902-586)

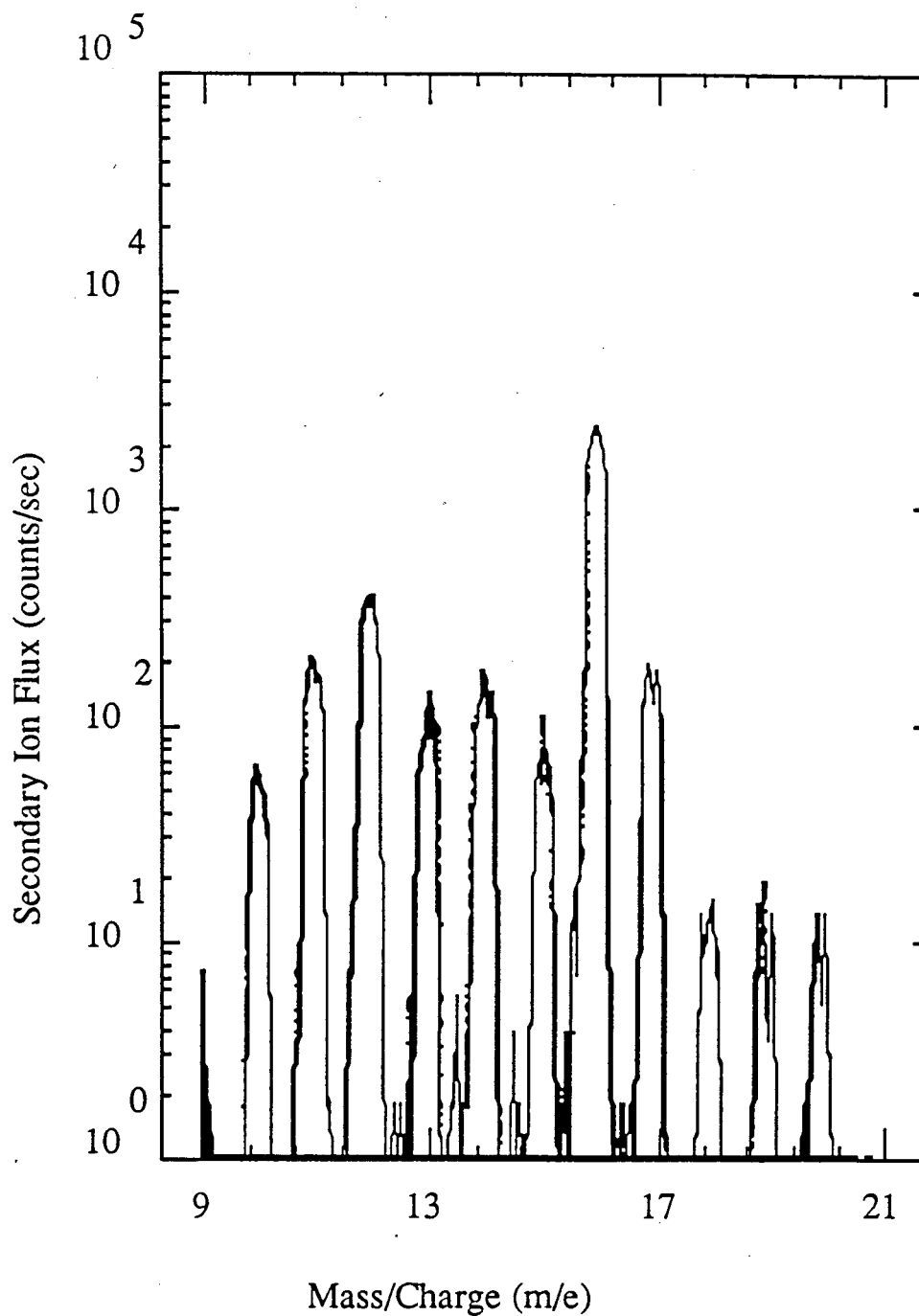


XBL 902-582

Figure 3.23. Amplitude of the 14 m/e signal during SIMS as a function of ion bombardment duration from a 10 mA/cm^2 modulated boundary layer deposit in $100 \mu\text{M}$ BTA electrolyte. Breakthrough into the Au substrate, as indicated by an increase in the amplitude of the 197 m/e (Au) signal, occurs following 35 min of ion bombardment. There are no modulations in the N content corresponding to the changes in rotation rate of the substrate. (XBL 902-582)

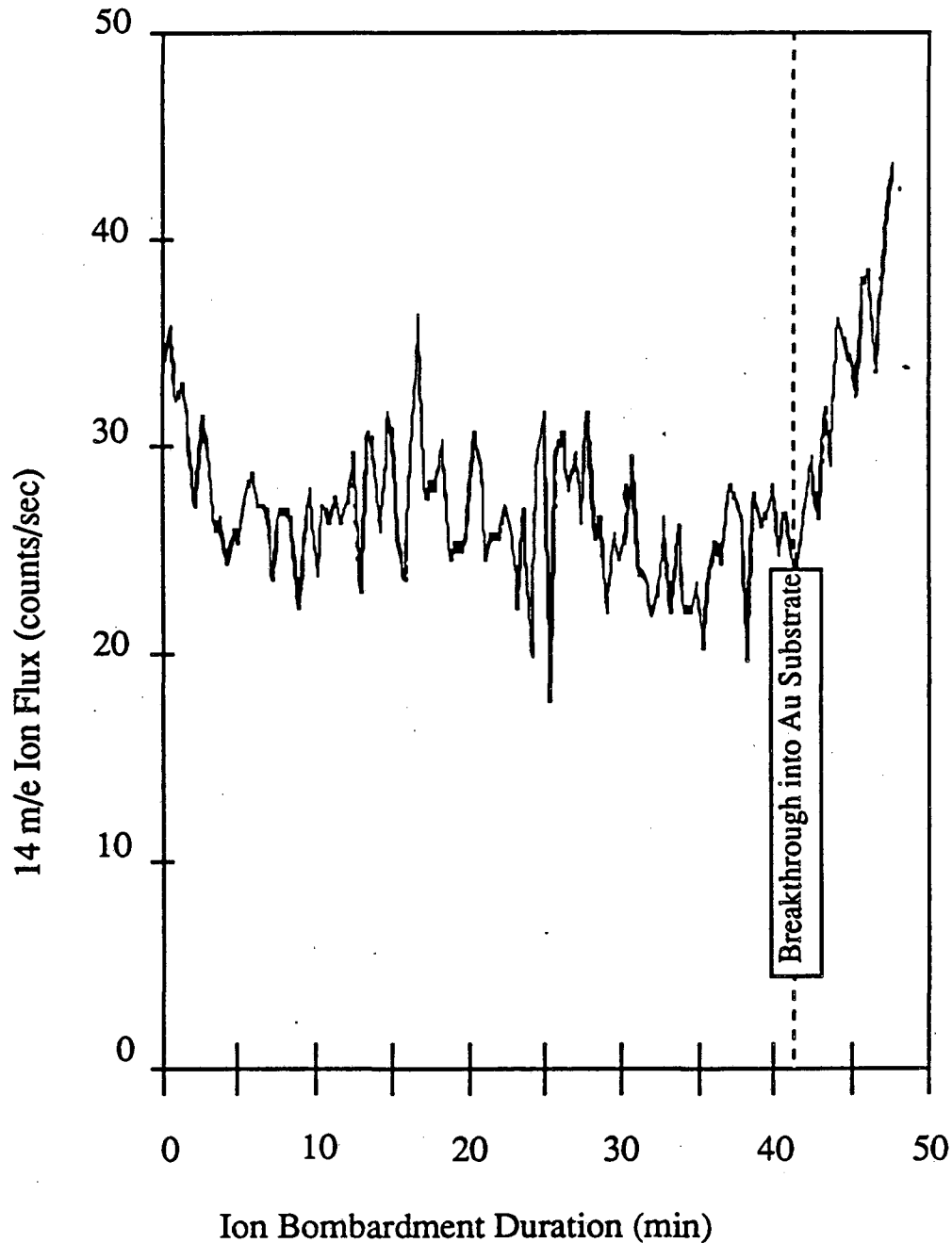
A concentration of $100 \mu\text{M}$ N in the electrolyte would be expected in the worst case of 10 ppm N in the salt. The nitrogen content of the BTA containing electrolyte was $300 \mu\text{M}$ from BTA and $100 \mu\text{M}$ from the CuSO_4 salt. Background nitrogen in the ultrahigh vacuum chamber was negligible. Another source of the 14 m/e peak is from doubly ionized Si. Doubly ionized Si will have peaks at 14, 14.5, and 15 m/e at the isotopic ratios of 0.923, 0.0468, and 0.0305 respectively. Figure 3.24 is from a high resolution mass survey of 0 to 30 m/e from copper deposited as above. The survey shows peaks at 14 and 15 m/e at comparable count rates and a count rate at 14.5 m/e of at most 0.01 of the peak at 14 m/e. These ratios are not in accordance with those expected for the Si isotopes. The ratio of 14 to 63 m/e signals was 3 times higher in the deposit from BTA containing electrolytes compared with no BTA in electrolyte. This ratio is approximately the same as the change in N content of the electrolyte and may be an indication that the incorporation of BTA is by occlusion of electrolyte between copper grains. In addition nitrogen was not detected on the deposit surface following ion bombardment by Auger electron spectroscopy (AES) or X-ray photoelectron spectroscopy (XPS). The sensitivity of the AES and XPS techniques are 1 and 0.1 % of a monolayer respectively.

Figure 25 shows the 14 m/e count rate during depth profiling of a 4000 Å deposit of which the first 2000 Å were formed at $20 \text{ mA}/\text{cm}^2$ and the last 2000 Å were formed at $10 \text{ mA}/\text{cm}^2$. Breakthrough into the Au substrate, as indicated by an increase in the amplitude of the 197 m/e (Au) signal, occurs following 48 min of ion bombardment. There are no modulations in the N content corresponding to the changes in current or rotation rate of the substrate. In addition following each 1000 Å of deposit the rotation rate was changed between 200 and 1800 rpm. Figure



XBL 902-587

Figure 3.24. High resolution survey of 8 to 22 m/e from a 10 mA/cm² modulated boundary layer deposit in 100 μM BTA electrolyte. There is no peak at 14.5 m/e corresponding to doubly charged Si²⁹. (XBL 902-587)



XBL 902-585

Figure 3.25. The count rate of 14 m/e during SIMS depth profiling of a 4000 Å deposit of which the first 2000 Å were formed at 20 mA/cm² and the last 2000 Å were formed at 10 mA/cm². Breakthrough into the Au substrate, as indicated by an increase in the amplitude of the 197 m/e (Au) signal, occurs following 42 min of ion bombardment. There are no modulations in the N content corresponding to the changes in current or rotation rate of the substrate. (XBL 902-585)

3.26 shows the current and rotation rate during deposition. There is no periodicity or inflection in the 14 m/e count rate from either changes in rotation rate or current density.

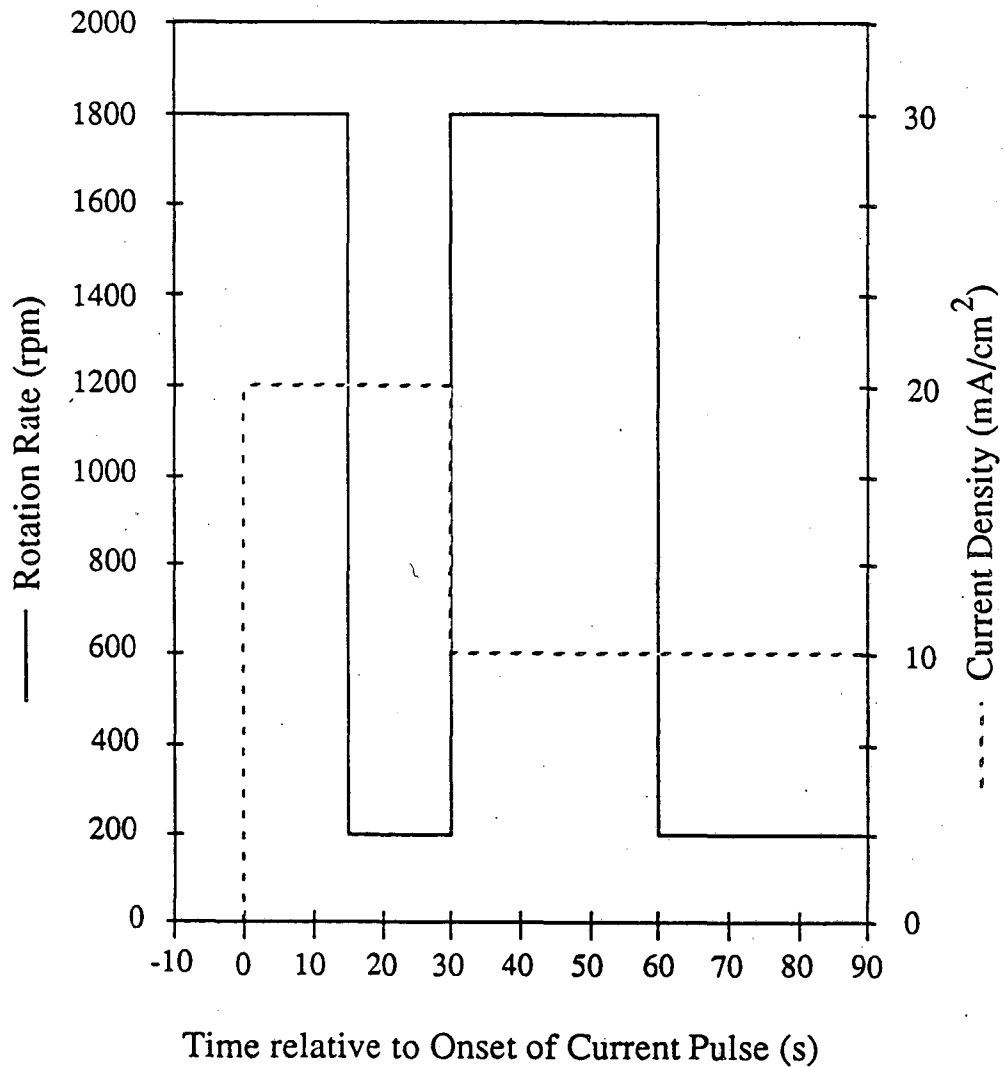
From these experimental results it is apparent that the incorporation rate is very small and that there is no dependence of incorporation rate on transport conditions or on current density.

3.4. Inhibition of Copper Reduction

3.4.1. Deposition rate as a function of potential and BTA concentration

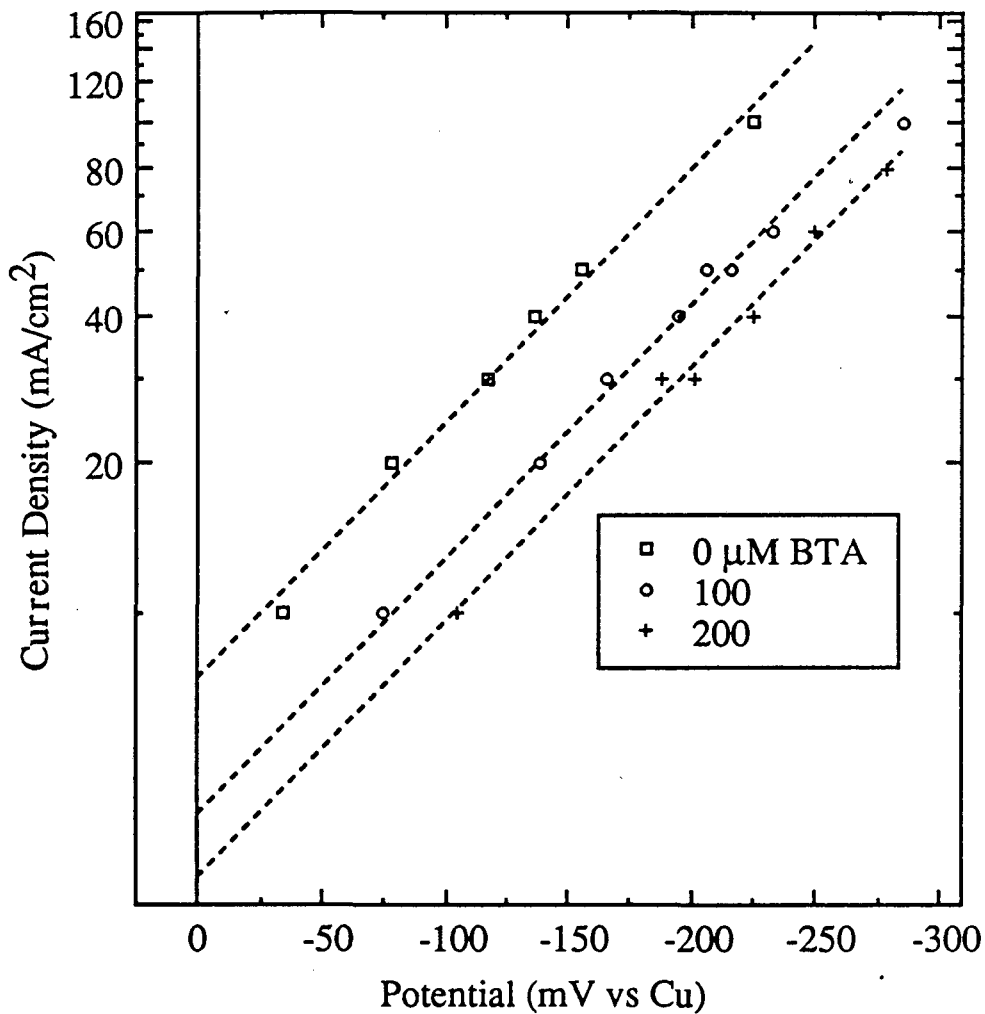
The most often cited mechanism of leveling and brightening is based on a concentration gradient of inhibitor between recesses and peaks of the surface. The presence of a concentration gradient of inhibitor at a rough surface results in a higher coverage of inhibitor on protrusions than in recesses. The ability of an inhibitor to brighten is then related to the dependence of the deposition kinetics on the inhibitor concentration. In this experiment the dependence of kinetics of copper reduction on the BTA concentration was measured.

Figure 3.27 is a Tafel plot of the dependence of current on potential for electrolytes with 0, 100, and 200 μM BTA. The potentials have been corrected for ohmic drop, R_{Ω} , of 2.3 Ω determined from impedance of the cell at 20 kHz.



XBL 902-608

Figure 3.26. Rotation rate and current density as a function of time during deposition of a 4000 A deposit of which the first 2000 A were formed at 20 mA/cm² and the last 2000 A were formed at 10 mA/cm². (XBL 902-608)



XBL 902-610

Figure 3.27. Tafel plot of the potential-current relationship for Cu deposition from 0.5 M H₂SO₄, 0.5 M CuSO₄, with 0, 100, and 200 μM BTA. Rotating disk, 700 rpm. Potential corrected for a 2.3 Ω ohmic drop through the cell. (XBL 902-610)

A comparison of measurements at a disk rotation rate of 700 and 175 rpm was made in order to establish whether there is a relation between mass transfer conditions and the kinetics. Figure 3.28 is a plot of measured potentials at 20, 30, and 40 mA /cm² for both 700 and 175 rpm. There is no dependence of the current-voltage behavior on rotation rate under these conditions which indicates that the concentration of BTA at the surface does not change. Prall and Shreir [3.2] have measured the BTA inclusion content of copper deposits under many conditions. Their results show an incorporation rate which is less than 1/5 of the diffusion limited supply in a solution containing 0.5 M CuSO₄, 0.5 M H₂SO₄, and 200 μM BTA. In addition they report virtually the same BTA inclusion content for current densities ranging from 2.5 to 40 mA /cm².

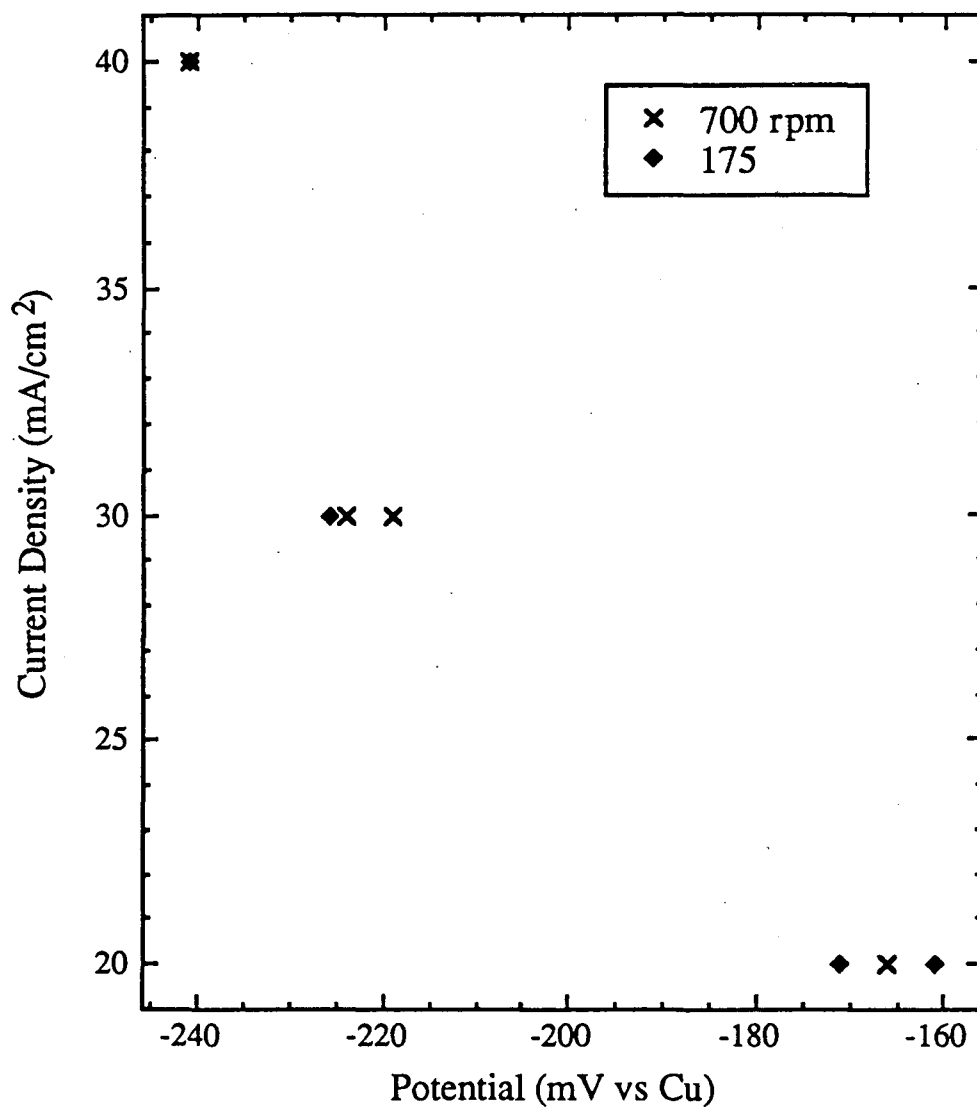
A Tafel slope of 200 mV per decade was measured at all BTA concentrations. The parallel Tafel plots indicate that the reaction mechanism is not affected by the presence of BTA. This Tafel slope corresponds to $\alpha_c = 0.3$ in the Butler Volmer equation

$$i = i_0 \left(\exp\left(\frac{\alpha_a RT \eta}{F}\right) - \exp\left(\frac{-\alpha_c RT \eta}{F}\right) \right) \quad (11)$$

where i is the current density, i_0 is the exchange current, α_c is the cathodic transfer coefficient, α_a is the anodic transfer coefficient, R is the gas constant, T is the temperature, F is Faradays constant, and η is the overpotential. A α_c of 0.5 is widely used in the literature. The overpotential, η , is defined by

$$\eta = V - V_{cu} - IR_{\Omega}$$

where V is the potential of the electrode, V_{cu} is the potential of copper in equilibrium with the solution, I is the current through the solution, and R_{Ω} is the



XBL 902-609

Figure 3.28. The effect of rotation rate on the measured potentials for Cu deposition from 0.5 M CuSO₄, 0.5 M H₂SO₄ for current densities of 20, 30, and 40 mA/cm². (XBL 902-609)

solution resistance. In order to obtain a α_c of 0.5 a value of $R_\Omega = 3.5$ must be assumed.

Table 3.4 tabulates the measured exchange current, i_0 , and the BTA coverage, θ_i , where $1-\theta_i$ is determined by the ratio of i_0 in BTA containing electrolyte to i_0 in BTA free electrolyte.

The different measured current-potential relationship for BTA free and BTA containing electrolytes can be interpreted in terms of the surface coverage by BTA. Assuming that negligible current passes on the fraction of surface covered by BTA, the total current is proportional to the BTA free surface. Since there was no noticeable effect of the rotation rate on the measured current, the BTA concentration at the surface is assumed to be the bulk concentration of BTA. Da Costa et al. [3.8] measured a Langmuir adsorption coefficient for BTA on Cu of $K = 8.8 \times 10^3 \text{ l/M}$ from weight loss measurements of copper coupons in BTA solutions. The BTA coverage derived from the measured exchange current compares favorably with the coverage calculated with the adsorption coefficient above (table 3.4).

3.4.2. UPD of Cu on Pt as a function of BTA Concentration

The deposition of a metal on a foreign substrate frequently occurs with a monolayer depositing anodic of E_0 for that metal. This phenomenon is referred to as a underpotential deposit, UPD. The charge passed for this first layer is usually represented by peaks in dQ/dV separated over a wide range of potential. The

BTA Concentration (μM)	Exchange Current (mA/cm^2)	BTA Coverage	BTA Coverage using Langmuir Adsorption with $K=8.8 \times 10^3 \text{ M}^{-1}$
0	7.0	0	0
100	4.1	0.41	0.47
200	2.8	0.60	0.64

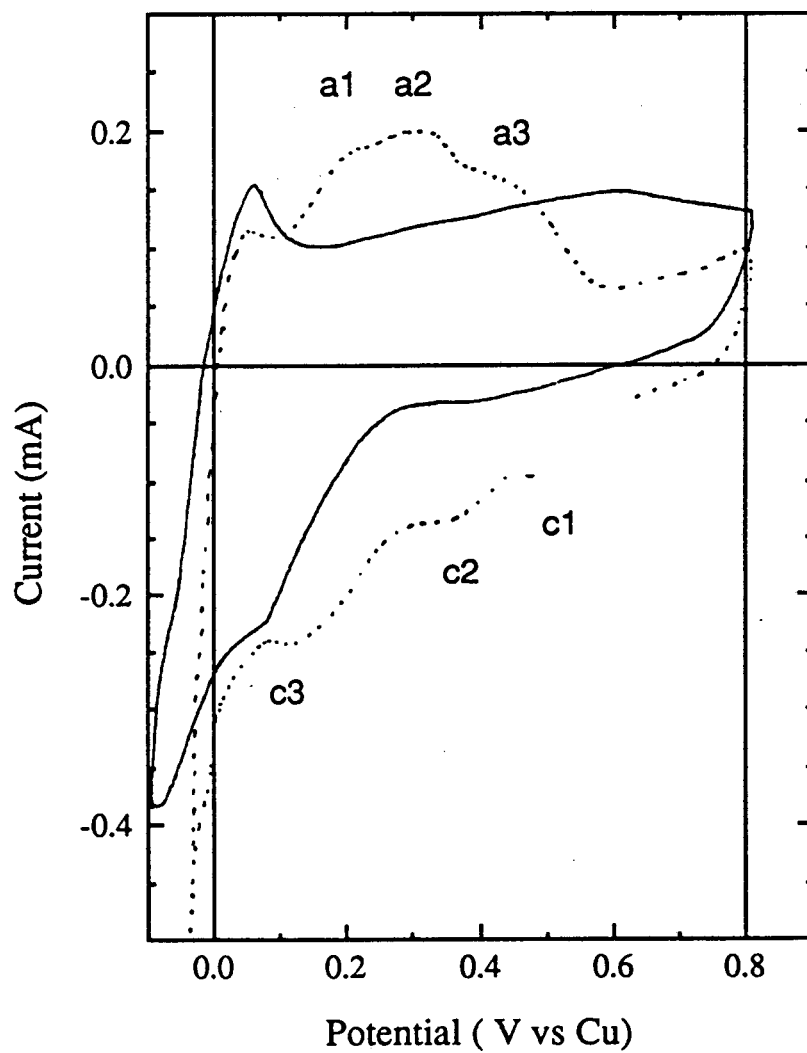
Table 3.4. Exchange current for Cu deposition and derived BTA coverage for a Cu electrode in 0.5 M CuSO_4 , 0.5 M H_2SO_4 with 0, 100, and 200 μM BTA. Also tabulated is the calculated BTA coverage at each BTA concentration using a Langmuir adsorption coefficient of $8.8 \times 10^3 \text{ l/m}$ [3.7].

separated maxima of dQ/dV have been associated to the coverage of the surface by plane, step, and kink sites [3.9]. The UPD of Cu on Pt was followed to determine whether there is any specific inhibition of the various sites by BTA.

The UPD of Cu on Pt in BTA free electrolyte and following addition of 10 μM BTA is shown in figure 3.29. The UPD in BTA free electrolyte has three peaks in current in the anodic sweep and two peaks in current in the cathodic sweep. Following addition of the 10 μM BTA only one cathodic peak and two anodic peaks appear and a 40% reduction in the charge passed between 0.8 and 0.0 V. In addition the potential of the most cathodic UPD peak occurs 110 mV cathodic of the corresponding peak in BTA free electrolyte.

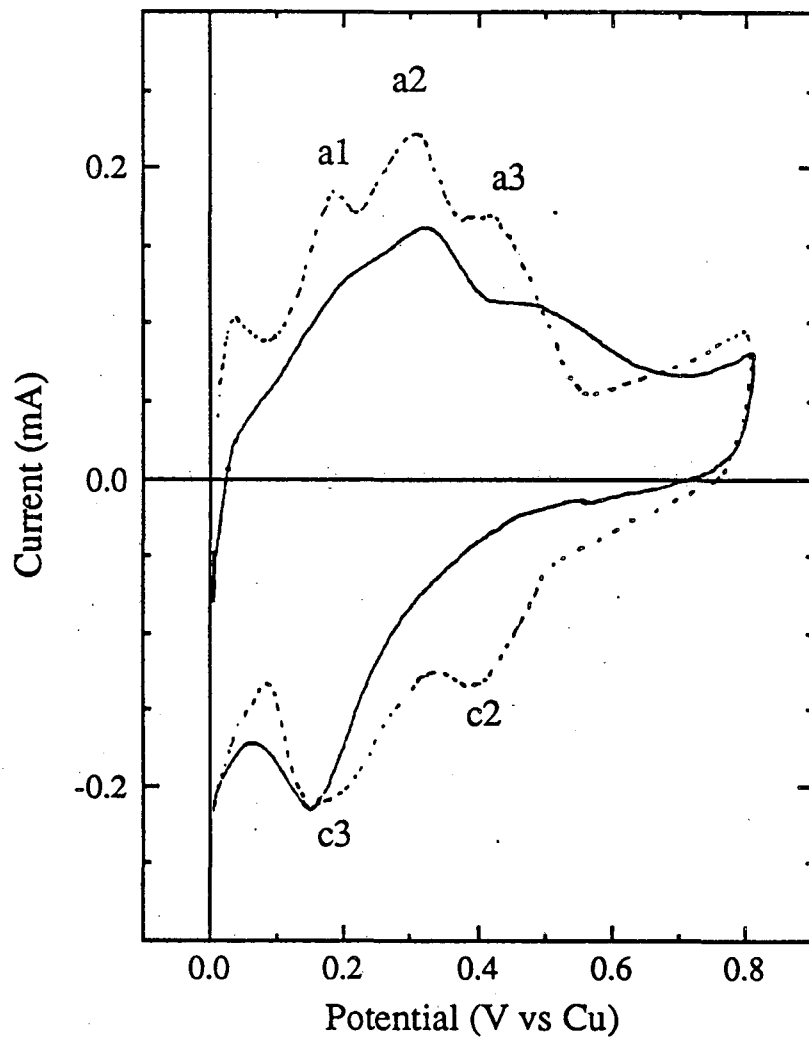
With 1 μM BTA all three anodic current peaks occur with the two most cathodic peaks, a1 and a2 of figure 3.30, at approximately the same potential as without BTA. The third anodic peak, a3, is shifted more anodic by approximately 70 mV.

The first conclusion from these experiments is that BTA strongly blocks portions of the Pt surface preventing Cu deposition. Secondly the change in the distribution of charge in the cathodic sweep from two separated UPD peaks to a single peak indicates a preferential inhibition of the most favorable deposition sites on the Pt electrode resulting in a uniform nucleation energy over the surface.



XBL 902-605

Figure 3.29. UPD of Cu on Pt in BTA free electrolyte, ---, and following addition of 10 μ M BTA, —. (XBL 902-605)



XBL 902-606

Figure 3.30. UPD of Cu on Pt in BTA free electrolyte, ---, and following addition of 1 μM BTA, —. (XBL 902-606)

3.5. Micro Topography

3.5.1. Growth of Copper Deposits

The following experiment was performed to investigate the continued growth of Cu films on Pt following nucleation. The composition of the electrolyte was 10 mM $\text{Cu}(\text{ClO}_4)_2$, 0.5 M NaClO_4 , and 0.1 M HClO_4 with and without 10 μM BTA.

A thick deposit of Cu from BTA free electrolyte was formed with a 30 sec pulse to -500 mV vs Cu with the tip removed from the surface. Following the pulse the potential was stepped to -25 mV vs Cu at which time continuous scanning of the surface by the tunneling probe began. The deposit from BTA-free electrolyte had long range order exceeding the width of the probe scan, 0.6 μm (fig. 3.31). These deposits were faceted with deposition observed at the edges. Short period roughness resulting from new nucleation is shown in the bottom right corner of figure 3.31b. Although rapid growth is observed in some areas of the electrode little change occurs in others, this can be seen by comparing the top and bottom portions of figures 3.31a and 3.31b. Nonuniform deposition of copper is also seen for deposition on Cu free Pt at low overpotentials. At low overpotentials three dimensional growth centers of copper develop next to regions of bare Pt. The deposit from electrolyte containing 10 μM BTA was initiated with a 0.5 sec pulse to -500 mV vs Cu. The tip was at tunneling distance from the surface during the initial pulse. Following the 0.5 sec pulse the potential was stepped to -20 mV vs Cu. Before Cu deposition the bare Pt surface showed a stepped appearance with 20 Å ledges and atomically flat planes in between (fig. 3.32a). Following the initial

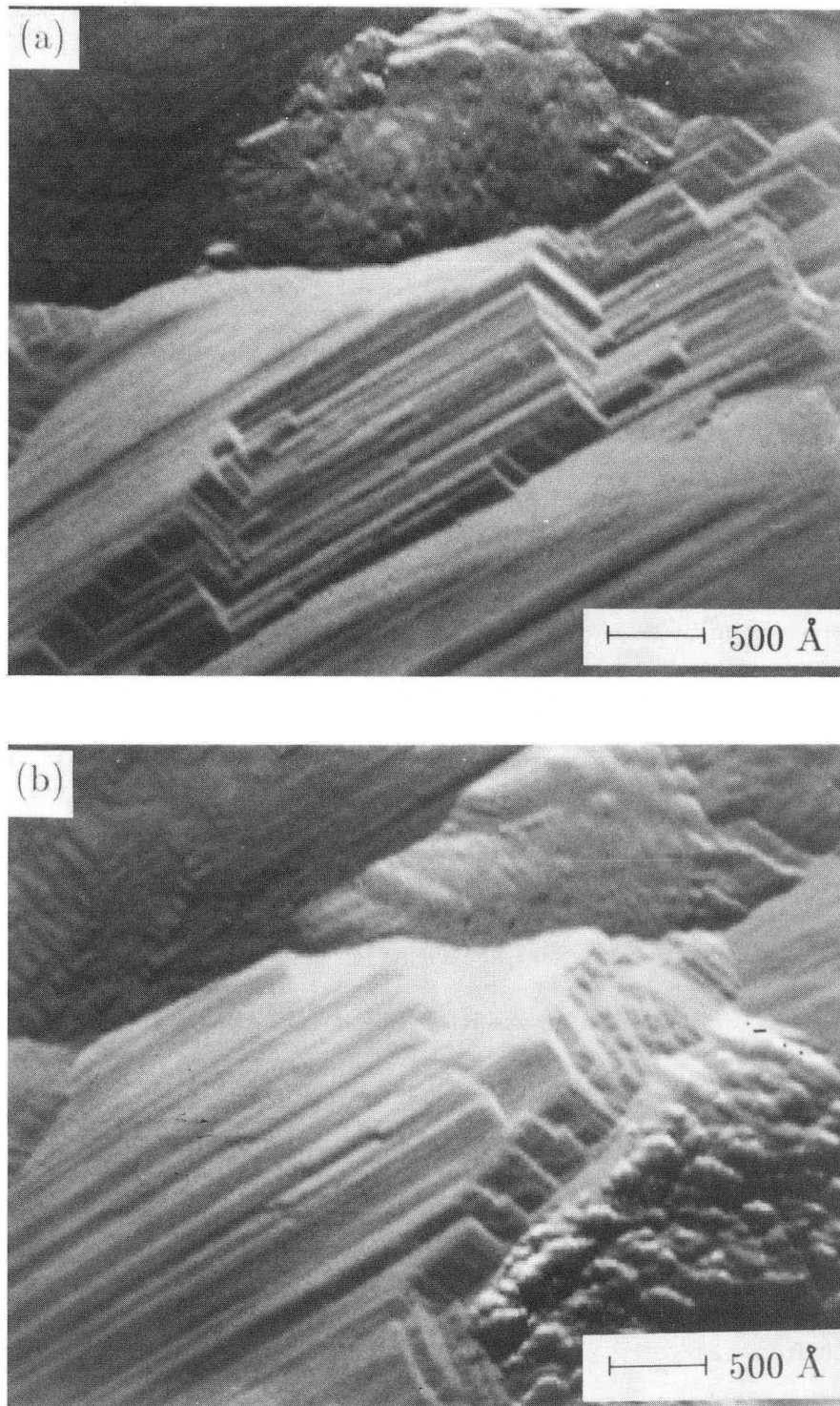


Figure 3.31. STM of a Cu deposit formed by a 30 s pulse to - 500 mV followed by a step to -25 mV vs Cu in BTA free electrolyte. a) initial deposit and b) following 30 seconds at -25 mV vs Cu. Shows propagation of crystal facets (20 Å height) from lower left corner of a) to center of b). (XBB 880-11214 Å)

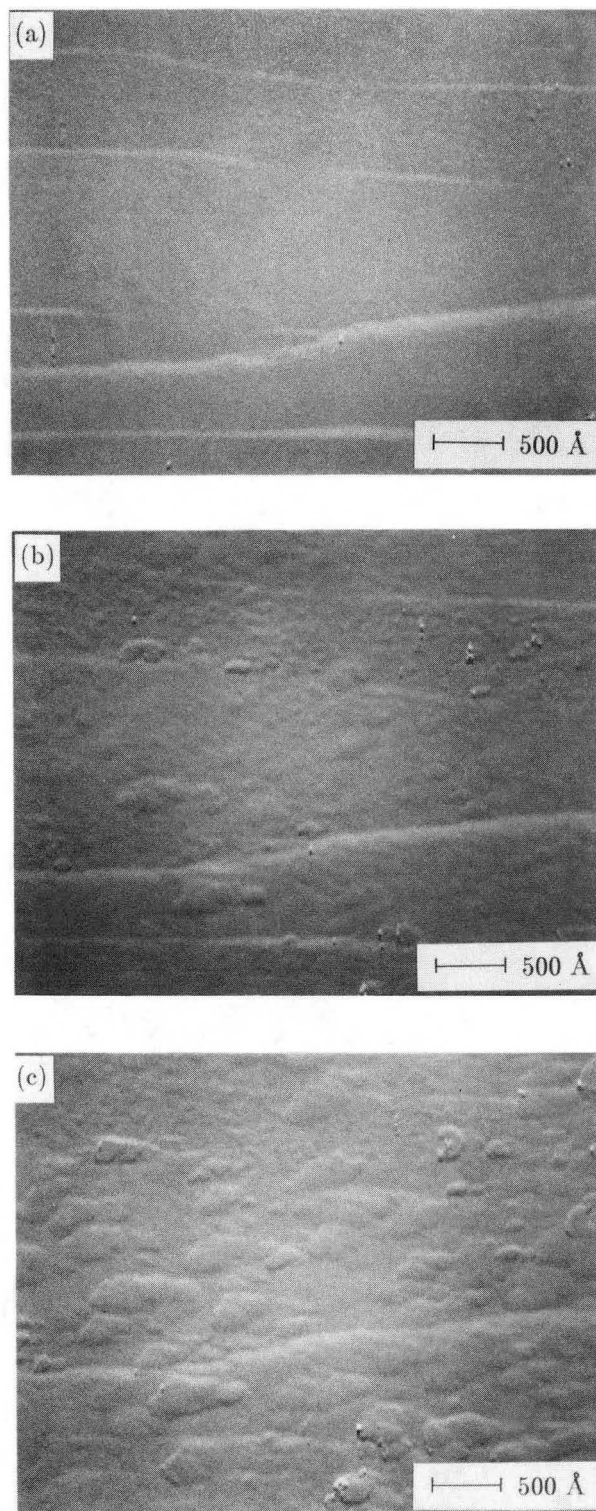


Figure 3.32. STM of a Cu deposit formed by a 0.5 s pulse to -500 mV followed by a step to -25 mV vs Cu in 10 μ M BTA, (a) Pt substrate, (b) 30 s after pulse, and (c) 90 s after pulse. Shows formation of 200 Å diameter islands of 5 Å height (b) and growth to 20 Å height (c). (XBB 880-11212 A)

pulse, deposition on the Pt planes resulted in a wavy surface with a period of approximately 200 Å and an amplitude of 5 Å (fig. 3.32b). This waviness is proposed to represent the island growth of the first two monolayers of deposit. Following further deposition, the development of larger oblong nuclei of approximately 20 Å height occurs. Unlike the BTA-free deposit (fig. 3.31), the deposit from the BTA-containing electrolyte was not faceted and did not have long range order (fig. 3.32b,c).

The propagation of edges and the long range order of the deposit from a BTA-free electrolyte indicates growth in preferred crystallographic directions. This preference is prevented by the action of BTA and random growth occurs. In the presence of BTA the Cu deposit develops from atomic height nuclei which coalesce into larger entities.

3.5.2. Nucleation Density

The following measurements were performed to determine the nuclei density of Cu on Pt in 50, 100, and 200 μM BTA. The nuclei density was measured following deposition of 15 C/cm² of Cu. A deposit thickness of 54 Å is expected assuming a compact layer of Cu.

Figure 3.33 is a derivative image of the Pt substrate. The substrate had rms roughness of 30 Å over a 3400 Å path across the surface. The substrate consisted of planes of less than 100 Å terminated with 10 to 30 Å steps. Figure 3.34, curve b, is a FFT of the substrate surface. The amplitude of the frequency components of the

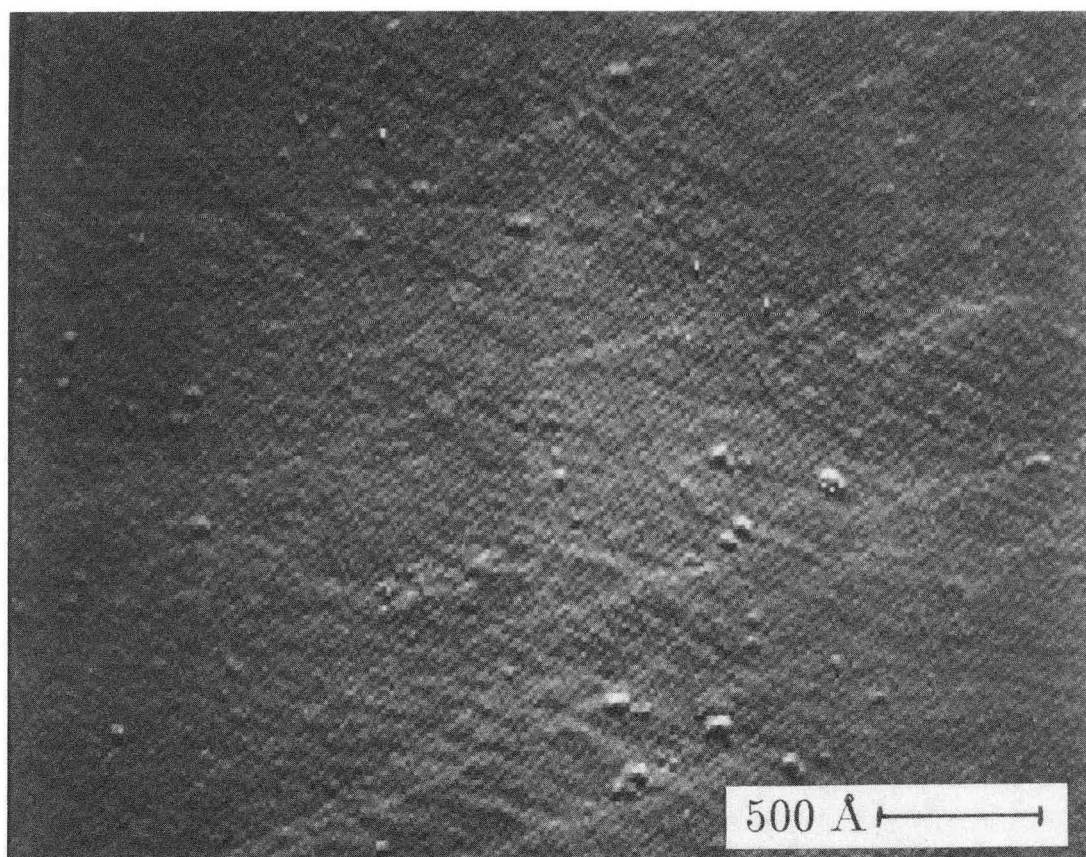
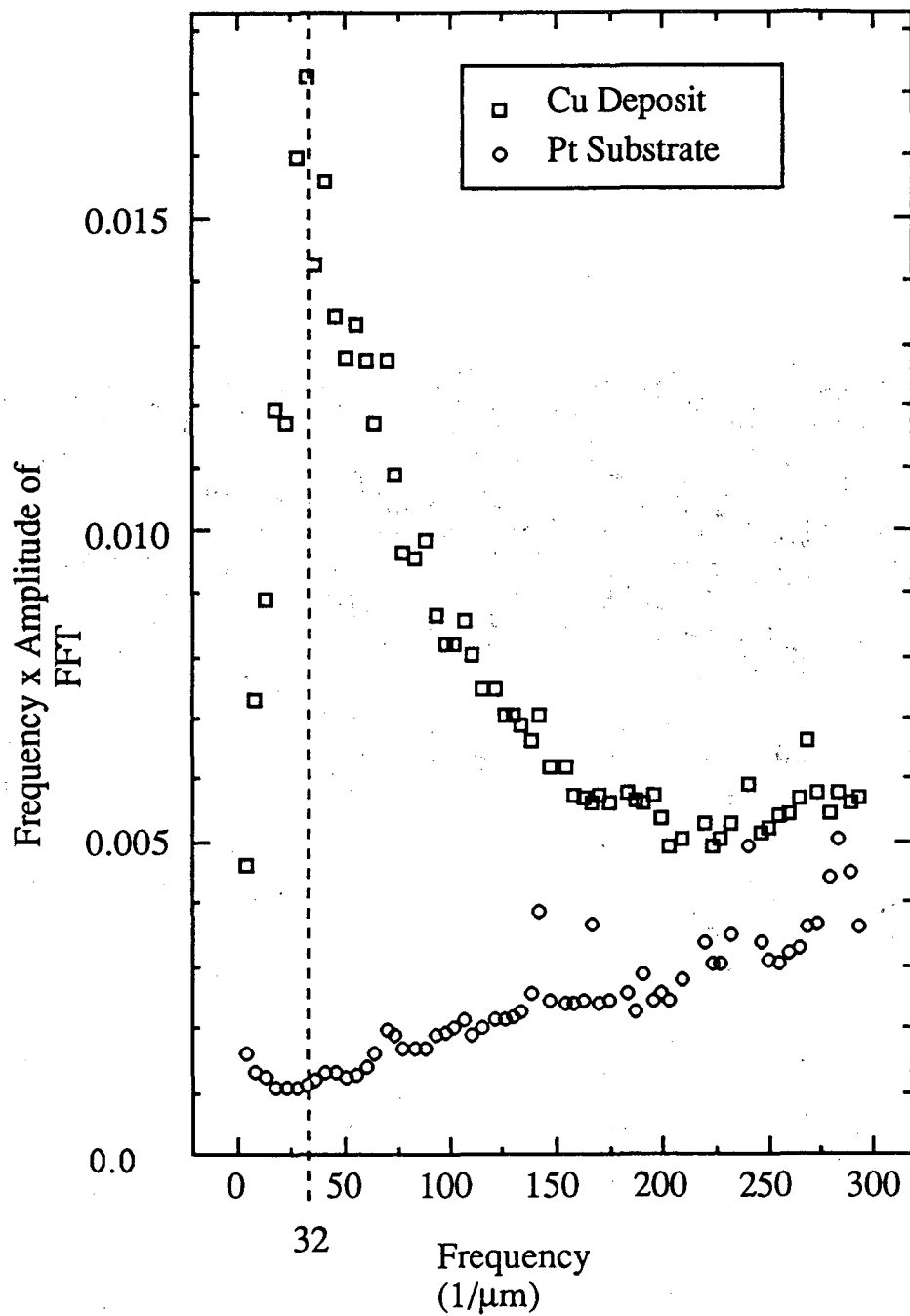


Figure 3.33. Grey scale image of $\frac{dz}{dx}$ of an annealed Pt substrate. The surface consist of 100 Å terraces terminated with 10 to 30 Å steps. There are a small number of protrusions on the surface. (XBB 901-555)



XBL 902-572

Figure 3.34. FFT of the probe height with respect to distance in the scan direction of (a) Cu deposit and (b) the underlying Pt substrate. The Cu deposit was formed with a 100 mA/cm^2 pulse for 200 ms from 0.5 M CuSO_4 , $0.5 \text{ M H}_2\text{SO}_4$, and 100 μM BTA . $32/\mu\text{m}$ corresponds to $9.8 \times 10^{10} \text{ nuclei/cm}^2$. (XBL 902-572)

FFT of the substrate was small compared to that for a nucleated deposit, figure 3.34, curve a.

Figure 3.35 is a derivative image of a deposit from electrolyte containing 100 μM BTA at an overpotential of 0.58 V vs Cu. The nuclei in figure 3.35 appear spherical in shape, have an average radius of 118 Å, and have a nuclei density of 7.5×10^{11} nuclei/cm² within the boundaries of a $0.029 \mu\text{m}^2$ area in the center of the figure. The peak value of the product of FFT amplitude and frequency from the data of figure 3.35 occurs at a wavelength, ω_n , of 320 Å. The nuclei density determined from the Fourier transformed data was 0.98×10^{11} nuclei/cm² as approximated by $N_d = \frac{1}{\omega_n^2}$ assuming the ω_n corresponds to the characteristic separation of nuclei on the surface. Comparison of the results of nuclei density from direct counting of nuclei to the use of Fourier transformed data compares with the scatter of the FFT nuclei density measurements. The nuclei densities reported in figure 3.36 are determined from FFT of STM data.

The nuclei density shows an upward trend with increasing η with no significant difference between electrolytes containing 0, 50, 100, and 200 μM BTA (fig. 3.36). This result indicates that the nucleation site density on the Pt surface is dependent only on the overpotential and is independent of the presence of BTA. On the assumption that the nucleation site density of copper is similarly unaffected by the presence of BTA, the following conclusion can be made. The reduction in bulk deposit grain size with increasing BTA concentration at constant current density is due to an increase in the density of active nucleation sites at the increased overpotential required in the presence of BTA.

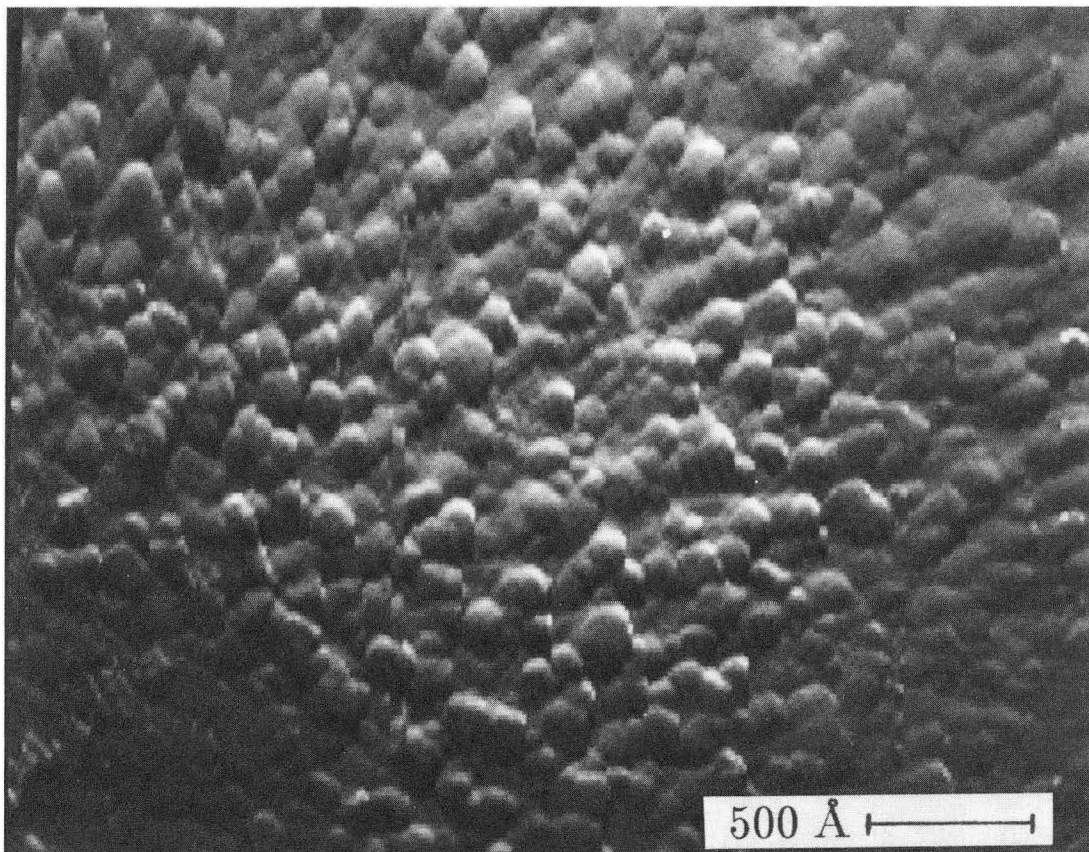


Figure 3.35. Grey scale image of $\frac{dz}{dx}$ of a 20 mC/cm^2 Cu deposit on Pt (shown in figure 3.36) from 0.5 M CuSO_4 , $0.5 \text{ M H}_2\text{SO}_4$, and $100 \mu\text{M BTA}$. The deposit was formed by a 100 mA/cm^2 pulse. FFT of the deposit contour indicates the nuclei have a periodicity of 320 \AA (9.8×10^{10}). (XBB 901-554)

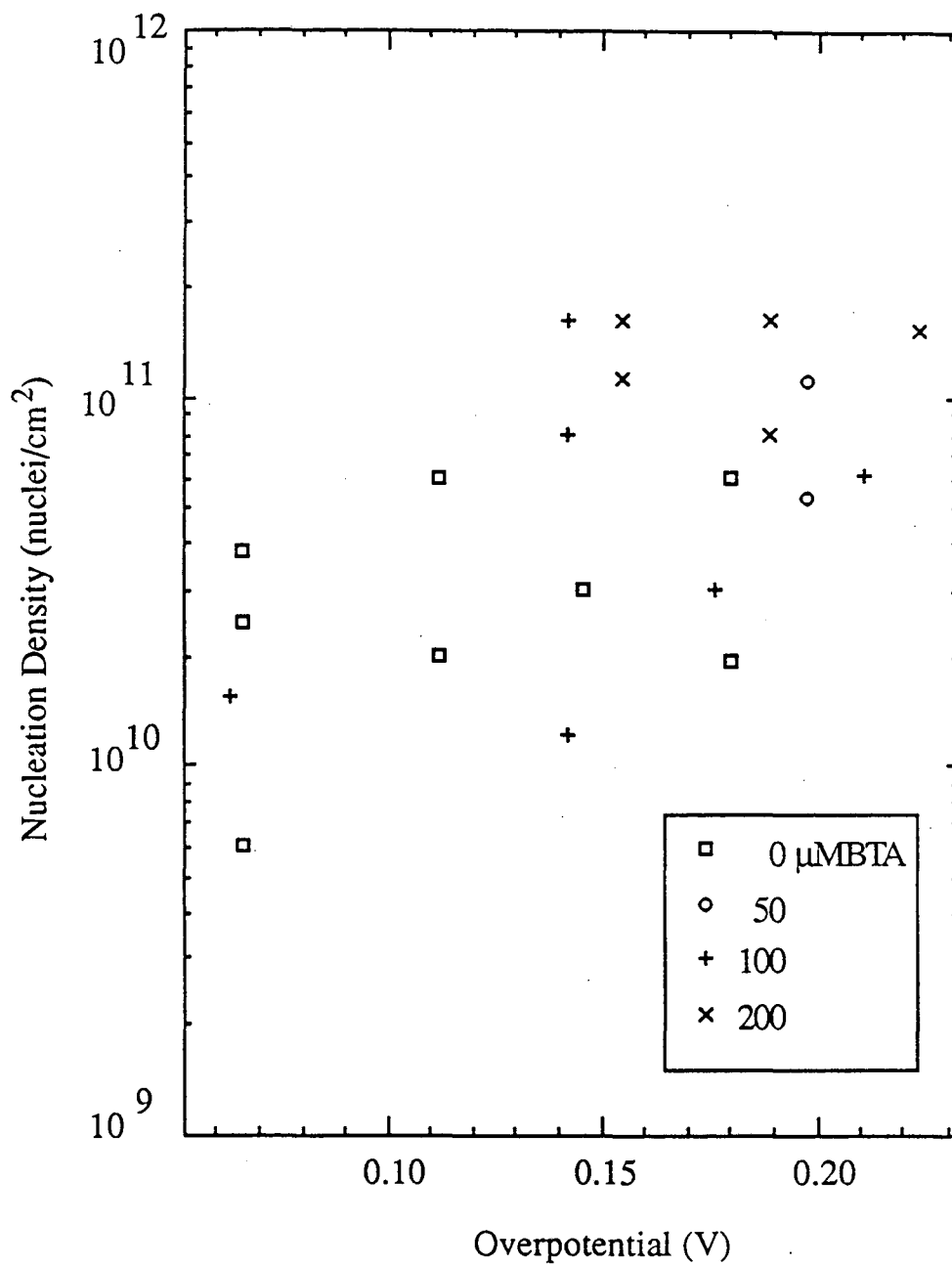


Figure 3.36. Nuclei density of BTA inhibited copper deposition on Pt $\langle 110 \rangle$, □ 0, ○ 50, + 100, and × 200 μ M BTA. (XBL 902-607)

References

- [3.1] J. C. Farmer and R. H. Muller, "Effect of Rhodamine-B on the Electrodeposition of Lead on Copper", *J. Electrochem. Soc.*, 132 (1985) 313
- [3.2] J. K. Prall and L. L. Shreir, "A Study of Benzotriazole as an Addition Agent for Acid Copper Sulphate Solutions", *Trans. Inst. Metal Finishing*, 41, 29 (1964)
- [1.3] O. Kardos and D.G. Foulke, "Applications of Mass Transfer Theory: Electrodeposition on Small-Scale Profiles", in *Advances in Electrochemistry and Electrochemical Engineering*, Vol 2, C.W. Tobias Ed., Interscience, New York, 1962
- [3.4] R. Morris and W. Smyrl, "Rigorous Treatment of Rotating Disk Electrode Impedance Data Over the Entire Frequency Range", *J. Electrochem. Soc.*, 137 (1990) 406
- [3.5] A. J. Bard and L. R. Faulkner, "Electrochemical Methods", John Wiley & Sons, USA, 1980, pp. 323-327
- [1.6] U. Bertocci and D.R. Turner, *Copper in Encyclopedia of Electrochemistry of the Elements* (A. J. Bard editor), Vol. 2, p 384, Marcel Dekker Inc., New York (1974)
- [3.7] S. L. F. A. DaCosta, J. C. Rubim, and S. M. L. Agostinho, "Spectroelectrochemical Study of the Corrosion of a Copper Electrode in Deaerated 1.0 M HCl Solutions Containing Fe(III) Effect of the Corrosion Inhibitor Benzotriazole", *J. Electroanal. Chem.* 220 (1987) 259

[3.9] A. Hamelin, "Underpotential Deposition of Lead on Single Crystal Faces of Gold. Part 1. The Influence of Crystallographic Orientation of the Substrate", *J. Electroanal. Chem.*, 165 (1984) 167

Chapter 4. Conclusions

In the following section a summary of conclusions from the experimental work will be presented. In addition areas of research will be suggested for future study.

4.1. Nucleation and Growth Phenomena

There is evidence in the SEM and STM images of copper deposited at a constant current, of a decrease in the deposit particle size upon addition of BTA to the plating electrolyte. Scanning electron microscopy of 2.4 μm thick copper deposits showed a decrease in the particle size with increase in the concentration of BTA. The characteristic length of particles in the plane of deposits formed at 50 mA/cm^2 was approximately 1 μm without BTA and less than 0.05 μm with 100 μM BTA. Scanning tunneling microscopy of Cu deposits nucleated on Pt indicated the same nuclei density at a given overpotential for electrolytes containing between 0 and 200 μM BTA. This result indicates that the nucleation density is dependent only on the overpotential. The addition of the BTA results in a higher overpotential and nucleation site density at a given current density. The addition

of inhibitor to plating electrolytes results in deposition at a high overpotential at low current densities such that the nucleation site density is high and roughening due to transport restrictions is low.

Randomized growth of copper deposits from BTA containing solutions was also found to occur. Measurements of the underpotential deposition (UPD) of copper on platinum indicated that BTA reduced the site specificity of the metal deposition process. The UPD of Cu on Pt from BTA free electrolyte occurs across a large potential range with peaks in dQ/dV (measured as a current during cyclic voltammetry) which are associated with the various crystal orientations on the surface. With BTA added to the electrolyte the UPD of Cu on Pt merges into one peak of dQ/dV which indicates that in the presence of BTA each crystal face orientation has the same energy and will have the same kinetics for copper deposition.

4.2. Summary of Conclusions

The following information on the process of copper deposition in BTA containing electrolytes has been obtained:

- 1) The rate of BTA incorporation into copper deposits from solutions containing less than 200 μM BTA is much less than the mass transfer limited rate of supply for BTA. Brightening due to a BTA concentration gradient does not occur during deposition of copper from BTA containing electrolytes since the BTA concentration gradient is

negligible.

- 2) A passivating film develops on copper in BTA containing solutions at low overpotentials.
- 3) The growth habit of deposit particles is randomized in the presence of BTA. The growth character changed from angular particles to rounded upon addition of BTA.
- 4) The nucleation site density of Cu on Pt is dependent on the overpotential and not on the presence of BTA. The brightening of Cu deposits is due to an increase in the overpotential required for deposition in the presence of BTA.

4.3. Future Directions

In the following sections several directions are presented for further exploration of the deposition of copper from BTA containing solutions. In addition some ideas are presented for improving and understanding the operation of the tunneling microscope in electrochemical systems.

4.3.1. Copper - Benzotriazole System

Areas of interest include the nucleation rate of copper on copper and foreign substrates, the formation of copper-BTA films on the deposit, and the structure of adsorbed BTA and Cu-BTA films. Specific examples of possible experiments are

presented in the following paragraphs.

STM of the nucleation of copper on platinum was performed in this study. Platinum has a low nucleation overpotential for copper with the result of a high Cu nucleation rate and density. It would be of interest to study the nucleation of Cu on a high nucleation overpotential surface such as highly ordered pyrolytic graphite (HOPG). Fewer and larger Cu nuclei would occur on such a surface.

Cuprous-BTA films have been shown to form at low overpotentials and low current density by this study. Scanning tunneling microscopy of the film formation prior to bulk copper deposition may be possible. Imaging the formation of the films on an atomically resolvable surface such as HOPG will allow direct monitoring of the film build up at the atomic scale even if atomic resolution of the Cu^+ -BTA molecule may not be possible. The film build up will be evident by its effect on the STM image of the substrate.

Bulk Cu^+ -BTA film growth can be measured with ellipsometry. The growth of this film is important for determining the brightening mechanism of the Cu/BTA system. Roughening of a copper substrate due to corrosion is a problem during an ellipsometric measurement of the Cu^+ -BTA film on copper. The development of bulk Cu^+ -BTA film should be measured on an inert substrate such as Pt or Au. The effect of potential, current density, and electrolyte composition on the Cu^+ -BTA film would be important parameters for establishing operating conditions where brightening by Cu^+ -BTA precipitation would be in effect. The measurement of Cu^+ -BTA film on a growing deposit is made very difficult by the changing morphology of deposited Cu. If the deposit were liquid, surface tension forces would

result in a planer surface during deposition. The use of a copper amalgam electrode would provided a liquid surface which remains smooth during deposition. The film thickness of Cu-BTA can be monitored by ellipsometry on the mercury electrode. These measurements would be useful for determining the effect of current density and the electrolyte composition on the Cu-BTA film thickness.

Modeling of the solution chemistry at the electrochemical interface would be useful for optimizing the electrolyte composition and overpotential for bright deposition. The model would need to include the interaction of the electrolyte components and account for concentration gradients at the surface to determine the gradient in inhibition on a rough surface.

4.3.2. STM Technique

The image of a surface is affected by the shape of the probe used for the scan. An accurate representation of shape of the surface is obtained only in the limiting case of a probe consisting of a singular point. In the limiting case of a relatively flat probe and a very sharp feature on the surface, the recorded image is of the shape of probe tip. In the application of STM where the radius of the probe tip and radius of features on a surface are comparable, the recorded image of the surface features reflect the shape of the probe. A mathematical method should be developed for deconvoluting the probe shape in those instances where the apparent object shape is altered by the probe shape. Developing a method for deconvoluting probe and object shapes will be very important for studying the initial stages of

three dimensional nucleation.

The presence of the probe tip next to the surface in electrolyte changes the potential gradient and mass transport in the local area. Not only does the probe block transport of reactants to the surface, it changes the electric field and is a charged surface on which electrochemical reactions can occur. Modeling of the probe/electrolyte/sample region is necessary to evaluate the effects of the probe on electrochemical reactions in the imaged region.

Appendix A -- Impedance Spectroscopy Software

1. Introduction

Impedance spectroscopy is performed here by superimposing a multimode waveform, composed of sine waves, on the electrode potential and measuring the frequency dependence of the amplitude and phase of the the current response. The programs described in the following sections serve to generate a multimode waveform, control of a PAR 273 potentiostat [A.1], and performing a fast Fourier transform (FFT) of the collected data. The programs run on a IBM PS II computer with a National Instruments [A.2] GPIB communications board. A PAR 273 potentiostat is controlled by the computer with commands sent with the GPIB interface. The following subsections describe programs used for the impedance spectroscopy.

2. Multimode waveform -- MKCV (make curve)

The program MKCV generates a multimode waveform digitally represented by 1024 chronological steps (fig. 2.3). Each frequency in the curve has a different phase offset, at the origin, which is determined with a random number generator in

the program. The output file is programmed into the PAR 273 potentiostat as a source curve with the program HEADSTRT [A.3]. HEADSTRT is a program distributed by Princeton Applied Research for controlling PAR 273 and PAR 173 (with PAR 276 interface) potentiostats.

The following is the text of the screen for input to the MKCV program.

Number of Frequencies *user response (integer)*

The program stores the output curve in the file "C.D" in the sub-directory "COMMAND". In order for MKCV to successively execute there must be a sub-directory "COMMAND" present in the directory the program is executed from. The source code listing of MKCV.FOR can be found in section 5.1 of this appendix.

3. Data acquisition -- ACQUIRE.C

The computer controls the potentiostat by sending a series of commands to the potentiostat in the programming language of the potentiostat. ACQUIRE.C commands the PAR 273 to record the current and potential while applying the waveform generated by MKCV. The measured rather than the programmed potential is used in the impedance calculation because the potentiostat fails to accurately follow the programmed waveform. A detailed explanation of the commands can be found in the PAR 273 manual [A.1]. What follows is a commented listing of the command set sent to the PAR to perform the measurement of the response of both I and V to the potential program.

command	comment
26	<i>Number of commands to follow</i>
DCL	<i>Restores default settings of potentiostat</i>
I/E -3	<i>Set current measurement scale to 10^{-9} A</i>
BW 1	<i>Set potentiostat mode to high speed</i>
SETE -50	<i>Set electrode potential to -50 mV vs reference electrode</i>
CELL 1	<i>Turn cell on</i>
P 1	<i>Pause 1 second</i>
FP 0	<i>Storage location of first point of curve 0</i>
LP 1023	<i>Storage location of last point of curve 0</i>
SCV 5	<i>Set location of the source curve to 5×1024. The source curve is the multimode waveform generated by MKCV and loaded into the potentiostat by HEADSTRT</i>
PAM 0	<i>Set point averaging mode to no averaging</i>
MR 0	<i>Set modulation range to 20 mV</i>
MM 2	<i>Set modulation mode to arbitrary waveform modulation</i>
EGAIN 50	<i>Set potential gain to X50, recommended for $V < 200$ mV</i>
IGAIN 1	<i>Set current gain to X1</i>
SIE 3	<i>Sample current and potential</i>
DCV 0	<i>Set destination curve to curve 0. Current will be stored in curve 0, location 0 to 1023, and potential will be stored in curve 1, location 1024 to 2047.</i>

- TMB 1000 *Set time base to 1000 μ s.*
- SAM 2 *Set sweep averaging mode to exponential averaging*
- SHF 4 *Set exponential averaging to follow $avg = \sum_{i=1}^n [\frac{x_i}{2^i} + avg_{i-1}(1 - \frac{1}{2^i})]$*
- SWPS 96 *Average over 96 sweeps of the multimode waveform*
- DT 0 *Set dead time between sweeps to 0*
- NC *Set potentiostat for new acquisition*
- TC *Start sweeps*
- WCD *Wait till sweeps are completed before executing any more commands*
- g 1 *Execute HEADSTRT subroutine 1 which transfers data from potentiostat to computer memory*
- g 2 *Execute HEADSTRT subroutine 2 which stores the transferred data to a file on the hard disk*

Several of the commands can be altered to customize the program for a particular experiment. SETE must be altered in order to set the cell bias to another value. EGAIN and IGAIN must be altered to reflect the potential and current range of the electrochemical process investigated. The frequency, f , range of the measurement can be altered by changing TMB, however below $TMB = 1000$ the potential and current can not be simultaneously measured.

$$\frac{10^6}{1024 \times TMB} < f \text{ (Hz)} < \frac{10^6}{2 \times TMB} \quad (\text{A.1})$$

4. Impedance calculation -- IMP-FFT

The output of the FFT is an array of complex numbers corresponding to the frequency dependent amplitudes of sine and cosine waves. The impedance is then determined by the ratio of the complex amplitude of potential to current. The program IMP-FFT reads data created by HEADSTRT running the ACQUIRE.C program and outputs the complex impedance to a file on the hard disk. The following is the text of the screen for input to the IMP-FFT program.

Input Data File *user response*

Output File *user response*

Below is a sample of output from the program IMP-FFT.

I(mA)	V(mV)		
.629E-01	13.1		
Frequency	Zr	Zi	Z
2	23.8	3.24	24.0
4	20.9	4.14	21.3

The values .629E-01 and 13.1 correspond to the measured current and potential averaged over the applied waveform. The source code listing of IMP-FFT.FOR can be found in section 5.2 of this appendix.

5. Source Code Listing

5.1. MKCV (fortran)

```

program curve
integer amplitude(1024),nf
real*8 sum(1024)
i2=-1
call editi('Number of Frequencies',nf)
do 999 i=1,1024
999  sum(i)=0.0
do 1000 j=1,nf,2
write(*,90)j
random=ran2(i2)*6.28318
do 1000 i=1,1024
x=i/1024.*2.*3.14159+random
90  format(t2,i4,f7.0,f7.0)
1000 sum(i)=sum(i)+100*sin(x*j)
do 1100 j=nf+1,512,512/nf
write(*,90)j
random=ran2(i2)*6.28318
do 1100 i=1,1024
x=i/1024.*2.*3.14159+random
1100 sum(i)=sum(i)+100*sin(x*j)
maxa=0
mina=0
do 1001 i=1,1024
amplitude(i)=sum(i)+0.5

```

```

maxa=max(amplitude(i),maxa)
1001 mina=min(amplitude(i),mina)
      if(maxa.gt.iabs(mina))then
          factor=8000/maxa
      else
          factor=8000/iabs(mina)
      endif
      do 1002 i=1,1024
1002  amplitude(i)=amplitude(i)*factor
      open(unit=1,file='command\c.d',status='old')
      write(1,100)(amplitude(i),i=1,1024)
100  format('1024',/(i6))
      stop
      end

```

FUNCTION RAN2(IDUM)

RAN2

```

PARAMETER (M=714025,IA=1366,IC=150889,RM=1.4005112E-6)
DIMENSION IR(97)
DATA IFF /0/
IF(IDUM.LT.0.OR.IFF.EQ.0)THEN
    IFF=1
    IDUM=MOD(IC-IDUM,M)
    DO 11 J=1,97
        IDUM=MOD(LA *IDUM+IC,M)
        IR(J)=IDUM
11  CONTINUE
    IDUM=MOD(LA *IDUM+IC,M)
    IY=IDUM
ENDIF
J=1+(97 *IY) /M
IF(J.GT.97.OR.J.LT.1)PAUSE
IY=IR(J)

```

```
RAN2=IY*RM  
IDUM=MOD(LA*IDUM+IC,M)  
IR(J)=IDUM  
RETURN  
END
```

5.2. IMP_FFT (fortran)

```

program IMP_FFT
logical flag
real raw_data_1(1024),raw_data_2(1024)
complex out1(1024),out2(1024)
Character*40 potential_file,current_file,Output_file
data potential_file/'command\r.prn' /
data period/'.' /
write(*,*)'IMP_FFT ver 2.1'
100 format(a40)
call EDITCH('Input Data file',potential_file)
open(unit=1,file=potential_file,status='old')
read(1,100)(output_file,i=1,4)
read(1,110)(a,b,raw_data_1(i),raw_data_2(i),i=1,1024)
110 format(g18.0,g18.0,g18.0,g18.0)
call twofit(raw_data_1,raw_data_2,out1,out2,1024)
close(unit=1)
do 20 i=2,1024
20 out1(i)=out2(i)/out1(i)
i=index(potential_file,'.')
if(i.eq.0)i=index(potential_file,' ')
write(unit=potential_file(i),fmt=3021)
3021 format('.imp')
3002 inquire(file=potential_file,exist=flag)
3012 format('debug logical flag ',l4)
if(flag)then
write(*,3000)potential_file
3000 format(' ',a40,/' Already exists, Overwrite ? (y,n) : ', $)
read(*,1009)output_file(:1)

```

```

1009      format(a1)
          if(output_file(1:1).eq.'y'.or.output_file(1:1).eq.'Y')then
              open(unit=1,file=potential_file,status='old')
              goto 3001
          else
              call editch('output file ',potential_file)
              goto 3002
          endif
      endif
      open(unit=1,file=potential_file,status='new')
3001      chk=1.0
          write(*,*)'writing output to ',potential_file
          write(1,*)'V (mV), A (mA) ',out2(1)/1000., out1(1)/1000.
          do 30 i=2,512
              if(cabs(out2(i)).gt.chk)then
                  write(1,120)i-1,real(out1(i)),aimag(out1(i))
&                  ,cabs(out1(i))
              endif
30          continue
120      format(i4,g10.3,g10.3,g10.3,g10.3,g10.3,g10.3)
          close(unit=1)
          stop
          end

```

```

SUBROUTINE TWOFFT(DATA1,DATA2,FFT1,FFT2,N)      TWOFFT
DIMENSION DATA1(N),DATA2(N)
COMPLEX FFT1(N),FFT2(N),H1,H2,C1,C2
C1=CMPLX(0.5,0.0)
C2=CMPLX(0.0,-0.5)
DO 11 J=1,N
    FFT1(J)=CMPLX(DATA1(J),DATA2(J))

```

```

11  CONTINUE
    CALL FOUR1(FFT1,N,1)
    FFT2(1)=CMPLX(AMAG(FFT1(1)),0.0)
    FFT1(1)=CMPLX(REAL(FFT1(1)),0.0)
    N2=N+2
    DO 12 J=2,N/2+1
        H1=C1 *(FFT1(J)+CONJG(FFT1(N2-J)))
        H2=C2 *(FFT1(J)-CONJG(FFT1(N2-J)))
        FFT1(J)=H1
        FFT1(N2-J)=CONJG(H1)
        FFT2(J)=H2
        FFT2(N2-J)=CONJG(H2)

```

```

12  CONTINUE
    RETURN
    END

```

```

SUBROUTINE FOUR1(DATA,NN,ISIGN)
REAL *8 WR,WI,WPR,WPI,WTEMP,THETA
DIMENSION DATA(*)
N=2 *NN
J=1
DO 11 I=1,N,2
    IF(J.GT.I)THEN
        TEMPR=DATA(J)
        TEMPI=DATA(J+1)
        DATA(J)=DATA(I)
        DATA(J+1)=DATA(I+1)
        DATA(I)=TEMPR
        DATA(I+1)=TEMPI
    ENDIF
M=N/2

```

FOUR1

```
1      IF ((M.GE.2).AND.(J.GT.M)) THEN
        J=J-M
        M=M/2
        GO TO 1
      ENDIF
        J=J+M
11     CONTINUE
        MMAX=2
2      IF (N.GT.MMAX) THEN
        ISTEP=2*MMAX
        THETA=6.28318530717959D0/(ISIGN*MMAX)
        WPR=-2.D0*DSIN(0.5D0*THETA)**2
        WPI=DSIN(THETA)
        WR=1.D0
        WI=0.D0
        DO 13 M=1,MMAX,2
          DO 12 I=M,N,ISTEP
            J=I+MMAX
            TEMPR=SNGL(WR)*DATA(J)-SNGL(WI)*DATA(J+1)
            TEMPI=SNGL(WR)*DATA(J+1)+SNGL(WI)*DATA(J)
            DATA(J)=DATA(I)-TEMPR
            DATA(J+1)=DATA(I+1)-TEMPI
            DATA(I)=DATA(I)+TEMPR
            DATA(I+1)=DATA(I+1)+TEMPI
12         CONTINUE
            WTEMP=WR
            WR=WR*WPR-WI*WPI+WR
            WI=WI*WPR+WTEMP*WPI+WI
13        CONTINUE
            MMAX=ISTEP
        GO TO 2
```

ENDIF
RETURN
END

References

[A.1] Model 273 Potentiostat/Galvanostat Operating Manual, Princeton Applied Research, P.O. Box 2565, Princeton, New Jersey, 08543-2565, USA

[A.2] National Instruments Inc., 12109 Technology Blvd., Austin, Texas, 78727-9825

[A.3] HEAD START Creative Electrochemistry Software Preliminary Operating Manual, 4200-0291, Princeton Applied Research, P.O. Box 2565, Princeton, New Jersey, 08543-2565, USA

Appendix B -- Scanning Tunneling Microscopy Software

1. Introduction

The programs described in the following subsections are for control, data collection, and display of scanning tunneling microscopy, STM. The programs run on a IBM-AT compatible computer which has a VGA compatible display and a Metrabyte DAS-20 A/D-D/A board. A Digital Instruments Inc. Nanoscope I scanning tunneling microscopy system is controlled and monitored by the computer with the Metrabyte DAS-20 board. The following subsections describe programs used for acquisition, display, and manipulation of STM data.

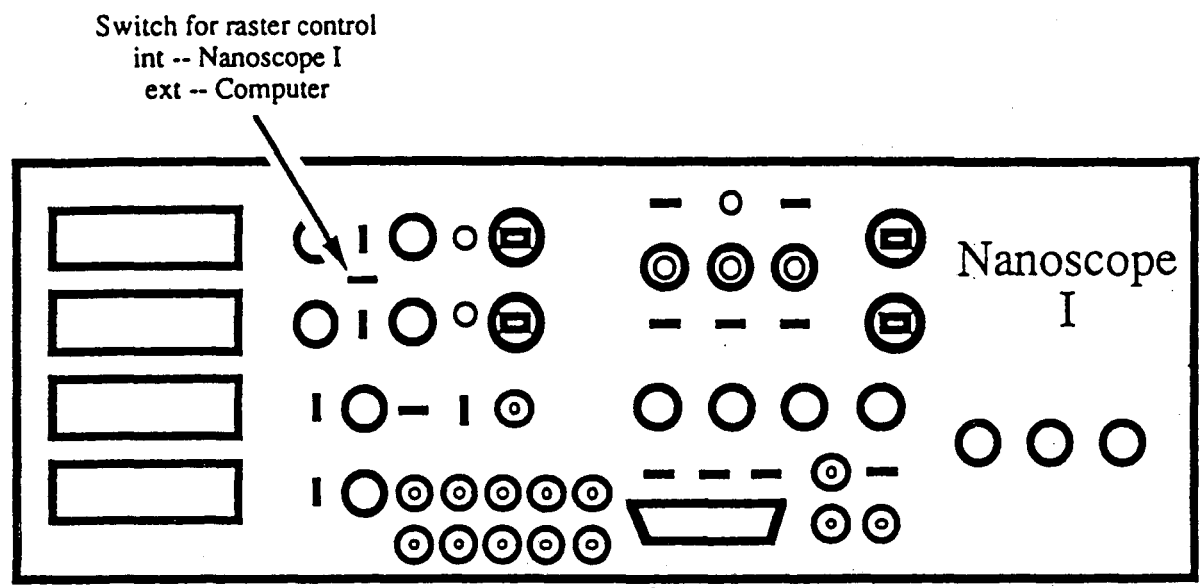
2. Data Acquisition

The Nanoscope I can be used with or without computer control. The instructions for operation of the Nanoscope I without computer control can be found in the instrument manual [B.1/]. The tunneling microscopy scan is performed by rastering the tunneling probe across the sample surface. This raster is generated internally in the Nanoscope I power supply when the switch highlighted in figure B-1 is positioned to INT and externally by the data acquisition system

when the switch is positioned to EXT. With internal control the x and y positions are varied with a saw tooth function. The x position varies rapidly at 1 to 200 Hz and y position varies slowly at 0.02 to 1 Hz. Under computer control the x and y positioning is discrete forming a 200 by 320 point grid. A digitally simulated triangle function is generated for the x position. Z position data are only collected in one x sweep direction. Following completion of each x sweep the Y position is updated. A complete 200 by 320 point scan can be completed in as little as 25 seconds when under computer control. More often the scan speed is limited by the ability of the STM to follow the surface contour such that in practice scan durations of 1 to 2 minutes are typical. The following programs are written for data collection from a Nanoscope I scanning tunneling microscope. The program STMPLE3 prompts the user for data display and storage following each scan. The program STMPLE4 scans continuously for a set number of scans and stores each scan automatically.

2.1. STMPLE3

The STM data acquisition program STMPLE3 was developed to perform single scans of a surface and allow viewing of the results. Input to the program includes raster length, sweep rate, z gain, and display mode. The raster length is the product of the scanner range, the software setting (.25, .5, 1, or 2), and the Nanoscope I controller setting (continuously variable between 0 and 1). When under control of the computer the resolution of the x-y probe position is limited by the resolution of the D/A converters of the data acquisition board. The D/A



XBL 902-575

Figure B-1. Nanoscope I control panel.

converters have a 12 bit resolution which corresponds to 4096 discrete potentials over the full range of the converters. The position of the tunneling probe in the z direction is represented by a -10 to +10 V output from the Nanoscope I power supply which corresponds to the full range of the scanner. The potential of the z output is measured with a A/D converter on the data acquisition board in the computer. The converter represents the measured potential as an integer value between -2048 and 2047 corresponding to a software selectable voltage range of -10 to +10 V, 0 to +10 V, -5 to 5 V, -0.5 to 0.5 V, or 0 to 1 V. A voltage range should be chosen such that the features which are of interest are within the range of the A/D converter. The scan speed can be set to any value below 5 kHz. The scan speed refers to the rate at which position of the tunneling probe is updated. The probe is placed at 128000 positions for each computer controlled image of the surface. Collisions with surface limit the high end of the raster speed and drift of the sample with respect to the probe limit the low end of the raster speed.

The following is the text of the screen for input to the STMPLE3 program.

Input scan range

A -- 2/1 Full scale

B -- 1/1

C -- 1/2

D -- 1/4

Y -- Change Gain

Z -- Frequency change

Q -- Quit

Selection :

Do you want to display data ? (Y/N)

A -- Line drawing

B -- Intensity Drawing

N -- No

Do you want autoscalling (Y/N) ?

Do you want leveling (Y/N) ?

This screen will repeat following display of the STM image. The x-y scale, z gain, or raster speed can be altered at the first prompt. The x-y scale can be chosen by pressing A through D. A scan of the surface will be taken automatically when a scale setting is chosen. The z gain can be altered by pressing Y. The possible values for the z gain are 1 to 5. Table B-1 shows the resolution for each gain setting for both the 9 and 0.6 μm STM scanners. The raster speed can be altered by pressing Z and inputing the desired raster speed. The value for the raster speed is in hertz and corresponds to the step rate in the x direction.

Following completion of the raster scan the screen will display options for viewing of the data. The options for display include A) line drawing, B) grey scale, or N) none. A line drawing and a grey scale plot of an STM scan are shown in figure B-2. If B is chosen a 64 shade grey scale image will be presented of the difference between the recorded z position and the z value of a plane intersecting three corners of the scanned area. The intensity levels are spread between the maximum and minimum values to be plotted. If A is chosen the user will be

Z Gain	Resolution	
	0.6 μm Scanner (\AA)	9.0 μm Scanner (\AA)
1	1.5	7.5
2	0.75	3.75
3	0.75	3.75
4	0.075	0.375
5	0.075	0.375

Table B-1. Resolution of the digitally recorded z data for the 9 and 0.6 μm scanners at the available gain settings.

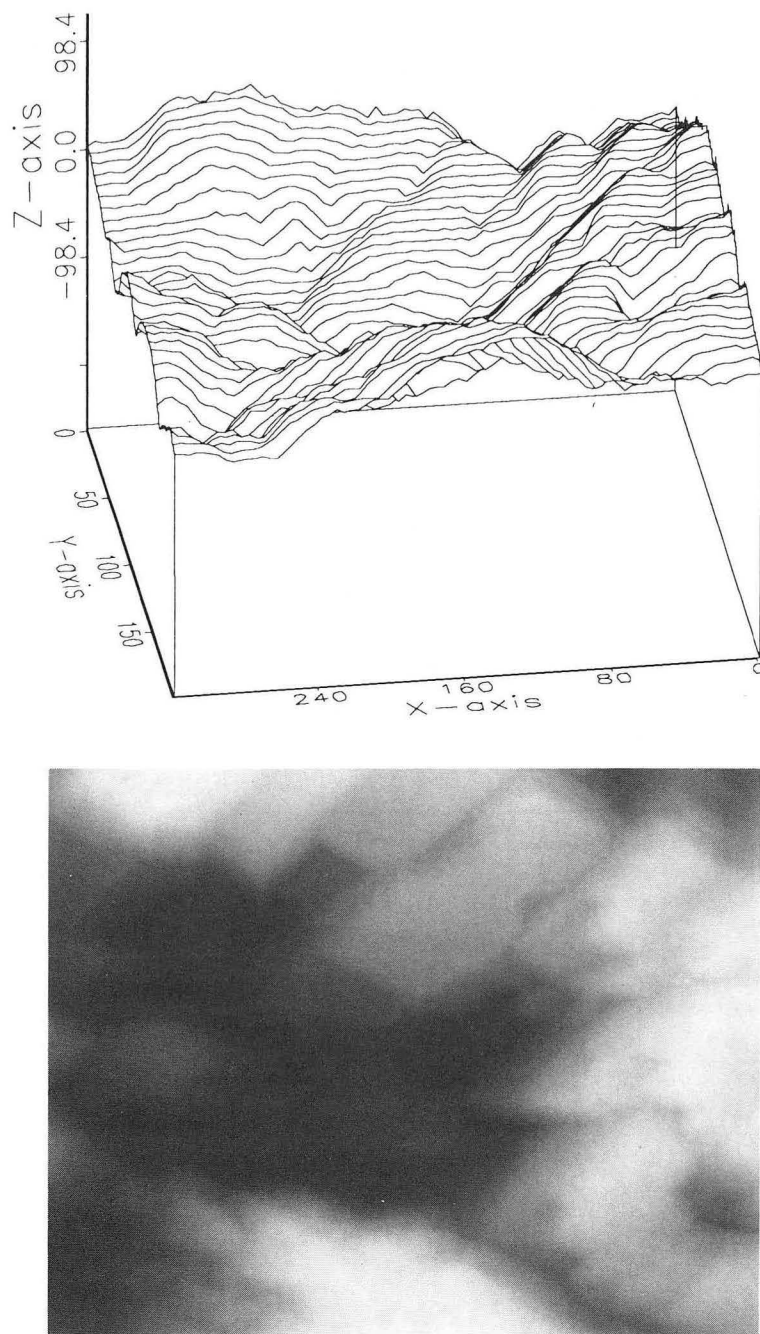


Figure B-2. STM scan of a copper deposit formed in 0.5 M CuSO_4 and 0.5 M H_2SO_4 . top) line drawing and bottom) grey scale plot. The scan area is 340 x 260 nm. (XBB 902-1429)

prompted to choose between automatic or manual scaling. If automatic scaling is chosen the z scale is set to three times the difference between the minimum and maximum values of the plotted data with the data centered on the axis. If manual scaling is chosen the user will be prompted to input the z axis scaling. Following input of the z axis scaling the user will be prompted for the option of leveling the data. If leveling is chosen the difference between the recorded z position and the z value of a plane intersecting three corners of the data matrix will be plotted. Following the line plot the user has the option of saving the line plot in a Tektronix formatted graphics file which can be printed on Tektronics compatible output devices.

2.2. STMPLE4

The STM data acquisition program STMPLE4 was written to perform multiple scans of a sample and record the data. The operation of the program is very similar to STMPLE3 with the exception that when the scale is chosen the user is prompted for a file name and the number of scans to be performed. The data are stored in multiple files having the inputted file name with an extension label equal to the sequence number of the scan, for example *name.003* is the third scan of series *name*. The inputted file name should not have an extension since one is added by the program. Each file contains the starting and finishing time recorded at the end of the data.

3. Data Display - RE2

The STM data can be recalled and displayed with the program RE2. This program is essentially the data display portion of the data acquisition program STMPLE3 with the addition of a prompt for inputting the file name of previously recorded data.

4. Data Manipulation

4.1. SUBTRACT

The program SUBTRACT is used to subtract one scan from another. The following prompts for input are printed by the program.

Input base file:

Input file from which "base" is subtracted:

Input file for difference:

Do you want to repeat ? (Y/N)

The data of the first file name inputted to the program is subtracted from the data of the second file name inputted. Following the subtraction the program prompts the user for an output file name. In order for this operation to be successful the STM must be operated with out drift. A possible improvement of the program would include correction for drift. The drift offset could be determined by superposition of images by the operator with an interactive program or by using

cross correlation of the z data.

4.2. ENHANCE

The program ENHANCE adds the value of the Laplacian operator, $\frac{d^2z}{dx^2} + \frac{d^2z}{dy^2}$, to the z values. The Laplacian value is averaged from a three by three matrix centered on the output storage location. The following equation is used for determining the stored value, $e_{i,j}$, of the program ENHANCE for location i,j of z value data.

$$e_{i,j} = z_{i,j} + \sum_{k=-1}^1 \sum_{l=-1}^1 (z_{i,j} - z_{k,l})$$

The following prompts for input are printed by the program.

File name of Z data:

Input file for storage of edge enhanced output:

Do you want to repeat ? (Y/N)

A grey scale image of the edge enhanced data will be plotted automatically (fig. B-3). The edge enhanced data can be stored by entering a name at the output file prompt. If no name is entered the data will not be stored.

4.3. DX

The program DX is used to take a derivative of the z location of the probe with respect to distance in the scan direction, $\frac{dz}{dx}$, from recorded STM data. The



Figure B-3. Grey scale display of an edge enhanced STM image of a copper deposit from 0.5 M H_2SO_4 and 0.5 M CuSO_4 . The scan area is 340 x 260 nm. (XBB 902-1428)

program uses a average of $\frac{dz}{dx}$ calculated from a 3 x 3 matrix centered on the storage location. The equation for the $\frac{dz}{dx}$ value for location i,j is as follows.

$$\frac{dz}{dx} = \frac{\sum_{l=-1}^1 (z_{i+1,l} - z_{i-1,l})}{6}$$

The following input prompts are printed by the program.

File name of Z data:

Input file name for storage of dZ/dX output:

Do You want to repeat ? (Y/N)

A grey scale image of the $\frac{dz}{dx}$ data will be plotted automatically (fig. B-4). The $\frac{dz}{dx}$ data can be stored by entering a name at the output file prompt. If no name is entered the data will not be stored.

4.4. SMOOTH

The program SMOOTH is used to filter high frequency noise from STM data. The program uses an average of a 3 x 3 matrix centered on the storage location with weighting on the center value by a factor of 8. The equation for the smoothed value, $s_{i,j}$ for location i,j is as follows.

$$s_{i,j} = \frac{\sum_{k=-1}^1 \sum_{l=-1}^1 (z_{i,j} + z_{k,l})}{16}$$

The following input prompts are printed by the program.

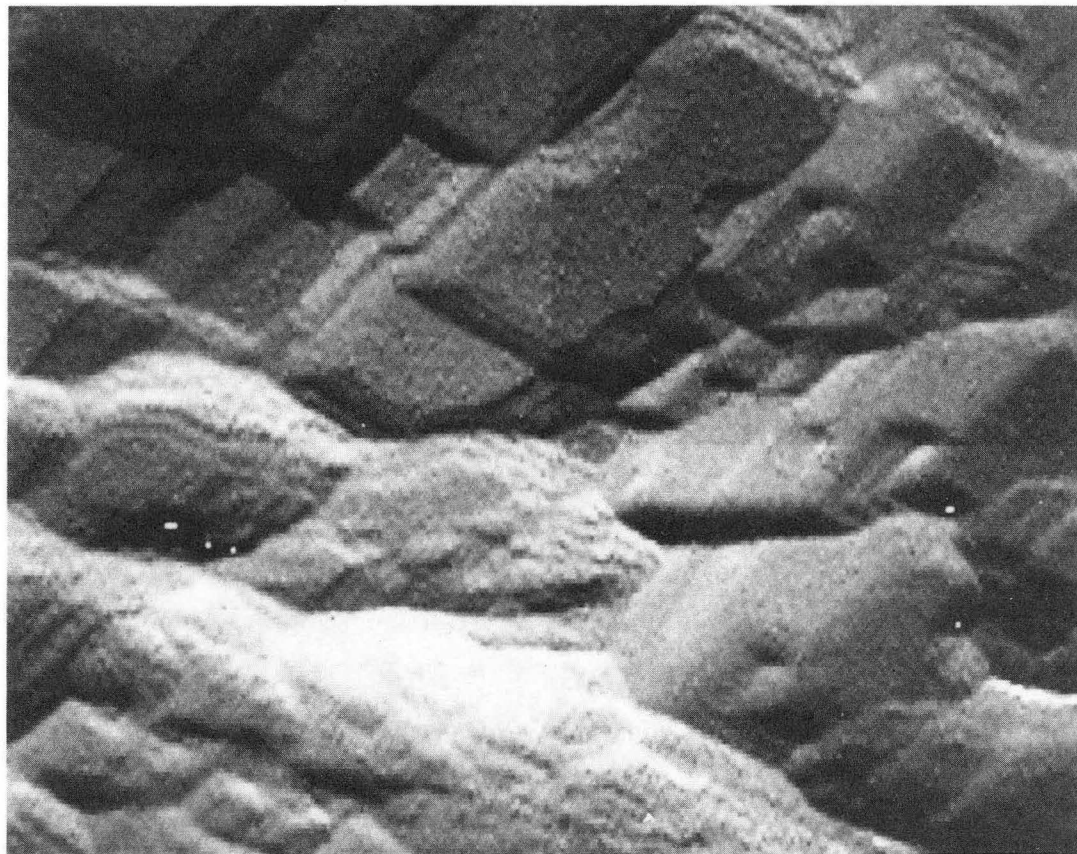


Figure B-4. Grey scale display of a $\frac{dz}{dx}$ STM image of a copper deposit from 0.5 M H_2SO_4 and 0.5 M CuSO_4 . The scan area is 340 x 260 nm. (XBB 902-1427)

Input number of passes:

Input file :

Input file name for data:

Do you want to repeat ? (Y/N)

Multiple passes of the smoothing routine can be performed by inputting a value greater than one at the prompt for the number of passes. The smooth data can be stored by entering a name at the output file prompt. If no name is entered the smoothed data will not be stored. Figure B-5 is a grey scale image of a STM image before and after it has been smoothed.

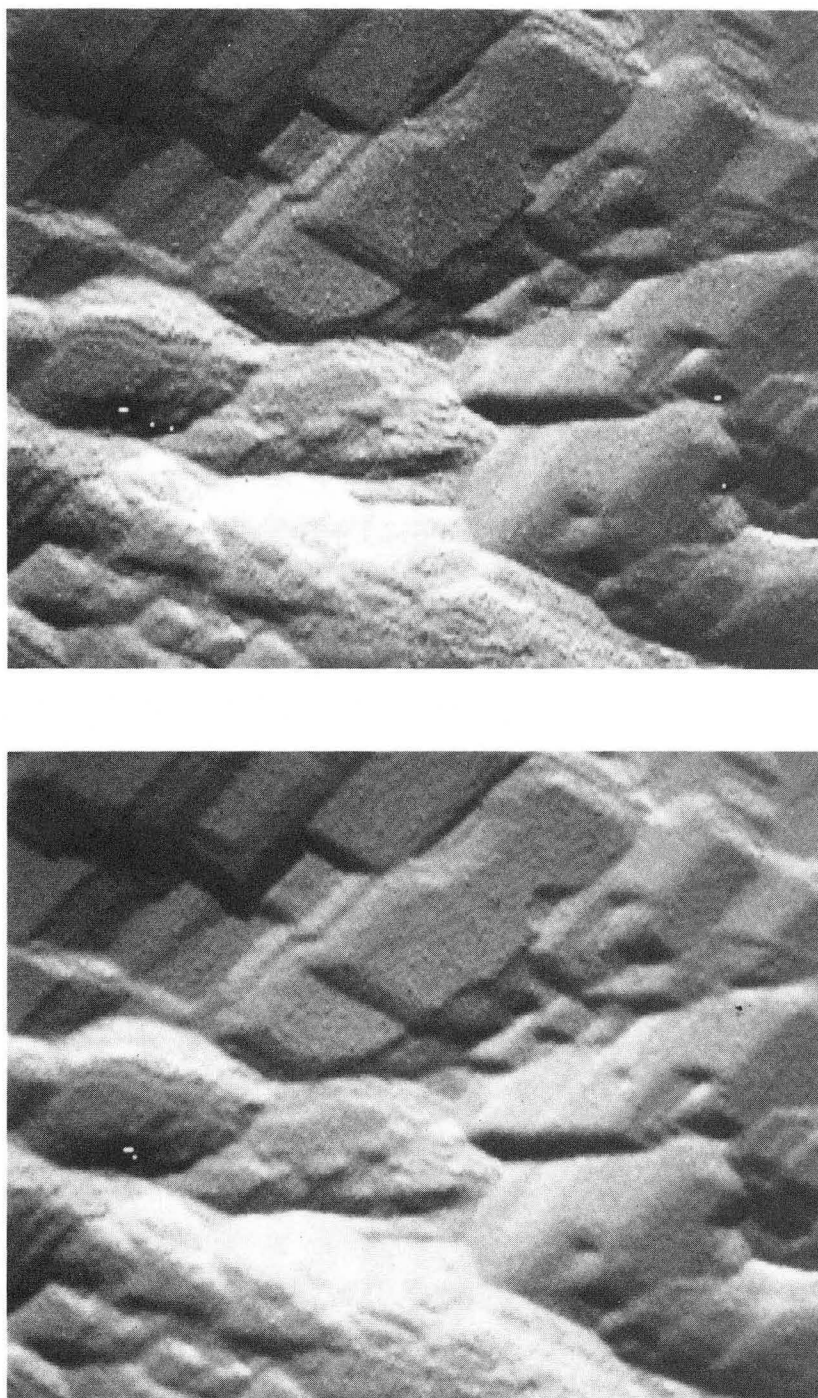


Figure B-5. Grey scale display of a STM image of a copper deposit from 0.5 M H_2SO_4 , 0.5 M CuSO_4 , and 100 μM BTA top) no smoothing and bottom) following one pass of SMOOTH. The scan area is 340 x 260 nm. (XBB 902-1430)

5. Source Code

5.1. STMPLE3

```

$include: 'stmp1e.inc'

    program STMPLE3
    integer *2 adarray(320,200),system
    integer *2 param(10),DAarray(400),rcode,tmp(200)
    integer *2 kbhit,getch,das20,offadr,segadr
    integer *2 base,int_level,dma_channel,imode,gain
    integer *2 response,scale,freq,I1,I2,I3,I4,I5
    INTEGER *2 zmax,zmin
    character *40 file_name

    freq=1000
    gain=1
    base=#300
    int_level= 2
    dma_channel= 1

*   Initialize board with mode 0
    param(1)=base
    param(2)=int_level
    param(3)=dma_channel
    imode=0
    rcode=das20(imode,param)

*   Set pacer clock to 1 kHz with mode 25
    param(1)=int(5000.)
    param(2)=0
    imode=25

```

```

        rcode=das20(imode,param)
*   Load the A/D control queue
        param(1)=0
        param(2)=1
        param(3)=2
        imode=1
        rcode=das20(imode,param)
        param(3)=0
        do 10 i=1,198
            rcode=das20(imode,param)
10       continue
        param(3)=1
        rcode=das20(imode,param)
607      write(*,2001)
2001     format(' Input scan range',/
&'   A — 1/1 Full scale',/
&'   B — 1/2 ',/
&'   C — 1/4 ',/
&'   D — 1/8',/
&'   E — 1/16',/
&'   F — 1/32',/
&'   G — 1/64',/'   Q — QUIT',/
&'   Y — Change gain',/
&'   Z — Frequency change',/
&'   selection: ')
401     response=getch()
        write(*,491)response
491     format('+ selection: ',a1)
        if(response.eq.ichar('Y'))then
*   Load the A/D control queue with new gain
        write(*,2037)gain

```

```

2037  format(/,' old gain = ',i5,'Input new gain',)$
      i=gain
      read(*,*)gain
      if(gain.eq.0)gain=i
      param(1)=0
      param(2)=gain
      param(3)=2
      imode=1
      rcode=das20(imode,param)
      param(3)=0
      do 109 i=1,198
          rcode=das20(imode,param)
109    continue
      param(3)=1
      rcode=das20(imode,param)
      goto 607
      endif
      if(response.eq.ichar('Z'))Then
          write(*,2013)freq
          i=freq
2013  format(' old freq. = ',i5,'input new value : ',)$
      read(*,*)freq
      if(freq.eq.0)freq=i
      param(1)=int(5000000./freq)
      param(2)=0
      imode=25
      rcode=das20(imode,param)
      goto 607
      endif
      IF(response.eq.ichar('Q'))stop
      if(response.lt.65.or.response.gt.71)goto 401

```

```
        scale=2***(response-65)
*   setup D/A control buffer
        do 20 i=1,200
            DAarray(i)=int(-2048./scale+(i-1)*4095./scale/199.)
            DAarray(401-i)=DAarray(i)
20      continue
*   Perform scan
        il=system('6.COM')
*   Set Y position (D/A channel 1)
        do 21 i=1,200
21      tmp(i)=int(-2048./scale*i/200.)
            imode=30
            param(1)=1
            param(2)=200
            param(3)=1
            param(4)=offadr(tmp(1))
            param(5)=offadr(tmp(1))
            param(6)=2
            param(7)=1
            rcode=das20(imode,param)
*   Check for end of line (mode 12)
            imode=12
327     param(2)=1
            rcode=das20(imode,param)
            if(rcode.ne.0)then
                write(*,*)'error on line'
                stop
            endif
            if(param(2).eq.0)goto 337
            goto 327
337     continue
```

```

*   Scan X line backwards(mode 30)
      imode=30
      param(1)=0
      param(2)=100
      param(3)=1
      param(4)=offadr(DAarray(301))
      param(5)=offadr(tmp(1))
      param(6)=2
      param(7)=1
      rcode=das20(imode,param)
*   Check for end of line (mode 12)
      imode=12
317   param(2)=1
      rcode=das20(imode,param)
      if(rcode.ne.0)then
          write(*,*)'error on line'
          stop
      endif
      if(param(2).eq.0)goto 307
      goto 317
307   continue
      do 32 i=1,320
*   Set Y position (D/A channel 1)
          IMODE=7
          param(1)=1
          param(2)=int(-2048./scale+(i-1)*4095./scale/319.)
          rcode=das20(imode,param)
*   Scan X line (mode 30)
          imode=30
          param(1)=0
          param(2)=200

```

```

    param(3)=1
    param(4)=offadr(DAarray(1))
    param(5)=offadr(tmp(1))
    param(6)=2
    param(7)=1
    rcode=das20(imode,param)
*   Check for end of line (mode 12)
    imode=12
3171  param(2)=1
    rcode=das20(imode,param)
    if(rcode.ne.0)then
        write(*,*)'error on line'
        stop
    endif
    if(param(2).eq.0)goto 3071
    goto 3171
3071  continue
    do 332 j=1,200
332  adarray(i,j)=tmp(j)
    IF(I.EQ.320)GOTO 32
*   Set Y position (D/A channel 1)
    IMODE=7
    param(1)=1
    param(2)=int(-2048./scale+(i)*4095./scale/319.)
    rcode=das20(imode,param)
*   Scan X line (mode 30)
    imode=30
    param(1)=0
    param(2)=200
    param(3)=1
    param(4)=offadr(DAarray(201))

```

```

        param(5)=offadr(tmp(1))
        param(6)=2
        param(7)=1
        rcode=das20(imode,param)
*   Check for end of line (mode 12)
        imode=12
31   param(2)=1
        rcode=das20(imode,param)
        if(rcode.ne.0)then
            write(*,*)'error on line'
            stop
        endif
        if(param(2).eq.0)goto 30
        goto 31
30   continue
32   continue
*   Set X and Y position to 0
        do 22 i=1,200
22   tmp(i)=int(2047./scale*(1-i/200.))
        imode=30
        param(1)=1
        param(2)=200
        param(3)=1
        param(4)=offadr(tmp(1))
        param(5)=offadr(tmp(1))
        param(6)=2
        param(7)=1
        rcode=das20(imode,param)
*   Check for end of line (mode 12)
        imode=12
3271 param(2)=1

```

```

        rcode=das20(imode,param)
        if(rcode.ne.0)then
            write(*,*)'error on line'
            stop
        endif
        if(param(2).eq.0)goto 3371
        goto 3271
3371    continue
        imode=30
        param(1)=0
        param(2)=100
        param(3)=1
        param(4)=offadr(DAarray(201))
        param(5)=offadr(tmp(1))
        param(6)=2
        param(7)=1
        rcode=das20(imode,param)
*
*   Display of Data
*
        il=system('10.COM')
795    write(*,2004)
2004    format(' Do you want to display data ? ',/
&'   A — Line drawing',/'   B — Intensity drawing',/
&'   N — No',,$)
403    response=getch()
        if(response.ne.ichar('A').AND.response.ne.ichar('N'))
&.and.response.ne.ichar('B'))goto 403
        if(response.eq.ichar('A'))Then
796    write(*,2014)
2014    format('/' Do you want autoscanning (Y/N) ? ',,$)

```

```

4013     yorn=getch()
        if(yorn.ne.ichar('Y').AND.yorn.ne.ichar('N')) goto 4013
        if(yorn.eq.ichar('Y')) then
            zmax=0
            zmin=0
        else
            WRITE(*,4113)ZMAX
4113     FORMAT(/' ZMAX ?('I6,') ', $)
        READ(*,*)ZMAX
            WRITE(*,4114)ZMIN
4114     FORMAT(/' ZMIN ?('I6,') ', $)
        READ(*,*)ZMIN
        endif
        write(*,2015)
2015     format(/' Do you want LEVELING (Y/N) ? ', $)
4014     yorn=getch()
        if(yorn.ne.ichar('Y').AND.yorn.ne.ichar('N')) goto 4014
        NORMAL=0
        if(yorn.eq.ichar('Y')) then
            NORMAL=1
        ENDIF
            CALL DISPLAY(ADARRAY(1,1),320,200,zMIN
&            ,ZMAX,NORMAL)
        endif
        if(response.eq.ichar('B'))Then
            call disp2(ADARRAY(1,1),320,200)
        endif
        if(response.ne.ichar('N'))goto 795

```

*

* File output if wanted

*

```
404      continue
      write(*,2002)
2002      format(/' Input file name for data : ', $)
      read(*,2003)file_name
2003      format(a40)
      if(file_name(1:1).eq.' ')goto 402
      open(unit=1,file=file_name,access='sequential',
&      form='BINARY',status='new')
      write(1)ADarray,scale
402      continue
      goto 607
      stop
      end
```

5.2. STMPLE4

```

$include: 'stmp4.inc'

program STMPLE4
integer *2 adarray(320,200),system
integer *2 param(10),DAarray(400),rcode,tmp(200)
integer *2 kbhit,getch,das20,offadr,segadr
integer *2 base,int_level,dma_channel,imode,gain
integer *2 response,scale,freq,I1,I2,I3,I4,I5
integer *2 ihr,imin,isec,i100th
integer scan_num,fnl
character *40 file_name

freq=1000
gain=1
base=#300
int_level= 2
dma_channel= 1

* Initialize board with mode 0
param(1)=base
param(2)=int_level
param(3)=dma_channel
imode=0
rcode=das20(imode,param)

* Set pacer clock to 1 kHz with mode 25
param(1)=int(5000.)
param(2)=0
imode=25
rcode=das20(imode,param)

* Load the A/D control queue
param(1)=0

```

```

param(2)=1
param(3)=2
imode=1
rcode=das20(imode,param)
param(3)=0
do 10 i=1,198
    rcode=das20(imode,param)
10    continue
    param(3)=1
    rcode=das20(imode,param)
607    write(*,2001)
2001    format(' Input scan range',/
&'   A — 1/1 Full scale',/
&'   B — 1/2 ',/
&'   C — 1/4 ',/
&'   D — 1/8',/
&'   E — 1/16',/
&'   F — 1/32',/
&'   G — 1/64',/'   Q — QUIT',/
&'   Y — Change gain',/
&'   Z — Frequency change',/
&'   selection: ')
401    response=getch()
        write(*,491)response
491    format('+ selection: ',a1)
        if(response.eq.ichar('Y'))then
*   Load the A/D control queue with new gain
        write(*,2037)gain
2037    format('/',' old gain = ',i5,'Input new gain',)$
        i=gain
        read(*,*)gain

```

```

if(gain.eq.0)gain=i
param(1)=0
param(2)=gain
param(3)=2
imode=1
rcode=das20(imode,param)
param(3)=0
do 109 i=1,198
    rcode=das20(imode,param)
109    continue
    param(3)=1
    rcode=das20(imode,param)
    goto 607
endif
if(response.eq.ichar('Z'))Then
    write(*,2013)freq
    i=freq
2013    format(' old freq. = ',i5,'input new value : ',%)
    read(*,*)freq
    if(freq.eq.0)freq=i
    param(1)=int(5000000./freq)
    param(2)=0
    imode=25
    rcode=das20(imode,param)
    goto 607
endif
IF(response.eq.ichar('Q'))then
    i5=system('c:\dos\10')
    stop
endif
if(response.lt.65.or.response.gt.71)goto 401

```

```

        scale=2*(response-65)
*   setup D/A control buffer
        do 20 i=1,200
            DAarray(i)=int(-2048./scale+(i-1)*4095./scale/199.)
            DAarray(401-i)=DAarray(i)
20        continue
        write(*,2002)
2002       format(/' Input file name for data : ', $)
        read(*,2003)file_name
2003       format(a40)
            if(file_name(1:1).eq.' ')goto 402
            fnl=index(file_name, ' ')
            if(index(file_name, '.').ne.0)fnl=index(file_name, '.')
402        continue
*   Perform scan
        WRITE(*,2101)
2101       FORMAT(' Input Number of scans ? : ', $)
        read(*,*)number_of_scans
            i5=system('c:\dos\6')
            do 2201 scan_num=1,number_of_scans
                WRITE(*,*)SCAN_NUM
                call gettim(i1,i2,i3,i4)
*   Set Y position (D/A channel 1)
            do 21 i=1,200
21          tmp(i)=int(-2048./scale*i/200.)
                imode=30
                param(1)=1
                param(2)=200
                param(3)=1
                param(4)=offadr(tmp(1))
                param(5)=offadr(tmp(1))

```

```
        param(6)=2
        param(7)=1
        rcode=das20(imode,param)
*      Check for end of line (mode 12)
        imode=12
327      param(2)=1
        rcode=das20(imode,param)
        if(rcode.ne.0)then
            write(*,*)'error on line'
            stop
        endif
        if(param(2).eq.0)goto 337
        goto 327
337      continue
        imode=30
        param(1)=0
        param(2)=100
        param(3)=1
        param(4)=offadr(DAarray(101))
        param(5)=offadr(tmp(1))
        param(6)=2
        param(7)=1
        rcode=das20(imode,param)
*      Check for end of line (mode 12)
        imode=12
3173     param(2)=1
        rcode=das20(imode,param)
        if(rcode.ne.0)then
            write(*,*)'error on line'
            stop
        endif
```

```
        if(param(2).eq.0)goto 3073
        goto 3173
3073      continue
        ICOUNT=0
*       Scan X line backwards(mode 30)
769      imode=30
        param(1)=0
        param(2)=200
        param(3)=1
        param(4)=offadr(DAarray(201))
        param(5)=offadr(tmp(1))
        param(6)=2
        param(7)=1
        rcode=das20(imode,param)
*       Check for end of line (mode 12)
        imode=12
317      param(2)=1
        rcode=das20(imode,param)
        if(rcode.ne.0)then
            write(*,*)'error on line'
            stop
        endif
        if(param(2).eq.0)goto 307
        goto 317
307      continue
        if(tmp(200).gt.2000.OR.ICOUNT.LT.30)then
        IF(TMP(200).LT.2000)ICOUNT=ICOUNT+1
        imode=30
        param(1)=0
        param(2)=200
        param(3)=1
```

```

        param(4)=offadr(DAarray(1))
        param(5)=offadr(tmp(1))
        param(6)=2
        param(7)=1
        rcode=das20(imode,param)
*   Check for end of line (mode 12)
        imode=12
3172   param(2)=1
        rcode=das20(imode,param)
        if(rcode.ne.0)then
            write(*,*)'error on line'
            stop
        endif
        if(param(2).eq.0)goto 769
        goto 3172
    endif
    do 32 i=1,320
*   Set Y position (D/A channel 1)
        IMODE=7
        param(1)=1
        param(2)=int(-2048./scale+(i-1)*4095./scale/319.)
        rcode=das20(imode,param)
*   Scan X line (mode 30)
        imode=30
        param(1)=0
        param(2)=200
        param(3)=1
        param(4)=offadr(DAarray(1))
        param(5)=offadr(tmp(1))
        param(6)=2
        param(7)=1

```

```

        rcode=das20(imode,param)
*   Check for end of line (mode 12)
        imode=12
3171   param(2)=1
        rcode=das20(imode,param)
        if(rcode.ne.0)then
            write(*,*)'error on line'
            stop
        endif
        if(param(2).eq.0)goto 3071
c       write(*,*)param(1),param(2),param(3)
        goto 3171
3071   continue
        do 332 j=1,200
332     adarray(i,j)=tmp(j)
        IF(I.EQ.320)GOTO 32
*   Set Y position (D/A channel 1)
        IMODE=7
        param(1)=1
        param(2)=int(-2048./scale+(i)*4095./scale/319.)
        rcode=das20(imode,param)
*   Scan X line (mode 30)
        imode=30
        param(1)=0
        param(2)=200
        param(3)=1
        param(4)=offadr(DAarray(201))
        param(5)=offadr(tmp(1))
        param(6)=2
        param(7)=1
        rcode=das20(imode,param)

```

```

*   Check for end of line (mode 12)
      imode=12
31   param(2)=1
      rcode=das20(imode,param)
      if(rcode.ne.0)then
          write(*,*)'error on line'
          stop
      endif
      if(param(2).eq.0)goto 30
c     write(*,*)param(1),param(2),param(3)
      goto 31
30   continue
32   continue
*   Set X and Y position to 0
      do 22 i=1,200
22   tmp(i)=int(2047./scale*(1-i/200.))
      imode=30
      param(1)=1
      param(2)=200
      param(3)=1
      param(4)=offadr(tmp(1))
      param(5)=offadr(tmp(1))
      param(6)=2
      param(7)=1
      rcode=das20(imode,param)
*   Check for end of line (mode 12)
      imode=12
3271 param(2)=1
      rcode=das20(imode,param)
      if(rcode.ne.0)then
          write(*,*)'error on line'

```

```
        stop
      endif
      if(param(2).eq.0)goto 3371
      goto 3271
3371    continue
        imode=30
        param(1)=0
        param(2)=100
        param(3)=1
        param(4)=offadr(DAarray(201))
        param(5)=offadr(tmp(1))
        param(6)=2
        param(7)=1
        rcode=das20(imode,param)
*   Output File including time start and finish
        call gettim(ihr,imin,isec,i100th)
        write(file_name(fnl:40-fnl),2103)scan_num
2103    format(' ',i3.3)
        open(unit=1,file=file_name,access='sequential',
&   form='BINARY',status='new')
        write(1)ADarray,scale,i1,i2,i3,i4,ihr,imin,isec,i100th
2201    continue
404    continue
        goto 607
      end
```

5.3. RE2

```

$include: 'stmple.inc'

    program recall
    INTEGER *2 zmax,zmin,system
    integer *2 a(320,200)
    COMMON /EXT /A
    integer *2 response,scale,getch,yorn,NORMAL
    character *40 file_name
    CHARACTER *80 COMMAND
    character *12 file_form
    logical exists
    WRITE(*,*)'—RECALL V2.1—'
10      write(*,100)
100     format(' Input file: ', $)
        read(*,200)file_name
200     format(a40)
        INQUIRE(FILE=FILE_NAME,EXIST=EXISTS,FORM=FILE_FORM)
        if(exists)then
            open(unit=1,file=file_name,access='sequential',
&      form='BINARY',status='old')
            read(1)A,scale
            close(unit=1)
795     write(*,2004)
2004    format(' Do you want to display data ? ', /
&      ' A — Line drawing', / ' B — Intensity drawing', /
&      ' N — No', $)
403     response=getch()
        if(response.ne.ichar('A').AND.response.ne.ichar('N')
&.and.response.ne.ichar('B'))goto 403

```

```

if(response.eq.ichar('N'))goto 20
if(response.eq.ichar('A'))Then
796 write(*,2014)
2014 format(/' Do you want autoscalling (Y/N) ? ', $)
4013 yorn=getch()
if(yorn.ne.ichar('Y').AND.yorn.ne.ichar('N')) goto 4013
if(yorn.eq.ichar('Y')) then
zmax=0
zmin=0
else
WRITE(*,4113)ZMAX
4113 FORMAT(/' ZMAX ?(',I6,') ', $)
READ(*,*)ZMAX
WRITE(*,4114)ZMIN
4114 FORMAT(/' ZMIN ?(',I6,') ', $)
READ(*,*)ZMIN
endif
write(*,2015)
2015 format(/' Do you want LEVELING (Y/N) ? ', $)
4014 yorn=getch()
if(yorn.ne.ichar('Y').AND.yorn.ne.ichar('N')) goto 4014
NORMAL=0
if(yorn.eq.ichar('Y')) then
NORMAL=1
ENDIF
CALL DISPLAY(A(1,1),320,200,zMIN
& ,ZMAX,NORMAL)
201 write(*,1301)
1301 format(/' Do you want to save the x.tek file ? (Y/N) ', $)
read(*,200)file_name
if(file_name(1:1).eq.'N')goto 20

```

```
        if(file_name(1:1).ne.'Y')goto 201
        write(*,100)
        read(*,200)file_name
        WRITE(COMMAND,1302)FILE_NAME
1302  FORMAT(' COPY F:HOLD.DAT ',A40)
        COMMAND(56:1)='\000'C
        response=SYSTEM(COMMAND)
        endif
        if(response.eq.ichar('B'))Then
            call disp2(A(1,1),320,200)
        endif
        GOTO 795
        ELSE
        WRITE(*,*)FILE_NAME,'FILE NOT FOUND'
        ENDIF
20      write(*,130)
130     format(/' Do you want to repeat ? (Y/N) ', $)
        read(*,200)file_name
        if(file_name(1:1).eq.'Y')goto 10
        if(file_name(1:1).ne.'N')goto 20
        stop
        end
```

5.4. SUBTRACT

```

$include: 'stmple.inc'
      PROGRAM SUBTRACT
      integer *2 a(320,200),b(320,200)
      integer *2 scale,GETCH
      character *40 file_name,yorn
      character *12 file_form
      logical exists
10      write(*,100)
100     format(' Input base file: ', $)
      read(*,200)file_name
200     format(a40)
      INQUIRE(FILE=FILE_NAME,EXIST=EXISTS,FORM=FILE_FORM)
      if(exists)then
      open(unit=1,file=file_name,access='sequential',
& form='BINARY',status='old')
      read(1)A,scale
      close(unit=1)
      ELSE
      WRITE(*,*)FILE_NAME,'FILE NOT FOUND'
      GOTO 10
      ENDIF
2001    write(*,110)
110     format(' Input file from which "base" is subtracted: ', $)
      read(*,200)file_name
      INQUIRE(FILE=FILE_NAME,EXIST=EXISTS,FORM=FILE_FORM)
      if(exists)then
      open(unit=1,file=file_name,access='sequential',
& form='BINARY',status='old')

```

```

read(1)B,scale
close(unit=1)
ELSE
WRITE(*,*)FILE_NAME,'FILE NOT FOUND'
GOTO 2001
ENDIF
call sub(a,b)
70 write(*,2002)
2002 format('/' Input file name for storage of subtract output: ', $)
read(*,200)file_name
if(file_name(1:1).eq.' ')goto 20
INQUIRE(FILE=FILE_NAME,EXIST=EXISTS,FORM=FILE_FORM)
if(exists)then
write(*,2004)
2004 format(' Output file name already exists.' /,
&' Should I replace it ? (OVERWRITE OR N) :', $)
71 read(*,200)yorn
if(yorn.ne.' OVERWRITE'.and.yorn.ne.' N')then
write(*,2005)
2005 format(' OVERWRITE or N : ', $)
goto 71
endif
if(yorn.eq.' N')goto 70
endif
open(unit=1,file=file_name,access='sequential',
& form='BINARY',status='UNKNOWN')
write(1)B,scale
close(unit=1)
20 write(*,130)
130 format(' Do you want to repeat ? (Y/N) ', $)
read(*,200)file_name

```

```
if(file_name(1:1).eq.'Y')goto 10
if(file_name(1:1).ne.'N')goto 20
stop
end
```

```
subroutine sub(a,b)
integer *2 a(320,200),b(320,200)
do 10 j=1,200
  do 10 i=1,320
    b(i,j)=b(i,j)-a(i,j)
  continue
return
end
```

sub

10

5.5. ENHANCE

```

$include: 'stmple.inc'

      program ENHANCE
      integer *2 a(320,200),B(320,200)
      integer *2 response,scale,getch
      character *40 file_name,yorn
      character *12 file_form
      logical exists
10      write(*,100)
100     format(' Input file name of Z data: ', $)
      read(*,200)file_name
200     format(a40)
      INQUIRE(FILE=FILE_NAME,EXIST=EXISTS,FORM=FILE_FORM)
      if(exists)then
      open(unit=1,file=file_name,access='sequential',
&       form='BINARY',status='old')
      read(1)A,scale
      close(unit=1)
      DO 40 J=2,199
          DO 40 I=2,319
40          B(I,J)=A(I,J) *9-A(I-1,J)-A(I+1,J)-A(I,J-1)-A(I,J+1)
&          -A(I-1,J+1)-A(I-1,J-1)-A(I+1,J+1)-A(I+1,J-1)
      DO 50 J=2,199
          B(1,J)=B(2,J)
50          B(320,J)=B(319,J)
          DO 60 I=2,319
              B(I,1)=B(I,2)
60          B(I,200)=B(I,199)
          B(1,1)=B(2,2)

```

```

B(1,200)=B(2,199)
B(320,200)=B(319,199)
B(320,1)=B(319,2)
    call disp2(B(1,1),320,200)
70    write(*,2002)
2002   format(/' Input file name for storage of edge enhance output: ', $)
      read(*,200)file_name
      if(file_name(1:1).eq.' ')goto 402
      INQUIRE(FILE=FILE_NAME,EXIST=EXISTS,FORM=FILE_FORM)
      if(exists)then
        write(*,2004)
2004   format(' Output file name already exists. '/,
&' Should I replace it ? (OVERWRITE OR N) : ', $)
71     read(*,200)yorn
        if(yorn.ne.' OVERWRITE' .and.yorn.ne.' N')then
          write(*,2005)
2005   format(' OVERWRITE or N : ', $)
          goto 71
        endif
        if(yorn.eq.' N')goto 70
      endif
      open(unit=1,file=file_name,access='sequential',
& form='BINARY',status='UNKNOWN')
      write(1)B,scale
      CLOSE(UNIT=1)
402   continue
      ELSE
      WRITE(*,*)FILE_NAME,'FILE NOT FOUND'
      ENDIF
20    write(*,130)
130   format(' Do you want to repeat ? (Y/N) ', $)

```

```
read(*,200)file_name
if(file_name(1:1).eq.'Y')goto 10
if(file_name(1:1).ne.'N')goto 20
stop
end
```

5.8. DX

```

$include: 'stmp1e.inc'

      program deriv
      integer *2 a(320,200),B(320,200)
      integer *2 response,scale,getch
      character *40 file_name,yorn
      CHARACTER *12 FILE_FORM
      LOGICAL EXISTS
10      write(*,100)
100     format(' File name of Z data: ', $)
      read(*,200)file_name
200     format(a40)
      INQUIRE(FILE=FILE_NAME,EXIST=EXISTS,FORM=FILE_FORM)
      if(exists)then
      open(unit=1,file=file_name,access='sequential',
& form='BINARY',status='old')
      read(1)A,scale
      close(unit=1)
      DO 40 J=2,199
          DO 40 I=2,319
40          B(I,J)=-A(I,J-1)+A(I,J+1)
      DO 50 J=2,199
          B(1,J)=B(2,J)
50          B(320,J)=B(319,J)
          DO 60 I=2,319
              B(I,1)=B(I,2)
60          B(I,200)=B(I,199)
              B(1,1)=B(2,2)
              B(1,200)=B(2,199)

```

```

B(320,200)=B(319,199)
B(320,1)=B(319,2)
    call disp2(b(1,1),320,200)
70    write(*,2002)
2002    format(/' Input file name for storage of dZ/dX output: ', $)
        read(*,200)file_name
        if(file_name(1:1).eq.' ')goto 402
        INQUIRE(FILE=FILE_NAME,EXIST=EXISTS,FORM=FILE_FORM)
        if(exists)then
            write(*,2004)
2004    format(' Output file name already exists.' /,
& ' Should I replace it ? (OVERWRITE OR N) :', $)
71        read(*,200)yorn
            if(yorn.ne.' OVERWRITE' .and.yorn.ne.' N')then
                write(*,2005)
2005    format(' OVERWRITE or N : ', $)
                    goto 71
            endif
            if(yorn.eq.' N')goto 70
        endif
        open(unit=1,file=file_name,access='sequential',
& form='BINARY',status='unknown')
        write(1)B,scale
        CLOSE(UNIT=1)
402    continue
        ELSE
        WRITE(*,*)FILE_NAME,'FILE NOT FOUND'
        ENDIF
20    write(*,130)
130    format(' Do you want to repeat ? (Y/N) ', $)
        read(*,200)file_name

```

```
if(file_name(1:1).eq.'Y')goto 10
if(file_name(1:1).ne.'N')goto 20
stop
end
```

5.7. SMOOTH

```

$include: 'stmple.inc'

      program smooth
      integer *2 a(320,200),B(320,200)
      integer *2 response,scale,getch
      character *40 file_name,yorn
      character *12 file_form
      logical exists
      WRITE(*,890)
890    FORMAT(' INPUT NUMBER OF PASSES: ', $)
      READ(*,*)NUM_PASS
10     write(*,100)
100    format(' Input file name of data to be smooth: ', $)
      read(*,200)file_name
200    format(a40)
      INQUIRE(FILE=FILE_NAME,EXIST=EXISTS,FORM=FILE_FORM)
      if(exists)then
      open(unit=1,file=file_name,access='sequential',
&      form='BINARY',status='old')
      read(1)A,scale
      close(unit=1)
      DO 61 IP=1,NUM_PASS
      DO 40 J=2,199
          DO 40 I=2,319
140          B(I,J)=(A(I,J)*8+A(I-1,J)+A(I+1,J)+A(I,J-1)+A(I,J+1)
&          +A(I-1,J+1)+A(I-1,J-1)+A(I+1,J+1)+A(I+1,J-1))/16
      DO 50 J=2,199
      B(1,J)=B(2,J)
50     B(320,J)=B(319,J)

```

```

DO 60 I=2,319
B(I,1)=B(I,2)
60  B(I,200)=B(I,199)
    B(1,1)=B(2,2)
    B(1,200)=B(2,199)
    B(320,200)=B(319,199)
    B(320,1)=B(319,2)
    WRITE(*,*)IP
    DO 61 I=1,200
    DO 61 J=1,320
61  A(J,I)=B(J,I)
70  write(*,2002)
2002 format(/' Input file name for storage of smooth output: ', $)
    read(*,200)file_name
    if(file_name(1:1).eq.' ')goto 402
    INQUIRE(FILE=FILE_NAME,EXIST=EXISTS,FORM=FILE_FORM)
    if(exists)then
        write(*,2004)
2004 format(' Output file name already exists. '/,
&' Should I replace it ? (OVERWRITE OR N) : ', $)
71  read(*,200)yorn
    if(yorn.ne.' OVERWRITE'.and.yorn.ne.' N')then
        write(*,2005)
2005 format(' OVERWRITE or N : ', $)
        goto 71
    endif
    if(yorn.eq.' N')goto 70
endif
if(file_name(1:1).eq.' ')goto 402
open(unit=1,file=file_name,access='sequential',
& form=' BINARY',status=' UNKNOWN')

```

```
write(1)B,scale
CLOSE(UNIT=1)
402 continue
ELSE
WRITE(*,*)FILE_NAME,'FILE NOT FOUND'
ENDIF
20 write(*,130)
130 format(' Do you want to repeat ? (Y/N) ', $)
read(*,200)file_name
if(file_name(1:1).eq.'Y')goto 10
if(file_name(1:1).ne.'N')goto 20
stop
end
```

5.8. Subroutines

5.8.1. *Display*

```

void display( int huge *, int ,int , int far * ,int far *,int);
double zfun(float ,float );
#include "graphic.h"
#include "stdio.h"
#include "dvapi.h"

/* minimum API version required
#define required 0x201 */

        int huge *adar;
        int c1,c2,c3,ni,nj;
void display( adarray, nx, ny, zmin, zmax ,normal)
/*
    adarray — huge array of "nx" by "ny"
    nx      — dimension of adarray
    ny      — dimension of adarray
    zmin,zmax— if these are equal auto scaling takes place
                else these values are used for the min and max
    normal  — if normal equals 1 the surface is flattend
*/
    int huge *adarray;
    int nx, ny,normal;
    int far *zmin,*zmax;
{
        int flag;

```

```

        long i,j;
        float plot,vx,vy,vz;
        float xmin,xstp,xmax,zmn,zmx,zst;

/* Does api exist flag */
    int api_flag=0;
/* actual API version number
    int    version;
    version = api_init();
    if (version < required) {
        api_flag=0;
    }
    else {
        api_flag=1;
        api_level (required);
    }
*/

    flag=0;
    adar=adarray;
    ni=nx;
    nj=ny;
    if( *zmax== *zmin)
    {
        *zmax=-2048;
        *zmin=2048;
        flag=1;
    }
    c1=c2=c3=0;
    if(normal==1)
    {
        c1=adarray[0];
        c2=adarray[nx-1];

```

```

i=1;
c3=adarray[i*(ny-1)*nx];
}
if(flag==1)
{
i=0;
while(i<32)
{
j=0;
while(j<32)
{
plot= adarray[i*nx/32+j*ny/32*nx]-c1-(c2-c1)*i
/31-(c3-c1)*j/31;
*zmin=( *zmin<plot)? *zmin : plot;
*zmax=( *zmax > plot)? *zmax : plot;
++j;
}
++i;
}
}
zmx=*zmax;
zmn=*zmin;
if(flag==1)
{
zst=( *zmax- *zmin);
zmx=*zmax+zst;
zmn=*zmin-zst;
}
}

```

```

printf("\nInput view position. (default 30.,200.,100.)");
scanf("%f %f %f", &vx, &vy, &vz);
printf("%f %f %f\n", vx, vy, vz);    */

vx=0;

if(vx==0.)
{
    vx=30.;
    vy=200.;
    vz=100.;
}
if(api_flag==1)
{
    api_beginc();
}
bgnplot(1, 'g', "e:\hold.dat");
font(4, "simplex.fnt", '\310', "triplex.fnt"
, '\311', "complex.fnt", '\312', "compgrma.fnt", '\313');
startplot(7);
color(0);
page(9.,6.5);
box();
area2d(7.5,5.5);
tickout(1);
survis("both");
x3name("\310X-axis");
y3name("\310Y-axis");
z3name("\310Z-axis");
volm3d(1.,1.,1.);
vuabs(vx,vy,vz);
xmin=0;
xstp=80.;

```

/* E

```

    xmax=320.;
    zst=(zmx-zmn)/5.;
    graf3d(0.,80.,318.,0.,50.,198.,zmn,
zst,zmx);
    base(1,0);
    surfun(zfun,80,320.,5,5.);
    d3head("\311STM output", 't');
    endplot();
    stopplot();
    if(api_flag==1)
    {
        api_endc();
    }
    return;
}
double zfun(float xx,float yy)
{
    double result;
    long cx,fx,cy,fy;
    float eta,theta;
    fx=floor(xx);
    fy=floor(yy);
    if(fx>318)fx=318;
    if(fy>198)fy=198;
    if(fx<0)fx=0;
    if(fy<0)fy=0;
    cx=fx+1;
    cy=fy+1;
    eta=xx-fx;
    theta=yy-fy;
    result=eta*theta*adar[cx+cy*ni]+(1-eta)*theta*adar[fx+cy*ni]

```

```
+(1-eta)*(1-theta)*adar[fx+fy*ni]+eta*(1-theta)*adar[cx+fy*ni]
-c1-(c2-c1)*xx/(ni-1)-(c3-c1)*yy/(nj-1);
return(result);
}
```

5.8.2. Grey64

```
#include <graph.h>
#include <stdio.h>
void grey64()
{
    long color,red,blue,green;
    short pixel;
    color = 0;
    pixel=0;
    /* where 0 <= red,green,blue ==> 63 */
    while(pixel<64)
    {
        red=green=blue=pixel;
        blue=blue *256;
        blue=blue *256;
        green=green *256;
        color=red+green+blue;
        _remappalette(pixel,red+green+blue);
        _remappalette(pixel+64,red);
        _remappalette(pixel+128,green);
        _remappalette(pixel+196,blue);
        ++pixel;
    }
}
```

5.8.3. *Disp2*

```
#include <stdio.h>
#include <graph.h>
#include <math.h>
#include <malloc.h>
void grey64(void);
void disp2(array,nx,ny)
int huge *array;
long nx,ny;
{
    int a1,a2;
    int maxz,minz,tmp;
    long i,j;
    int c1,c2,c3;
    int icolor;
    short color;

    _setvideomode(_MRES256COLOR);
    grey64();
    _setcolor(3);
    _clearscreen(_GCLEARSCREEN);
    minz=2048;
    maxz=-2048;
    c1=array[0];
    c2=array[nx-1];
    i=1;
    c3=array[i*(ny-1)*nx];
    j=0;
    while(j<ny)
```

```

{
    i=0;
    while(i<nx)
    {
        tmp=array[i+j*nx]-c1-(c2-c1)*i/(nx-1)-(c3-c1)*j/(ny-1);
        minz=(minz < tmp) ? minz : tmp;
        maxz=(maxz > tmp) ? maxz : tmp;
        i=i+2;
    }
    j=j+2;
}
j=0;
while(j<ny)
{
    i=0;
    while(i<nx)
    {
        tmp=array[i+j*nx]-c1-(c2-c1)*i/(nx-1)-(c3-c1)*j/(ny-1);
        icolor=floor(0.5+63.0*(tmp-minz)/(maxz-minz));
        color=icolor;
        _setcolor(color);
        _setpixel(-i+160+nx/2,j+100-ny/2);
        ++i;
    }
    ++j;
}
getch();
_setvideomode(3);
}

```

References

- [B.1] Digital Instruments Nanoscope I Scanning Tunneling Microscope Instruction Manual, Version 1.1, 1987, Digital Instruments Inc. , Goleta, California, USA

LAWRENCE BERKELEY LABORATORY
UNIVERSITY OF CALIFORNIA
INFORMATION RESOURCES DEPARTMENT
BERKELEY, CALIFORNIA 94720